April 2010

Flywheel-Accumulator for Compact Hydraulic Energy Storage

Angel A. Martinez
Worcester Polytechnic Institute

Rachel J. Grau
Worcester Polytechnic Institute

Rahul Mahtani
Worcester Polytechnic Institute

Robert Emmett Sayre
Worcester Polytechnic Institute

Project Number: ME-JDV-0904

Flywheel-Accumulator for Compact Hydraulic Energy Storage

A Major Qualifying Project Report
Submitted to the Faculty
of the
WORCESTER POLYTECHNIC INSTITUTE
in partial fulfillment of the requirements for the
Degree of Bachelor of Science
in Mechanical Engineering

by

Rahul Mahtani

Angel Martinez

Rachel Salvatori

Robert Sayre

Date: April 29, 2010

Approved:

Prof. J. D. Van de Ven, MQP Advisor

Keywords:
1. Variable Inertia Flywheel
2. Hydraulic Accumulator
3. Increased Energy Density

Abstract

The energy density of a hydraulic hybrid drive train pales in comparison to current competing technologies in industry, such as electrical and mechanical systems. A solution to bridge this gap is to improve the energy storage per unit mass of a hydraulic accumulator by storing energy as potential and rotating kinetic energy in a flywheel-accumulator. A flywheel-accumulator is a cylindrical pressure vessel with an oil and gas volume separated by a piston, which is rotated about the central axis. The goal of this project is to verify the increase in energy density and to validate that a parabolic pressure distribution exists on the hydraulic fluid side of the accumulator due to centripetal acceleration. To meet this goal, a low-energy bench top prototype was designed and fabricated. The system utilizes multiple sensors for data acquisition that incorporates: strain measurements to verify a FEA model, a transparent acrylic chamber to observe fluid flow, video capture in order to monitor the piston position, and pressure sensor readings that are relayed via a wireless data acquisition system to confirm the pressure distribution. The verification of increased energy density has the potential to revolutionize compact hydraulic accumulator energy storage.

Acknowledgments

The group would like to thank Professor Van de Ven for his expert guidance and constructive criticism of this project. He allowed the group to formally come to their own designs and conclusions with enough involvement to fully develop ideas, while supporting independence. Without his supervision the project would have not been a success.

We would also like to thank Adam Allard of US Hydraulics for his advice on hydraulic aspects and components of the project. Additionally, we would like to thank him for the precision machining and polishing of the acrylic cylinder, which is a crucial component to the flywheel-accumulator.

We are grateful for the assistance from Adam Sears, Toby Bergstrom, and Dan Flavin of Washburn shops on the proper techniques for machining parts. Without their help this project would have taken much longer to complete.

We would furthermore like to thank Professor Nestinger for his general guidance on the project, particularly regarding the electronic aspects of the project.

We would also like to thank Professor Furlong for his assistance with the data acquisition system and setting up the strain gauges.

Table of Contents

Table of Figures

List of Tables

1. Introduction

The energy crisis has sparked widespread investigations by automotive manufacturers into greater energy density storage units and alternative fuels. A notable outcome of this research is the advent of the hybrid electric vehicle, which has become fairly popular amongst leading car manufacturers. Methods to improve performance, durability, and longevity are the primary goals in furthering hybrid research technology.

An alternative system that provides these desired characteristics is a hydraulic system. Hydraulic components, such as pumps and motors, have a larger power density than competing technologies, such as electrical systems. The leading drawback to hydraulics is the accumulator, which provides energy storage in the system. Accumulators have a lower energy density in comparison to batteries in competing electrical systems [**1**]. The significant difference in energy density between the two domains is one of the main reasons the electric hybrid system is the preferred method of energy storage in a hybrid vehicle. Overcoming the problem of low energy density in hydraulic systems enhances the feasibility of its implementation into hybrid vehicle designs.

Another method of storing energy is through the use of a flywheel. Flywheels are one of the oldest and more commonly used mechanical kinetic energy storage mechanisms. Flywheels have an average energy density that is in the same order of magnitude as electrical systems and is discussed later in the paper. Energy is extracted from a conventional flywheel by reducing its angular velocity. To further manipulate the energy output, the mass moment of inertia can be varied, thus making it a variable inertia flywheel. Consequently, the energy capacity depends on not only the angular velocity, but the changing inertia as well. The types of variable inertia flywheels range from band variable flywheels to those that modify their inertia by adding and subtracting fluid.

An innovative solution to improving the energy density of an accumulator is to utilize a flywheel-accumulator that involves rotating a cylindrical piston-style accumulator. By rotating the accumulator like a flywheel, it can store energy in two forms: the traditional potential energy and the added rotating kinetic component. Potential energy is stored by compressing the gas by adding hydraulic fluid, causing the gas side acts as a spring. When there is a need for the energy, the oil is released. Rotating kinetic energy is stored in the flywheel portion of the system. In the rotating flywheel-accumulator, a parabolic pressure distribution is predicted to develop in the hydraulic fluid due to the centripetal acceleration on the high-density fluid. This results in a decrease in the system pressure at the center, but a higher pressure at the outer walls. This combined system is theorized to increase the energy density of the system by about one order of magnitude.

The flywheel-accumulator is expected to provide higher durability and a longer life compared to electrical systems. A typical battery is a chemical storage device that unfortunately does not support a large number of cycle times prior to replacement. On the other hand, compressed gas storage and flywheels excel because the number of cycles are dependent on the fatigue strength of the material. These systems are frequently designed to withstand 10,000 cycles or more as compared to about 1,000 cycles of a lead acid battery [**2**]. Thus, compressed gas storage mediums and flywheels have a much longer lifespan than their battery storage counterparts.

The integration of hydraulic and mechanical flywheel power that yields a flywheel-accumulator is a potential solution to the current drive train problem. The power density and durability advantages of hydraulic components coupled with the high energy density of flywheels results in an ideal system. This system can be applied to a hybrid hydraulic vehicle and in other hydraulic applications.

The goal of this project is to verify the increase in energy storage density and validate that a parabolic pressure distribution exists in the hydraulic fluid side of the accumulator by:

- Researching and developing system requirements and performance specifications,
- Designing a scaled prototype, and
- Manufacturing, assembling, and testing a bench top prototype.

2. Background

Understanding the dynamics and characteristics of flywheels and hydraulic systems is critical in developing design parameters to create a working prototype. First, the team researched the basic characteristics of hydraulics, as well as the advantages and disadvantages of the system. An investigation on possible techniques to increase the energy density in hydraulic systems was also performed. Next, the team conducted research into flywheels, more specifically variable inertia flywheels in the form of existing technologies and previous patents. These examples provided insight into the various methods that can be utilized to vary the inertia, which reflects the behavior of the flywheel-accumulator.

2.1. Hydraulics

The subject of fluid power is defined by transmitting energy via the use of a fluid under pressure. The reliability, durability, and the power density of hydraulics are a few of the reasons the team is considering it as a replacement for electric hybrid drive trains. The largest disadvantage and the motivation for this project is the low energy density of hydraulics systems, specifically the limitations to the hydraulic accumulator.

Hydraulics utilizes oil or water to transmit energy through a system in a confined space [**3**]. A basic hydraulic circuit involves a pump that is connected to a reservoir that stores the hydraulic fluid for the system. The pump generates fluid flow at an increased pressure, which is conducted through pipes or hoses and can be stored in an accumulator or diverted into other components via the outflow in Figure 1.

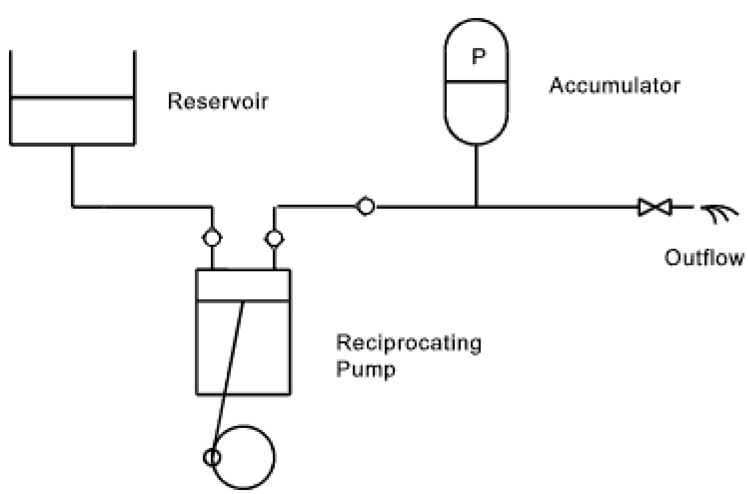

Figure 1: Basic Hydraulic Circuit [4**]**

A hydraulic accumulator is a means of storing energy in a hydraulic system. A common configuration consists of liquid and gas chambers separated by a sliding piston, which can be considered as a “closed” design. The gas chamber is pre-charged to a nominal pressure, after which energy is stored by pumping pressurized oil into the accumulator, thus reducing the volume of the stored gas. Energy is extracted when the gas forces the oil back out the accumulator. Accumulators supplement the hydraulic pump by releasing energy when more power is required than the pump can supply. Consequently, less pump power is needed to achieve the same transient peak performance with an accumulator, and thus operating costs are reduced and enhanced efficiency is attained [**5**]. Also, an accumulator can act as a safety device if the pump fails or if a leak forms in the system by providing power to components for a short period of time [**6**]. If there is a rapid temperature change, the accumulator can provide a place for the fluid to go if there is no expansion tank, which prevents lines from bursting under sudden pressure.

The hydraulic system can maintain a constant pressure because it requires no additional energy to sustain the applied force, as opposed to electrical systems that require a continuous voltage or current to maintain the same amount of force [**7**]. The high power density of hydraulics in comparison to electrical systems reduces the size of components required to maintain the same performance. The large power density of hydraulics varies from 500 to 1000 W/kg compared to electrical systems that range from 30 to 100 W/kg [**8**].

The durability difference between hydraulics and electrical components is another factor that favors the use of a hydraulic system. The primary method of storing energy in electrical systems is the battery. This chemical storage device unfortunately does not support a large number of cycle times. This is an area where compressed gas storage, and other technologies, such as flywheels excel. Since the maximum number of cycles for compressed gas storage and flywheels is dependent on the fatigue strength of the material, these devices are typically designed to withstand 10,000 cycles or more [**2**]. This is many more cycles than a chemical is capable of; therefore, compressed gas storage mediums and flywheels have a much longer lifespan than their battery storage counterparts.

Drawbacks of hydraulics include working with flammable fluids with the possibility of hazardous leaks and the low energy density in comparison to other systems. In general, leaks and flammable fluids are not of a concern, as long as the system is properly installed and maintained.

The limitation of the energy storage in a hydraulic accumulator is a major reason for hydraulics not being used commercially in hybrid cars. The energy density of a composite accumulator is about 6 kJ/kg, which is significantly less than a battery that provides about 432 kJ/kg [**1**]. Improvements to the accumulator's efficiency could make hydraulics a better fit in the application of hybrid vehicles than an electrical system.

A method of increasing the hydraulic energy storage density is by allowing the compression and expansion of the gas in the accumulator to be as isothermal as possible. This is attempted by placing an elastomeric foam in the gas chamber, which absorbs heat energy during gas compression and releases the heat during expansion. The foam aids in maintaining the gas temperature at a relatively constant value, which could increase the energy density by up to 40%. Another way to improve the isothermal nature of the process involves the use of fine metallic strands bonded to the casing, which improves heat exchange with the surroundings [**9**].

An alternative method to storing energy in an accumulator is the "open" approach, in which compressed gas is expelled to and drawn from the atmosphere. This approach is able to obtain considerably more energy from the same compressed gas since it is able to expand all the way down to atmospheric pressure. The system is not required to accommodate the volume of gas or oil, so the energy density has potential to improve up to twenty fold over that of the closed accumulator system [**9**]. Energy is stored and extracted through a pneumatic compressor or motor.

2.2. Flywheels

Flywheels have many benefits, including high energy and power density, long life, and minimal wear over its lifespan [**10**] [**11**]. The energy capacity of a flywheel is primarily dependent upon the mass, speed, and geometry of the rotor [**12**]. One method to further increasing flywheel energy capacity is to utilize a variable inertia flywheel, which changes the energy output by altering the mass of the system. The three most relevant variable inertia flywheel designs that came out of the group's research were the band variable inertia flywheel and two fluidic based flywheel patents.

Band Variable Inertia Flywheel

One of the first existing technologies that the team researched was the band variable inertia flywheel (BVIF) concept. One of the configurations consists of an inner hub and an outer cylindrical casing with a flexible band in between. Since these two components rotate independently, their varying velocities result in winding and unwinding of the band. The change in the amount the flexible band is wrapped around the inner hub represents versus the outer hub dictates the mass moment of inertia of the flywheel [**13**].

Proper function of the BVIF depends on the method of connection of the hub to the casing. The inner hub is connected to the carrier arm of a planetary gear set, the outer casing to the ring gear of the set, and the sun gear is linked to the inertial load. The concept is successful if the band can store enough energy to accelerate the load to a certain speed and then decelerate it for a fixed period of time. Also, it can replace the original drive train in performing this task at the same speed and with the same acceleration. The size of the system is determined by the amount of stored energy that is required to perform this task. When tested, the band initially winds about the inner hub and then unwinds inside the outer casing.

The BVIF concept will not work if enough energy is not stored in the band to accelerate the load to the required speed. If the stored energy does not provide the same speed and same acceleration as the original drive train, it will not be a suitable replacement. It is also heavier as compared to a continuously variable transmission. For the application of this MQP, the BVIF method would not be suitable. Therefore, the following patents introduce two different variable inertia flywheels that use fluid to modify the inertia.

Energy Storage Flywheels Using Fluid Transfer to Vary Moments of Inertia (US 5,086,664)

The patent, titled "Energy Storage Flywheels Using Fluid Transfer to Vary Moments of Inertia," uses a pair of variable inertia flywheels to store energy within a continuously variable transmission (CVT). An older design of these flywheels, for the same application, utilized radial displacement of solid masses to vary moments of inertia. In this new design, fluid may be added to or removed from the flywheel, which is much like the concept for this MQP [**14**]. Relative advantages include ease of control of fluidic flywheel and high ratio of maximum to minimum moments of inertia. The operator has greater control over the system by manipulating the fluid intake and thus changing the inertia. This patent is important to note because it promotes similar benefits to those proposed in this MQP, such as higher energy density by using fluid to create a variable inertia flywheel.

Variable Inertia Flywheel (US 6,883,399)

US patent 6,883,399, which is titled “Variable Inertia Flywheel,” describes a flywheel that has multiple chambers that can be filled with a fluid to change the inertia. The system uses chambers that are spaced radially on the flywheel and can be filled with electrolytic fluid using electromagnetic pumps [**15**]. A portion of the chamber system can be seen below in Figure 2. The patent describes how this flywheel design is more robust than the mostly mechanical design of variable flywheels due to the use of electromagnetic pumps that do not use moving parts. The pumps use the electro-osmotic flow to transfer the fluid, which can change the inertia of the flywheel. Slip rings are used to maintain the electrical connections during operation. The flywheel’s control was designed to react quickly to the requirements of an operating process, which has been a disadvantage to using variable flywheels of the past that took too long to adjust and react.

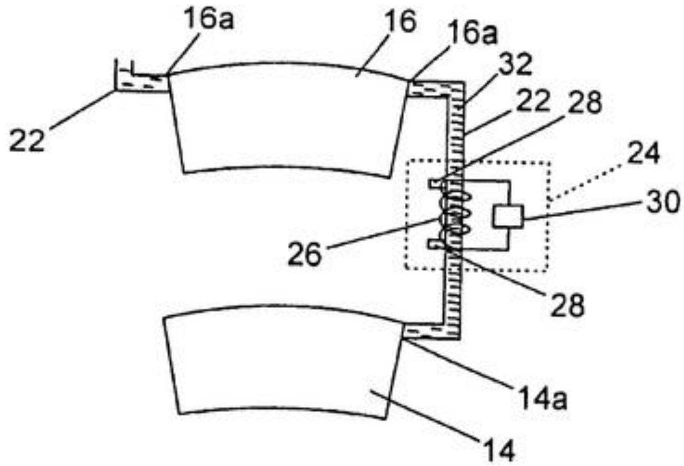

Figure 2: Two of the Chambers used to Vary Inertia [15**]**

This flywheel is similar to the flywheel-accumulator, but unlike the general design because there will be mechanical parts to compress the oil in the accumulator. Also, this design allows the fluid to be transferred to multiple locations and controlled independently, which is not the case in the flywheel-accumulator. This patent provides useful information on multiple ways of changing the inertia of a flywheel, one of which is employing a fluid to change the inertia.

In the end, the group came to the conclusion that there are not any existing designs that directly compare to the flywheel-accumulator created for this MQP. Implementation of hydraulic systems yields many benefits, including high power density, but one major disadvantage is the low energy density of the storage unit. This obstacle must be overcome before widespread usage occurs. To resolve this issue, this MQP team designed and manufactured a prototype of the flywheel-accumulator.

3. Design

This section begins with a goal statement and task specifications that were determined in the early stages of the project. Every design decision was made carefully by evaluating each concept against these two parameters.

3.1. Goal Statement

To design and prototype a fluidic variable inertia flywheel-accumulator that can be applied to a hydraulic hybrid vehicle.

3.2. Task Specifications

- The maximum pressure allowable by the system should be 500 psi.
- The shaft and flywheel will not exceed a maximum of 3000 RPM.
- The diameter of the flywheel-accumulator will be within the range of 3-8 inches.
- The motion of the fluid must be observed visually during operation.
- Material must not yield under applied loads and pressure.
- Hydraulic oil must be able to be pumped into accumulator while rotating.
- Pressure, strain, angular velocity, and piston position must be recorded while the system is rotating.
- A dynamic piston seal must isolate the gas from the oil side of accumulator and vice versa.
- The supports for the system must withstand all loads and maximum torque generated during operation.
- The pressure and hoop stress along the walls of the flywheel must be monitored.
- Data acquisition should be compared to the theoretical.
- Footprint of the system less than 48” x 12” x 12”.
- The system should not exceed a power requirement of 110VAC at 20A.
- The entire system must be enclosed in a safety structure in case any parts fail.

3.3. Conceptual Design of System

Before detailed design could commence, a conceptual design of the system was developed. The preliminary conceptual design can be viewed below in Figure 3.

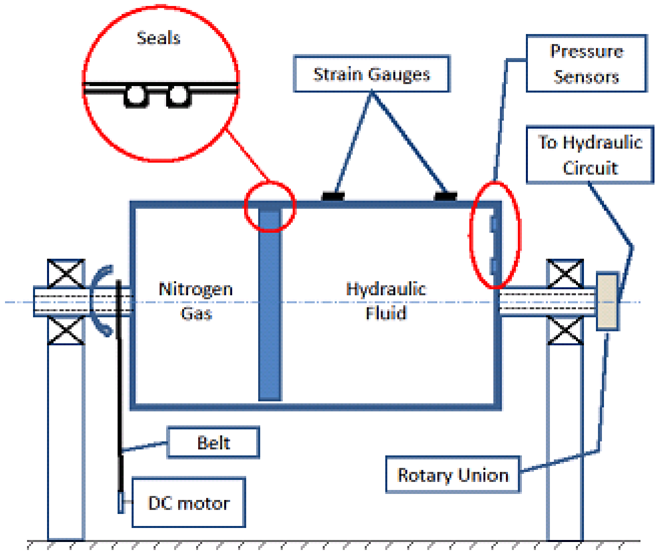

Figure 3: Conceptual Design of Rotating Assembly

The description of all the components in the drawing is as follows:

Since this system is a piston type accumulator, there is a sealed gas on the left side of the cylinder, isolated by a piston with two seals, followed by hydraulic fluid on the right side. The accumulator is mounted horizontally and rotates about a central axis; in this orientation the load is shared equally between two bearings. The system requires fluid to enter and exit while rotating and under pressure, so a rotary union is used to facilitate this fluid movement, which can be seen on the right in the figure above. Also, the entire system must be securely fastened to a surface and have a safety enclosure to ensure safety while the system is running. An aluminum base plate that is 46 inches long and 12 inches wide was available in the lab, along with a Lexan™ and wood enclosure. Thus, the plate and safety enclosure was adapted to fit the system including motor and clutch, so significant cost and time savings were achieved.

In a hybrid hydraulic vehicle, the torque would be applied using a pump, powered either by a combustion engine or through regenerative braking. Since this is a controlled experiment, there needs to be a way to apply torque to the system and control the angular velocity. Therefore, a DC or AC motor is attached to the accumulator.

In a typical piston type accumulator, the pressure distribution on both sides of the piston would both be linear and uniform. Since the system is rotating and the oil has a higher density than the gas, the centripetal acceleration on the oil is expected to result in a parabolic pressure distribution that varies with radius. As the angular velocity increases, the centripetal acceleration increases, thereby increasing the pressure at the edges of the accumulator. A main objective of this project is to verify and characterize this non-linear pressure distribution, which is illustrated in Figure 4. Thus, there are three pressure sensors on the hydraulic side, two on the end cap, and a third at the center in the hydraulic line. Since there will be three data points, an exponential or linear curve fit can be determined. On the gas side, it is believed there is a uniform, linear pressure distribution. To confirm this, there are two pressure sensors on the left side, which will indicate if there is uniform pressure trend or not.

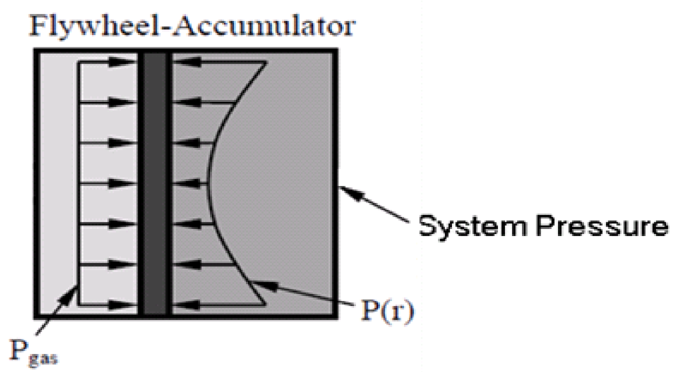

Figure 4: Pressure Distribution

In addition to the four onboard pressure sensors, there are two strain gauges on the outer wall of the pressure chamber; one is mounted in the radial direction, and one is mounted in the axial direction. These two strain gauges serve the purpose of verifying the deflections calculated by hand, as well as the FEA model deflections.

Once this preliminary design concept was established, the individual components, such as the end caps, piston, shafts, and DAQ system were further investigated and final designs were chosen. First, it must be determined if a clear chamber is even achievable for this MQP and if it can be machined to our specifications.

3.4. Hydraulic Circuit

The hydraulic circuit is used to pump fluid in and out of the system. Two designs were considered for the circuit: a double 2-way, 2-position valve setup and a 4-way, 3-position valve. The two valve configuration can be seen in Figure 5. Both circuits contain several components, including a gear pump with a built-in relief valve, tank, valve, pressure transducer, and accumulator. A two valve setup would allow for fluid to enter and exit at the same time; however, this increases the number of components, cost, and complexity of the system. Due to this increased complexity and the fact that a 4-way, 3-position valve was already present in the lab, the double valve configuration was not pursued.

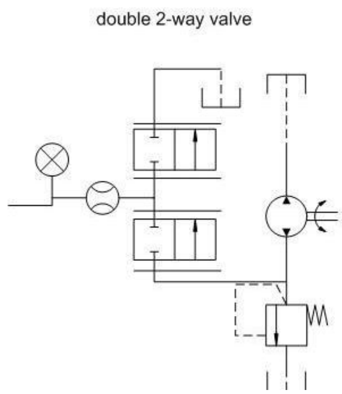

Figure 5: Double 2-way Valve Configuration

The final hydraulic circuit can be seen in Figure 6: Hydraulic Circuit. The accumulator can be seen at the top in its simplified form with an electronic pressure gauge attached. The valve is a 4-position, 3-way valve with one port blocked. The center position of the valve blocks all ports, which results in increased pump pressure since flow cannot move to the tank. While this is fine for testing purposes, it should be noted a valve that allows the pump to flow into the tank at the center position would be advantageous. Again, the valve available to the group in the lab fit the needs of the system and was of no additional cost.

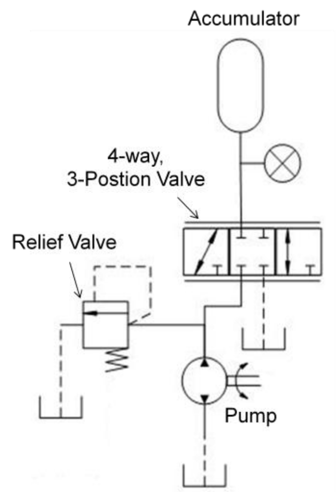

Figure 6: Hydraulic Circuit

Between the valve and accumulator there is a 4-way fitting, along with two quick disconnects, a mechanical pressure transducer, and an electronic pressure transducer, which is identical to the ones onboard the accumulator. Any pressure drop observed by the external sensor should be negligible. The fitting can be seen attached below in Figure 7, along with the two pressure transducers.

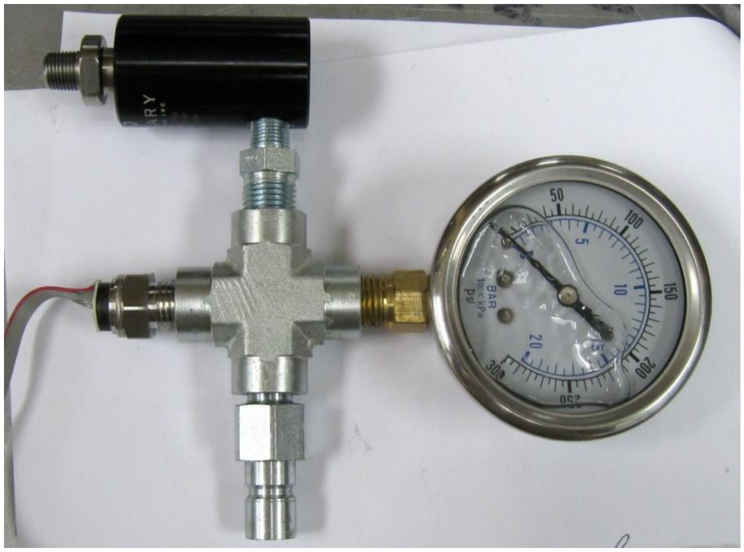

Figure 7: Inline Pressure Sensor

3.5. Accumulator

The first requirement of the accumulator is for it to be transparent in order to facilitate in observing experiments and fluid motion within the chamber. This specification was interesting because most hydraulic accumulators are made from steel or aluminum to accommodate for the high pressures being generated. These materials are not feasible in this project since they are not transparent; therefore, research into high impact polymer tubes that could be spun under the maximum running pressure of 500 psi and not fail was conducted.

The first material that was considered was high impact polycarbonate because it is transparent and has a reasonable yield strength of about 8400 psi [**16**]. The manufacturers were able to provide various tubes sizes with different thicknesses. Given the properties of the polycarbonate, the team calculated the stresses and safety factor of the tube under our maximum operating conditions.

The method for calculating the stresses and safety factor utilized the principal stresses in the tangential, radial, and axial directions due to pressure and the effects of acting as a flywheel due to the angular velocity that the system encounters [**17**]. The analysis involved input values based on the material properties of yield strength, Sy, weight density, γ, Poisson's ratio, υ, and elastic modulus, E. The dimensions and characteristics of the cylinder were also used with the desired safety factor, which the team chose to be three in order to maintain a certain level of assurance. By adding each component of stress together, the Von Mises stress can be calculated and used to determine the safety factor for the chamber via the yield strength. Given the calculated stresses, the expected maximum strain of the cylinder can be evaluated using Young's modulus of elasticity for polycarbonate.

Pressure Induced Stresses:

Axial Stress

$$\sigma_{ap}\,(p_i) = \frac{p_i r_i^2}{r_0^2 - r_i^2} \qquad \text{(Eq. 1)}$$

Tangential Stress

$$\sigma_{tp}\,(p_i) = \frac{r_i^2 p_i}{r_0^2 - r_i^2}\left(1 + \frac{r_0^2}{r^2}\right) \qquad \text{(Eq. 2)}$$

Radial Stress

$$\sigma_{rp}\,(p_i) = \frac{r_i^2 p_i}{r_0^2 - r_i^2}\left(1 - \frac{r_0^2}{r^2}\right) \qquad \text{(Eq. 3)}$$

Flywheel Stresses:

Tangential Stress

$$\sigma_{tf} = \frac{\gamma}{g}\omega^2\left(\frac{3+\upsilon}{8}\right)\left(r_i^2 + r_0^2 + \frac{r_i^2 r_0^2}{r^2} - \frac{1+3\upsilon}{3+\upsilon}r^2\right) \qquad \text{(Eq. 4)}$$

Radial Stress

$$\sigma_{rf} = \frac{\gamma}{g}\omega^2\left(\frac{3+\upsilon}{8}\right)\left(r_i^2 + r_0^2 - \frac{r_i^2 r_0^2}{r^2} - \frac{1+3\upsilon}{3+\upsilon}r^2\right) \qquad \text{(Eq. 5)}$$

The process, parameters, and equations for the chamber stress calculations are provided in Appendix A: Analytical Chamber Stress & Strain. During the data analysis, it was observed that the majority of the stresses were caused by the pressure that is exerted on the system, and a remaining portion was attributed to the flywheel stresses. Additionally, provided the material properties of polycarbonate and the possible cylinder dimensions were determined the chamber was found to not be adequate enough to handle the system pressure. Not to mention, polycarbonate is difficult to machine. After determining that polycarbonate was not an option, one other polymer was considered.

Acrylic was the next option because it had a similar tensile yield strength ranging from 6 to 75.8 MPa (11 ksi) and is easier to machine than polycarbonate [**18**]. The modulus of elasticity for the acrylic is 2.93 MPa, while all other properties of the material can be reviewed in Appendix B: Acrylic Material Properties. Once again, given the material properties and cylinder dimensions, the stresses, the strains, and the safety factor were computed using the method in Appendix A: Analytical Chamber Stress & Strain. Table 1, which is provided below, depicts the targeted chamber size and angular velocity given several pressures with corresponding safety factor, strain, and the change in pressure from the center to the outer edge of the chamber. The change in pressure, Δp, was computed given the system operating parameters of pressure and angular velocity. Equations describing the gas, system, and radial pressure in the system were utilized to calculate a theoretical pressure gradient assuming that the pressure would follow a parabolic distribution. The calculation of the pressure gradient given maximum operating conditions can be reviewed in Appendix C: System Pressure Model.

Table 1: Chamber Design Parameter

Analysis of Pressure Chamber (6" OD x 3/4")									
	Working Pressure (psi)								
Angular Velocity	**500**			**400**			**300**		
ω (rpm)	**Safety Factor**	**ΔP (psi)**	**Radial Strain (in)**	**Safety Factor**	**ΔP (psi)**	**Radial Strain (in)**	**Safety Factor**	**ΔP (psi)**	**Radial Strain (in)**
3000	2.943	20.478	9.937*10^-3	3.647	20.478	8.046*10^-3	4.792	20.478	6.155*10^-3

The chamber selection table aided in noticing the relationship between the angular velocity and the rate at which the pressure gradient increases the complete table is provided in Appendix D: Chamber Selection Tables. The pressure gradient in interest varies according to the rate at which the chamber is spinning and the pressure inside the chamber. The equation for the energy of a flywheel has an angular velocity term that is squared the gradient rate of change increases at a larger rate when the angular velocity is modified due to this term. A reasonable pressure gradient is necessary in order to use pressure sensors that will be able to record the pressure gradient with enough resolution. The gradient that was deemed suitable for the project was computed to be about 141.2 kPa (20.5 psi). Analyzing of the data revealed that the most effective way to increase the pressure gradient, while keeping stresses at a minimum, was to increase the angular velocity of the system and decrease the pressure.

The dimensions of the vessel determine the amount of pressure the chamber can withstand and provide a gradient with sufficient resolution for sensors to register data. Inputting the data into table format allowed the team to narrow down the selection of a feasible design can be seen in Table 1 that would perform all the requirements needed safely. The total Von Mises stresses the chamber would experience at maximum operating conditions would be about 14.14 MPa. A complete table of parameters that was used to determine the proper chamber selection is provided in Appendix D: Chamber Selection Tables. The tables also contributed in setting the operating parameters of the prototype, which are defined in the task specifications. The results of Table 1 confirmed that a transparent chamber with an outside diameter of 152.4 mm (6 inches) and a thickness of 19.05 mm (0.75 inches) could be utilized.

3.6. End Caps

Once the initial chamber design was completed, the next logical step was to determine a way to enclose the ends of the chamber. The end caps are the components that will effectively clamp the chamber on both sides and retain the pressure of the system. Additionally, the end caps need to incorporate the shafts that the accumulator would be supported by during rotation. The end caps would be made of 6061 aluminum in order to withstand the pressure that would be exerted inside the chamber. Making the end caps out of a lightweight material would aid in the manufacturability of a rather large stock material. Two designs were considered; one attaches the end caps directly to the acrylic tube, and the other clamps the end caps together externally.

The original design required physically attaching the end caps into the tube walls. The tube itself would need to be tapped, and the end caps would be fastened using threaded bolts. This concept would function in theory because the end caps would rigidly fasten onto the chamber, but a problem arose in the fact that acrylic threads are fairly weak. Additionally, the pressure the end caps would need to oppose could strip the threads and cause the chamber to fail. In terms of sealing, this chamber design posed a problem in sealing the chamber because of the limited contact area. Not to mention, the acrylic would be difficult to drill and tap because of its brittle nature, and the group did not have the machining capabilities on site. The following CAD model in Figure 8 illustrates the original design.

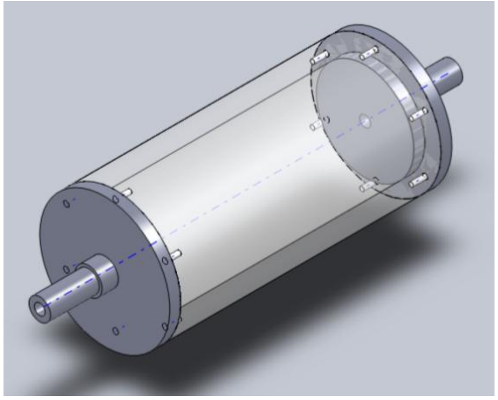

Figure 8: Original End Cap Design

The implemented design clamps the end caps together using threaded rod (see Figure 10). The tie rod design avoids the risk of damaging the chamber and still maintains a proper clamping force on the chamber. A secondary addition to the concept adds a feature that partially fits into and over the acrylic to increase the contact surface, which is provided in Figure 9: End Cap Groove. These features also limit the amount the chamber is able to deflect at the clamping areas in order to facilitate proper sealing.

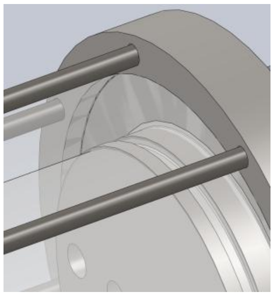

Figure 9: End Cap Groove

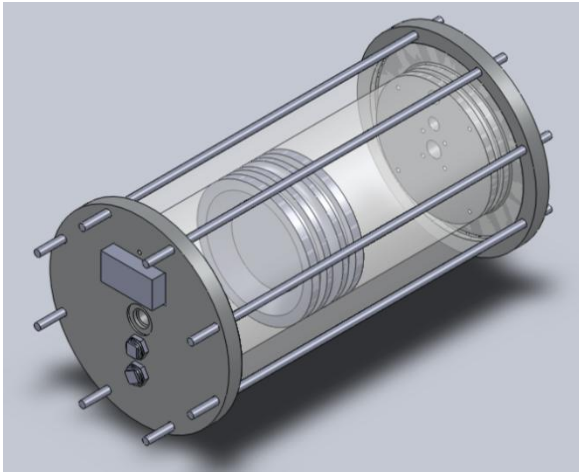

Figure 10: Tie Rod End Cap Design

In addition to clamping to the chamber, the end caps have to accommodate the accumulator shafts, as well as provide a place to mount the pressure sensors to record data. The end caps need to support the shafts while allowing flow through the center into the chamber. A standard method to achieve this is to use a porting tool. In this case, a dash six porting tool that utilizes o-rings to create a seal on the surface of the part and provides a through hole in the end cap. The end caps must also allow for sufficient space to mount two pressure sensors to record the mid and outer pressure range of the accumulator.

In order to reduce vibration and maintain dynamic balance, it is necessary to counterbalance the pressure sensors. The sensors not only needed to be balanced, but required a power source that was determined could help in statically balancing the end caps. Since the mass of the sensors is known to be 24 grams, and the mass of a 9V battery is known to be 45.6 grams, the battery can be placed on the end cap to offset the mass of the sensors and power the sensor simultaneously. If a force balance is performed, on the end caps, the equation becomes $m_1r_1 + m_2r_2 - m_br_b = 0$. Since the mass of the sensors and batteries are known and the pressure sensors should be spaced equally with the one closest to the edge leaving enough material to not fail, the balance distance of the battery can be determined. The balance diagram can be seen in Figure 11. With accounting for the material removed for the sensor holes and battery pocket, the battery cancels the shaking force at 1.7 inches away from the center. Thus, there is a battery on each end cap to counter balance the sensors. Since the batteries and pressure sensors are in relatively the same plane compared to the distance away from the center a static balance was performed and not a dynamic balance.

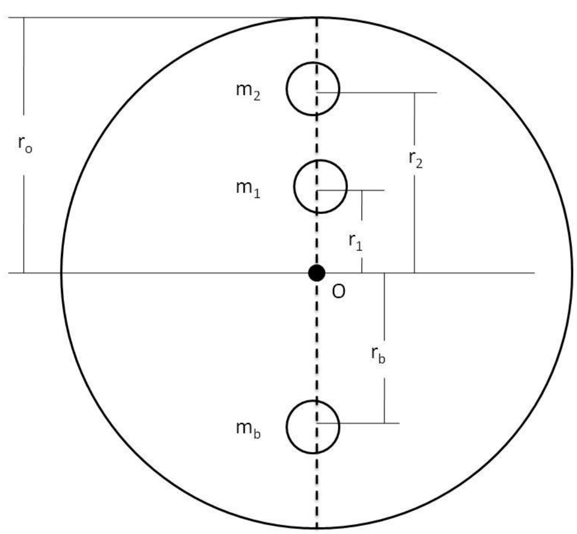

Figure 11: Mass Balance of End Caps

3.7. Analysis of Accumulator with End Caps

Further analysis using finite element analysis (FEA) was required to confirm the results of the hand calculations in Appendix A: Analytical Chamber Stress & Strain. The use of FEA was required due to the complex interactions between the end caps and the chamber; an analytical approach would be more difficult to calculate. The FEA was completed given the design of the end caps that seal the chamber.

The FEA model began with importing a computer-aided design (CAD) model of the flywheel-accumulator into ANSYS 12. Building the model began by defining the material properties of the acrylic chamber and the components that would constrain the chamber and maintain pressure in the system. The problem boundary conditions were defined based on the task specifications and the system configuration. The conditions used for the FEA model involved cylindrical supports that would allow for the system to rotate around the central axis and still be constrained. An addition frictionless support was inserted at the ends of the end caps in order to prevent any horizontal motion. The chamber CAD model used in ANSYS was a simplified version in order to decrease processing time without major effects to the analysis. The holes for the pressure sensors and the porting tool geometry were suppressed. The mesh was generated using the programs default mesh parameters and inputting a medium resolution setting. The maximum pressure of 3.44 MPa (500 psi) was applied on the inner face of the cylinder and a rotational velocity of 3000 rpm was placed on the outer circumference of the chamber.

The model evaluated the solution to the problem and plotted graphs depicting the stress and strains of the chamber, which Figure 12 below demonstrate.

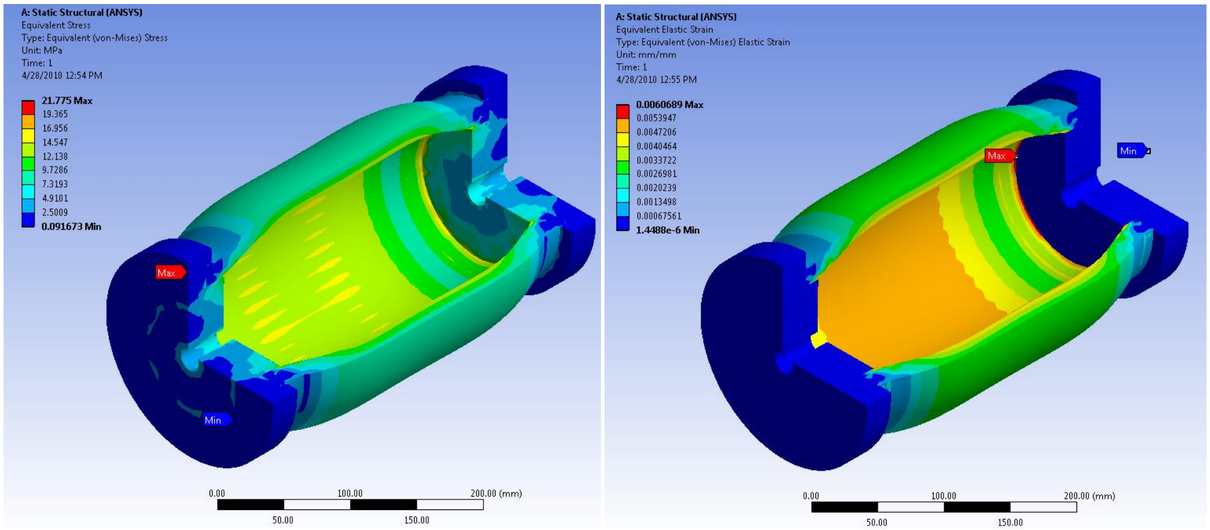

Figure 12: Pressure Chamber Stresses and Strains

The data also more accurately modeled the complex interactions between the clamping components that were not included in the hand calculations. The comparison between the analytical data calculated and the FEA data is provided in Table 2: FEA and Analytical Data Comparison. The table verifies the accuracy of the FEA model because its values closely correlate to the analytical model of estimated the strains and safety factor with an error of about twenty percent. The error can most likely be attributed to the fact that the analytical solution does not incorporate the end cap geometry. The largest discrepancy occurs with how the stresses are concentrated at the interaction areas and due to the complexity of the end cap design. Utilizing the analytical solution the FEA model can be verified because it is within the range of values that were calculated and are slightly more conservative in regards to illustrating that larger stresses exist that would lower the safety factor.

Table 2: FEA and Analytical Data Comparison

FEA Model Verification			
	Maximum Von Mises Stress (MPa)	**Maximum Strain**	**Minimum Safety Factor**
FEA Model	21.773	0.0060689	2.341
Analytical Model	14.143	0.004968	2.943
Percent Error (%)	53.94895001	22.15982287	20.4553177

The safety factor of the accumulator is portrayed below in Figure 13. The FEA model was able to account for the interactions with the sealing surfaces and determine that the chamber would fail before any other component.

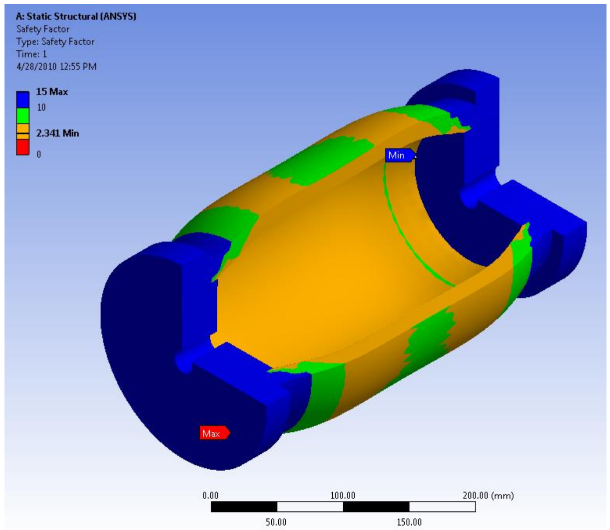

Figure 13: Safety Factor of the Pressure Chamber

The FEA model aided in the selection of seals because the proper sealing method depends on the amount the chamber deflects. Given the evaluated strain measurement of about 6 μ-strain, appropriate seals can be chosen for the piston seal and clamping components, which will be discussed in a later section.

The number of tie rods that would be used on the diameter of the end caps was also determined using FEA to compute the stresses. The model actually uses the original design in which bolts were to be inserted into the chamber. An analysis evaluating the difference in utilizing different hole configurations was useful to determine a setup that balances the number of holes and the reduction of stresses. Three different models were generated with configurations of six, eight, and ten holes.

The analysis used modified end caps that had small inserts in the positions for the tie rods that would be inserted into the acrylic cylinder. Using the same parameters as the previous FEA model except for new boundary conditions in order to constrain the cylinder to only the inserts. By bonding the inserts to the cylinder all the reaction forces will act on the inserts and not on the end caps. The first analysis is portrayed in Figure 14 under the maximum loading condition.

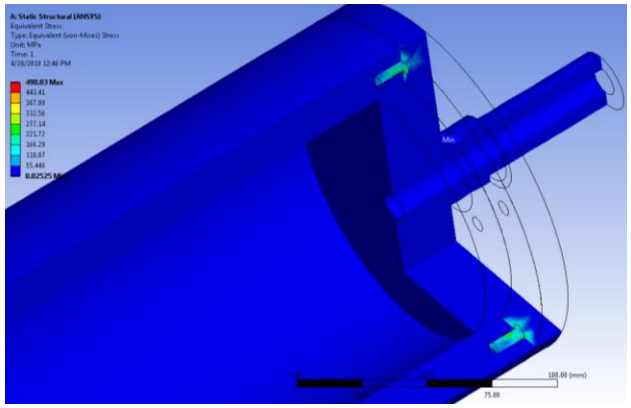

Figure 14: Four Hole Configuration Stresses

The figure displays the maximum stress as 498.83 MPa after evaluating the problem. The force will be dispersed along the inserts, so in a small number of insert configuration larger stresses will be experienced throughout the inserts. As the number of holes increases the area of contact increases and the stresses are divided into each insert lowering the stress that individual inserts exhibit. The figure portrays that the largest stress concentrations occur at the base of the insert.

The next analysis is illustrated in Figure 15 where the number of holes is increased in order to reduce the stresses distributed throughout the insert. The maximum stress in this model is 72.251 MPa, which is significant difference of about 426 MPa from the previous analysis.

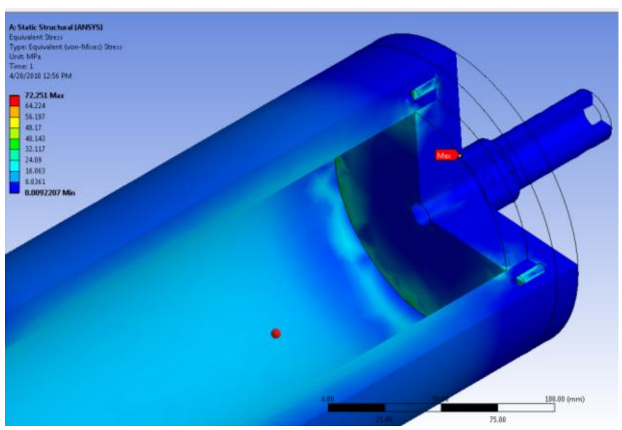

Figure 15: Six Hole Configuration Stresses

The final analysis increases the number of holes again in Figure 16 to further improve the stress distribution. The maximum stress is about 69 MPa, which is only about a 3 MPa difference. Comparing each of the models against each other facilitated in the determination of the appropriate hole configuration.

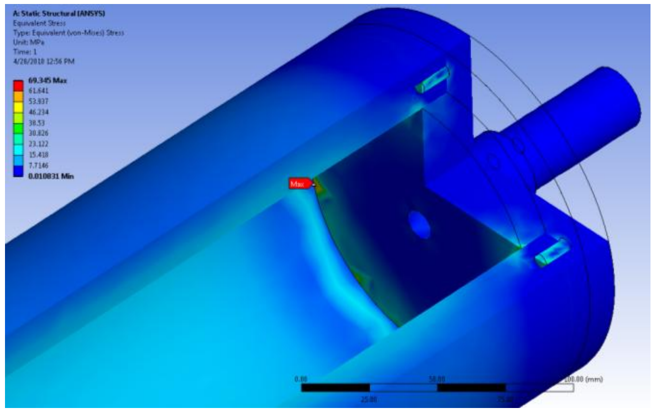

Figure 16: Ten Hole Configuration Stresses

Given the values that were determined using the FEA models the eight hole design yields the best results. It was the pattern that balanced the number of holes and the stress distribution effectively. The analysis done on the original design were the fastening points were closer to the center of the accumulator compared to the tie rod design can still be utilized to generalize the final design. The tie rod diameter size was determined by defining the clamping force that is needed during operation to counteract the force induced by the pressure inside the chamber.

The maximum force generated by the pressure at the end caps is 35.373 kN. The tie rods need to be able to exert a larger force in order to prevent the end caps from becoming detached from the cylinder. With an effective configuration of holes determined the diameter of the rods was needed to be determined.

An investigation into threaded rod began due to the availability, cost, and functionality that threaded rod can provide. The first common size that was explored was 6.35 mm (0.25 in) diameter steel rod, which generates a clamping force of 56.368 kN. The clamping force is obtained by multiplying the number of rods by the preload force [**19**]. The calculation of preload force involves multiplying a certain percentage of the proof strength of a fastener by its tensile area, the entire calculation of the preload force and torque is provided in Appendix E: Bolt Preload Calculation. To preload these bolts to exert the appropriate force the preload torque was calculated using Equation 6 that relates the coefficient of friction, the preload force, and the diameter of the fastener to yield a torque. This value can then be used to clamp the accumulator according to the amount the fasteners are torque.

$$T_i = K_i F_i d \qquad \text{(Eq. 6)}$$

The loads that the rods will encounter vary during operation due to the reacting forces of the pressure and the small deflections of the cylinder. The rods will essentially compress the cylinder and during operation will deflect. These deflections can be related to the loads that the tie rods will experience. Under maximum operating parameters the tie rods will experience a load of about 83.785 N, which was computed using relative stiffness relationship that are provided in a full analysis in Appendix F: Bolt Loading (Norton 2009).

The amount of analysis that the accumulator underwent was to properly size and design it to function properly. Most of the analysis of the accumulator was used to aid in the design of other components.

3.8. Piston

The first part that relied on the FEA analysis previously discussed above was the piston. There were three conceptual designs that the team considered for the piston. The first was the simplest, which essentially is a thin cylindrical part. It was created by extruding a circle and adding a single slot for a seal (see Figure 17). The piston could also be made thicker in order to accommodate two channels for two seals that would improve the chance of success.

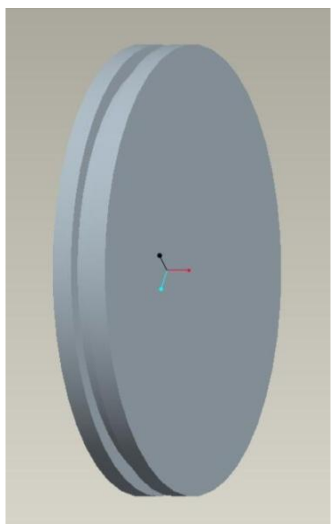

Figure 17: Piston 1 – Isometric View

The second piston design builds off of the first by adding an extruded rod for stabilization (see Figure 18). The rod, which would need to be attached to an end cap, was added because the group worried that the piston might become unstable and possibly become lodged and negatively affect the system. The drawback of this design is that the interface between the rod and end cap would be complex. Since gas or fluid need to be pumped in through the end caps, the piston rod would be challenging to design. Not to mention, an additional seal would be required at the end cap.

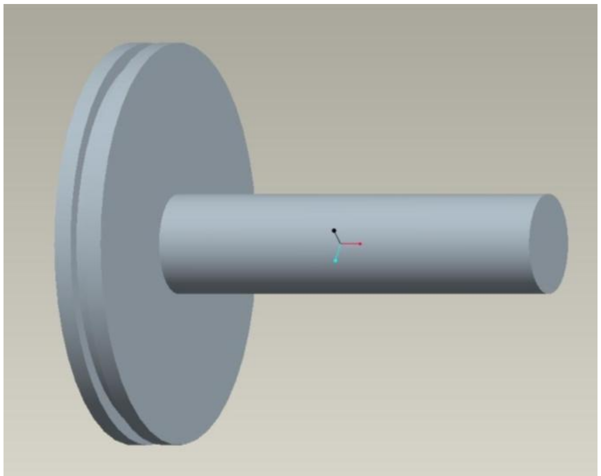

Figure 18: Piston 2 – Isometric View

The final proposed design adds additional stability in relation to the first concept, but is more compact than the second option (see Figure 19). Unlike the last two designs, this piston was created by revolving a sketch of the cross section about the central axis. This design incorporates two notches for two piston seals and a tapered pocket on either side. The pockets allow for greater thickness at the outer edge, but decrease the mass of the piston and do not take away as much volume from the fluid and gas chambers as a solid piston would.

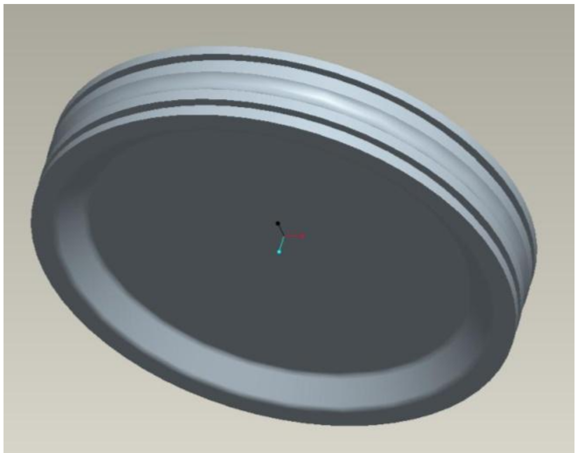

Figure 19: Piston 3 – Isometric View

The third piston design was further refined to its final state (Figure 20). The dimensions were optimized to allow for the largest bearing surface without drastically decreasing the volume of the gas and oil chambers. Additionally, the weight of the piston was minimized since it is a dynamic part.

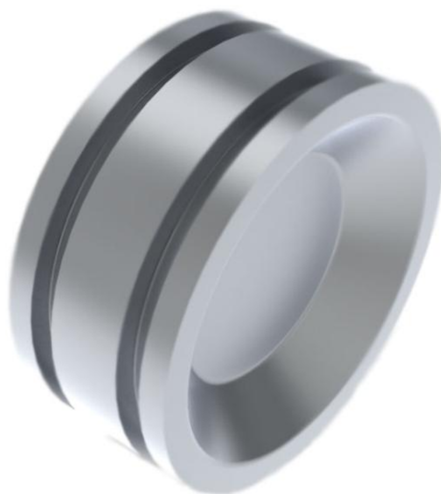

Figure 20: Final Piston Design

The final piston design incorporates two grooves for two seals, and the specific seals that were chosen will be discussed next.

3.9. Sealing the Piston and End Caps

Various types of seals were implemented at different connections and interfaces within the system, but the two most crucial were for the piston and end caps. Both the piston and end caps seals interface with the acrylic cylinder, as well as seal off gas and/or hydraulic fluid. Although these parameters are similar, other requirements differ, so ultimately different seals were specified at the two locations. The end caps needed a static seal, while the piston seal had to be dynamic. Additionally for the piston seal, it had to account for radial strain at mid-length of the tube, but this was not a concern for the end caps. The first type of seal considered for either application was an o-ring.

O-rings are a type of mechanical seal that are frequently used in a variety of engineering applications. An o-ring is simply a closed loop that has a circular cross-section (see Figure 21).

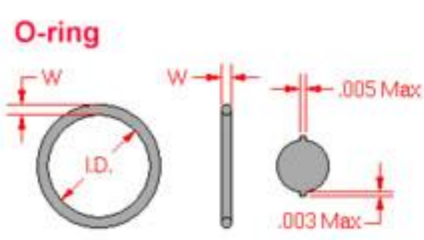

Figure 21: O-Ring Schematic [20]

Many companies sell o-rings in standardized sizes and tolerances, so various diameters are readily available. Once the o-ring is chosen, a groove should be sized based on the dimensions shown in Figure 22. The groove must be accurately dimensioned in order to create the appropriate seal squeeze, which ensures a proper seal between the mating surfaces.

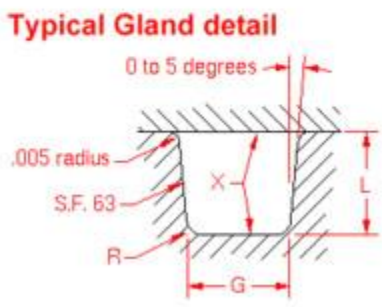

Figure 22: O-Ring Critical Dimension Considerations [**20**]

O-rings can be used in static or dynamic applications. For the end caps, it was determined that o-rings would provide the necessary static seal for this MQP. Therefore, a 4.5 inch (11.43 cm) outer diameter was chosen for the seal with an eighth of an inch thickness (10.795 cm inner diameter). Based on this selection and the company's specifications, the groove dimensions were determined.

In the case of the dynamic piston seal, lubrication would have to be utilized with the o-ring to prevent friction and thus excessive wear. It is not feasible to lubricate the piston seal on a regular basis because it would require excessive maintenance between runs. Not to mention, it would require the fluid to be drained and refilled each time, which adds time to the testing. The standard small amount of leakage (film) would probably provide sufficient lubrication, but the group was not willing to take those chances. Therefore, a more frictionless option was pursued for the piston seal.

The top options considered for the piston seal were the Multiseal® by Precision Associates, Inc, the polyurethane piston seal by Hercules, and the U-seal. Through research, the group was able to narrow down the choices based upon the defined specifications. The piston seal had to seal off both the gas and hydraulic fluid areas of the chamber, be dynamic, and strain with the acrylic cylinder.

The Multiseal® design by Precision Associates Inc. is similar to an o-ring in its application, but has an altered cross section. The company claims many benefits in comparison to standard o-rings, such as better seal and lubrication, resistance of spiral failure, and low friction [**21**]. To ensure no contamination between the gas and liquid side, two of these seals would need to be used in tandem.

Figure 23: Cross-section of Multiseal® by Precision Associates [21**]**

The polyurethane piston seal was next researched for the piston seal (see Figure 24). Polyurethane allows for better wear resistance and lower friction compared to o-rings [**22**]. Additionally, only one would be necessary if used in conjunction with two outer bearings.

Figure 24: Cross-section of Polyurethane Piston Seal [**22**]

Ultimately, the best fit for this application was determined to be a U-seal, which is a lip type seal (see Figure 25). A U-seal was chosen for its greater tolerance in comparison to the other seals considered. Additional measures were taken to further improve the seal against the changing radius. The two U-seals were installed in an opposing manor, which means that the open ends face away from the center of the piston. Any gas or pressure that would push against the seal would actually increase the seal force because it pushes the lip of the seal against the surfaces being sealed. Also, the grove diameter was increased by 0.010 inches to ensure proper seal squeeze even when the acrylic is radially strained.

Figure 25: Cross Section View of U-Seal [23]

The company the team ordered the piston U-seal from was Hercules. The specific product is HRU25-4.00-25 with a 4.5 inch outer diameter and 4 inch inner diameter. The groove width was determined to be 0.281 inches plus or minus 0.010 inches, and the groove diameter is 4.010 +0/-0.003 inches.

3.10. Shafts

After the seals were specified, the shafts were designed to allow the transport of fluid in and out on one side and gas on the other and to support the weight of the complete accumulator assembly. The diameter of the shafts is limited to a maximum of 0.969 inches or 24.6 mm since this is the diameter of the spot face on the end caps into which the shaft fits. A dimensional constraint on the shafts is the length of the shoulder between the spot face on the end cap and the bearing. This distance has to be at least 1 inch to allow enough clearance between the pressure sensors that extrude from the end cap and the bearing, as shown in Figure 23.

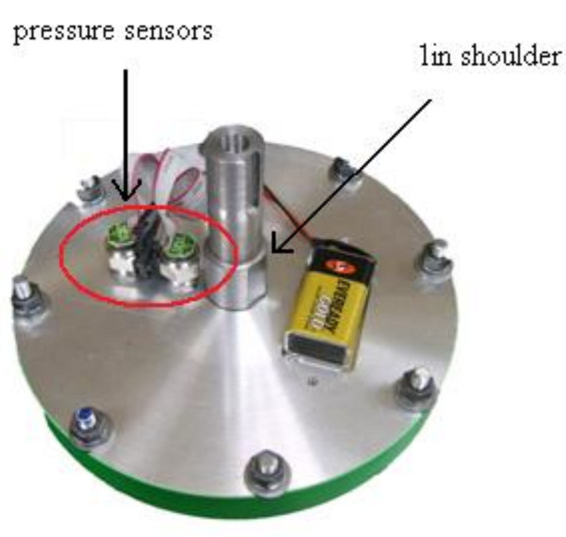

Figure 26: Shaft Attached to End Cap

In order to calculate the maximum shaking forces, a concentricity offset from the central axis of 1/8 inches or 3.175 mm was estimated for the accumulator system. The weight of each component in the accumulator assembly had to be measured, and are shown in Table 2 below:

Table 3: Weights of Components in Accumulator Assembly

Component	End Cap (x2)	Piston	Chamber	Rods + Batteries	Total
Weight (lb/kg)	3.5 / 1.6	2 / 0.9	6 / 2.7	2 / 0.9	17 / 7.7

Converted to kilograms, the mass of the empty accumulator system is 7.711 kg. The volume of the maximum amount of fluid that can be accommodated in the chamber is found when the piston is all the way towards the gas valve side. This is considered the extreme loading case for the bearings from which a maximum possible fluid weight is calculated given the density of Mobil DTE15 oil. Thus, the total mass of the accumulator system is 9.773 kg.

Given a rotational speed of 3000 rpm and an offset from the central axis of 3.175 mm, the maximum acceleration of the accumulator system is found. This results in a force of 3062 N in total. Since the force is distributed among two bearings, each one is required to withstand a maximum force of 1531 N. The calculations are shown in Appendix G: Shaft Calculations.

The low carbon steel 1018 was chosen as the material for the shafts as the stock was already available for use. This steel has yield strength of 303MPa and an ultimate tensile strength of 414MPa. It is also inexpensive and easily available.

The various factors considered when iterating to find a minimum required diameter for the shaft are listed in the calculations in Appendix G: Shaft Calculations. The effective ultimate tensile strength of the steel is then equated to the maximum stress experienced at the step in the shaft, after accounting for a safety factor of 1.7 and the stress concentration factor due to difference in diameters at the step.

The resulting recommended minimum diameter of the section supporting the bearing is 0.8 inches or 20.32 mm. Since bearings of 20 mm diameter are easily available, 20 mm is chosen for the outside diameter of the bearing end of the shaft. A k5 press fit is chosen for the shaft in the bearing, for which the tolerances in the shaft diameter can be obtained from the fit and tolerance chart in

Appendix H: Tolerance Charts.

The final shaft designs are shown in Figure 27 and Figure 28.

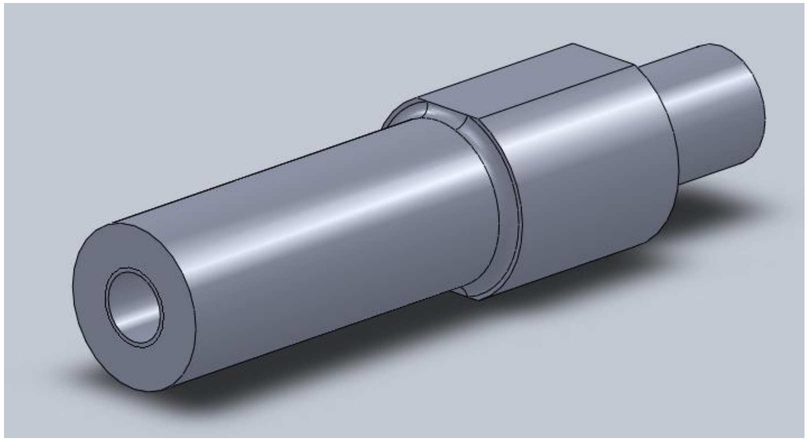

Figure 27: Fluid Side Shaft

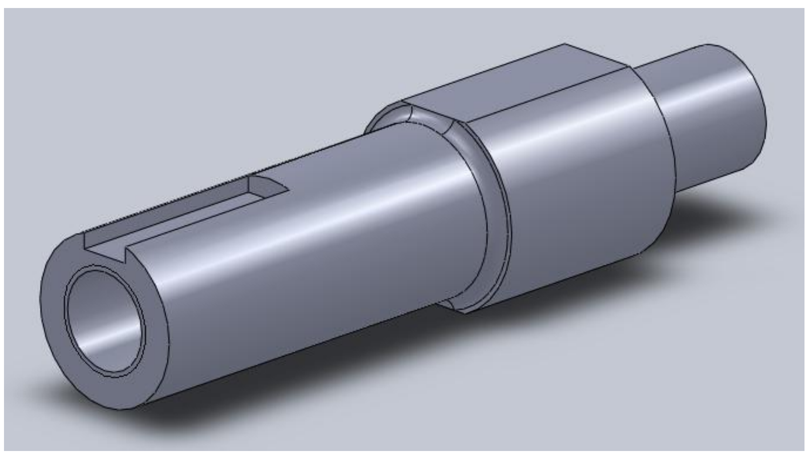

Figure 28: Gas Side Shaft

3.11. Bearings

Once the shafts were dimensioned, the bearings were specified based on the following requirements. Two bearings are required to support the accumulator assembly, one on each side. Since there is no force applied in the axial direction of the accumulator, the bearing is not required to support any axial loads. Only radial forces need to be dealt with here. The inner diameter of the bearing has to support a shaft of 20 mm diameter. The bearings should also be able to support the shaking forces in the accumulator assembly when it is being run at its maximum speed of 3000 rpm.

A few different types of bearings meet the requirements, but the cheapest one that performs the desired function is the deep groove ball bearing from Simply Bearings [**24**] and is shown in Figure 29. It has an inner diameter of 20mm, an outer diameter of 47 mm, and width of 14 mm.

Figure 29: Metal Shielded Deep Groove Ball Bearing [24**]**

The bearing is capable of supporting a maximum dynamic load of 13.5kN and a static load of 6.55kN. It has metal shields inserted into the outer raceway for protection against light mechanical damage, and the shields prevent the pre-filled grease from being contaminated. It does not require any additional lubrication.

Bearing mounts were designed as shown in Figure 30. The through hole in the bearing mount allows an H8 press fit for the bearing, and the machining tolerance can be obtained according to the fit and tolerance chart in

Appendix H: Tolerance Charts.

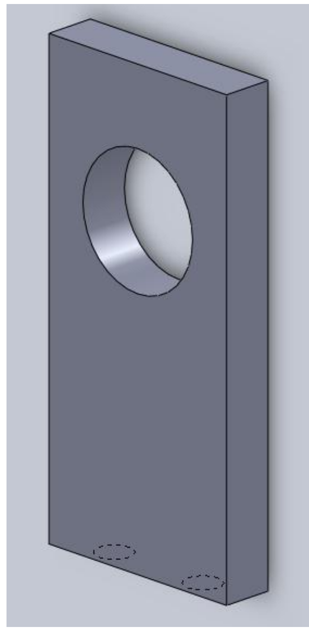

Figure 30: Bearing Mount CAD Model

3.12. Rotary Union

Tackling the problem of pumping fluid into a body that is spinning at a high speed was one that needed to be addressed at the beginning of the project in order to pursue further design in the system. The entire accumulator is required to rotate and needs to have an attachment or fitting that would allow flow into the system in order to vary and record the pressure data as the fluid volume varies. The attachment would need to meet the task specification of being able to spin at 3000 rpm and withstand a maximum pressure of 500 psi. The component would also need to have a relatively low amount of friction compared to the friction in the bearings holding the accumulator. Commercial solutions were pursued in the selection of the rotating hydraulic fitting.

Utilizing a live swivel was recommended by the advisor who had previous experience with the fitting. The live swivel is a fitting that allows full 360 degrees of rotation while allowing fluid to flow through the body of the swivel. Figure 31, provided below, is a picture of a live swivel.

Figure 31: Live Swivel [25**]**

The live swivel, however, had a significant amount of friction while rotating. The friction prompted communication with the supplier to determine whether a high performance swivel is available to fit our application, but the live swivel is not intended to rotate at high speeds in a hydraulic system. The supplier did recommended looking into rotary unions that would most likely fit our needs.

Rotary unions are very similar to live swivels because they can rotate 360 degrees continuously and provide fluid flow though its body to a system. Unlike the live swivel, the rotary union is designed to rotate at high speeds ranging from hundreds to thousands of rpm. The rotary union has a unique bearing seal that allows it to rotate like a bearing meanwhile pumping fluid whether it is air or oil. Given the system parameters, the 008 series single passage union met all the requirements. It can spin up to 4000 rpm and withstand a maximum hydraulic pressure of 1000 psi and is a small compact unit that is provided below in Figure 32.

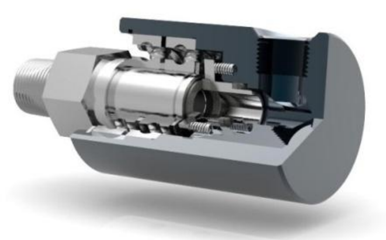

Figure 32: Rotary Union [26**]**

3.13. Valves

Along with the hydraulic pump, additional components are required to regulate the pressure and flow of liquid in the system. In this situation, a component is desired that regulates the rate of liquid flow in a particular direction, and this flow rate will be continuously monitored by an input command. The ideal component for this purpose is either a proportional or servo valve, which are types of electro-hydraulic valves. Other factors that dictate the specification of the valve are the fluid used, supply pressure, force requirements, dynamic response required, and load resonant frequency.

Hydraulic valves are designed to be sensitive to changes in supply pressure as opposed to direct-driven valves, which are unaffected by changes in pressure. The fluid type is an important factor when considering changes in performance due to effectiveness of the seal and changing viscosities over varying temperatures. The force requirements include accounting for static and dynamic loading on the system, and inertia forces must be considered when sizing valves in high speed applications.

Servo valves are those that use closed-loop control. They monitor and feed back the main-stage spool position to a pilot stage or driver either mechanically or electronically. Thus, they have an in-built error correction capability. Proportional valves, on the other hand, move the main-stage spool in direct proportion to a command signal, but they usually do not have any means of automatic error correction (feedback) within the valve. The spool displacement is proportional to the current driving solenoids.

Another option is a continuously variable proportional valve in which a varying control current results in a controlled output variable, which could be flow, pressure, or position of the spool.

If manual operation of the valve is desired, a proportional valve connected to the output of a pulse width modulation circuit can be used. Since proportional valves are expensive, pulsing a solenoid valve on and off using a manual control such that it behaves like a proportional is a feasible solution that performs the same function.

A potentiometer connected to a pulse width modulation (PWM) circuit allows analogous control of the valve. The solenoid valve chosen is a 24V, 4-way, 3-position on-off solenoid valve. The 4-way valve has an extra port that is not required; however, this port can be blocked, making it a 3-way valve.

Since the valve only has on and off states, it is pulsed at a frequency of 4.35Hz. Using the formula for frequency of the output wave given by $f = 1/(2.3*R6*C3)$, the capacitor value C3 and resistance R6 were chosen as 1μF and 100kΩ respectively, so that the input wave frequency is 4.35Hz. This is low enough to accurately affect the state of the valve.

The pulse width modulation circuit requires an input DC voltage of 12V, and using two operational amplifiers from the LM324 quad operational amplifier package, produces a triangle waveform. The frequency of this wave is determined by the formula below the schematic in Appendix I: PWM Circuit. Finally, a square wave is generated at node 13 using a third operational amplifier as shown. The positive input terminal of the valve is connected to a 24V rail, and the negative terminal to the square wave output by the PWM circuit.

By varying the duty cycle of the square wave received by the valve, the fraction of the time period for which the valve is open and closed can be varied, thus controlling the rate of fluid flow into the cylinder. The duty cycle is varied using a 100kΩ key 'A' potentiometer as shown in the schematic.

3.14. Motor and Torque Arm

In the lab, there was a 280W DC scooter motor available for use, the only problem being the maximum speed was 2300 RPM, This would require gearing the motor up in order to reach 3000 RPM. Neglecting friction if the motor were to be geared up to spin at 3,000 RPM the accumulator could be spun up in approximately 5 seconds, which indicated the motor was fine for use. However, now gears are required, as well as a DC power source which adds to the complexity of the design. Since the system required some sort of clutch as well, a ¾ HP AC motor, 22amp variac, and electromagnetic clutch were purchased for $180 altogether. While these parts are slightly used, it saved both time and money. By removing the motor mount built into the motor, the motor could be suspended on bearings, allowing it to rotate and allow the group to measure the torque applied by the motor.

The simplest method to measure the motor torque was to attach a torque arm to the motor and a load cell to the arm. A load cell measures force, so by using the relation that torque, τ, equals force, F, times distance, d, torque can be found (see the following equation, Eq. 7).

$$\tau = F * d \qquad \text{(Eq. 7)}$$

In order to make this possible, a new motor mount system had to be designed. The motor has to be able to freely rotate instead of being rigidly held in place. The design the team came up with is pictured below in Figure 33.

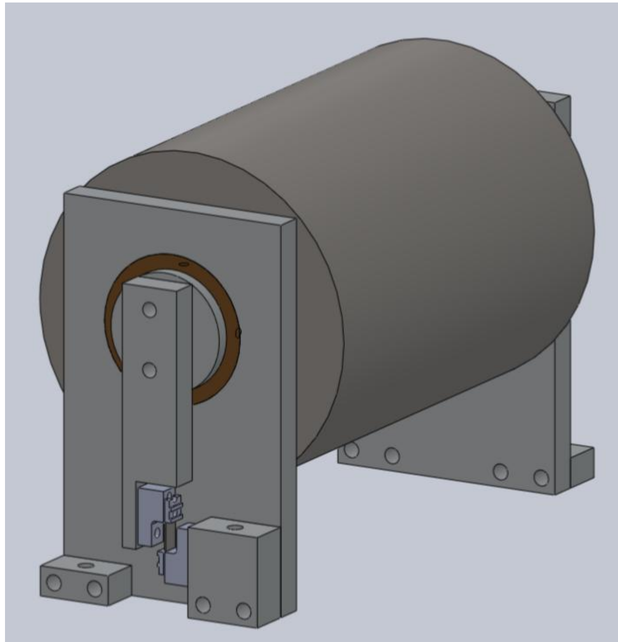

Figure 33: View of Load Cell Assembly

Two vertical plates serve as the basis of the design because all components connect to it. An oil-impregnated brass bushing is press fit into each plate (see Figure 34). Attached to the motor itself is a custom ring that interfaces with the bushing. The bushing and ring have a free running clearance.

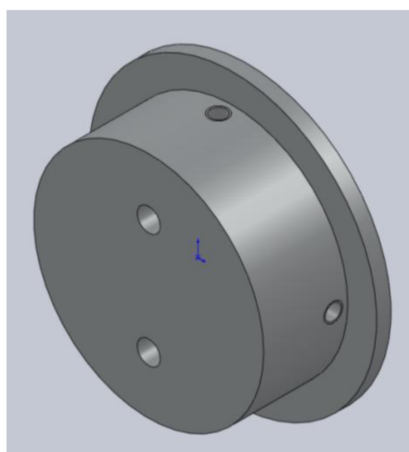

Figure 34: Isometric View of Custom Ring for Torque Arm

The custom ring was designed so that the torque arm could be attached with two screws, which are equally spaced from the axis of rotation.

The torque arm, shown in Figure 35, is simply a rectangular block with a notch cut out for the load cell to sit in. Ideally, the load cell itself should be in line with the center of axis of the motor; therefore, the load cell was aligned as close as possible with the screw holes without making the width of the torque arm greater than one inch.

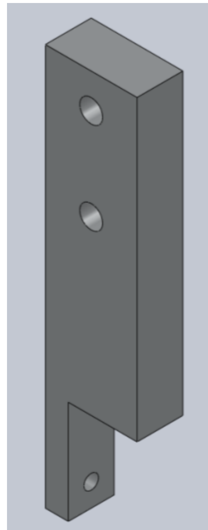

Figure 35: Isometric View of Torque Arm

The load cell is then attached from the torque arm to the ground block with the purchased kit, which can be seen assembled as shown in Figure 36 below.

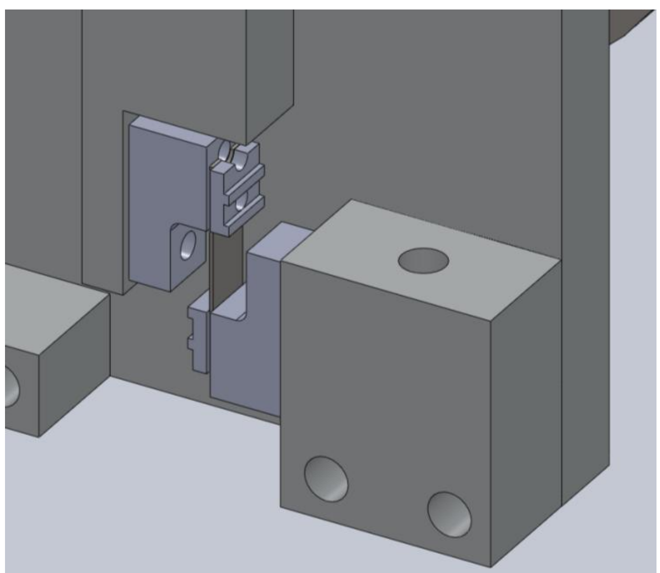

Figure 36: Zoomed-in Photo of Load Cell Assembly

The load cell chosen for this application was a full-bridge thin-beam load cell from Omega [**27**]. Each model is rated at a maximum force, ranging from 0.25 pounds to 40 pounds. To choose the right model for this MQP, the team calculated the maximum force the motor would produce at the given horsepower (see Appendix J: Load Cell Force Calculations for calculations). The force was approximately 4.216 lbf; thus, the five pound load cell would be the best choice.

3.15. Clutch

The clutch design was fairly simple and for the most part provided to the team. Once the system parameters were determined, a clutch that could withstand 3000 rpm was all that was required. Through a colleague of our professor the team was able to procure an electromagnetic clutch at a reasonable price. The design aspect of the clutch was how to mount and couple it to the other components in the system.

The clutch had an existing hole patterns that could be utilized to mount parallel plates. Measurements were taken to fit the plates on the clutch and to elevate the clutch to 4.5 inches from the base plate in order to allow all other components to be able to rotate freely without contacting the base plate.

The plates then needed a method to attach to the base plate and in the use of modularity mounting blocks were designed to mount two blocks on each plate. These blocks would then be able to be used on the motor mounts that will be discussed later as well. In Figure 37 below the model of the clutch is depicted.

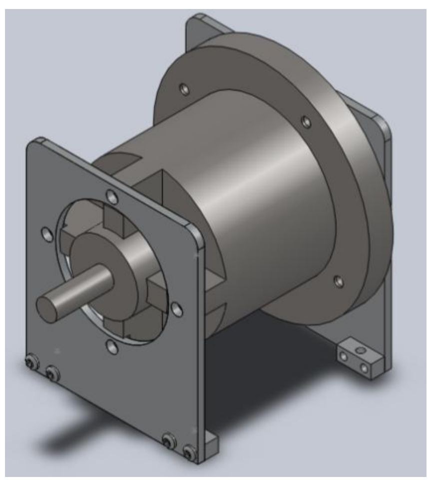

Figure 37: Clutch Mount Assembly

Another aspect of the clutch design arose when the clutch had only one input shaft when the project would require an input and output shaft. The clutch had an input shaft and a female coupler and by evaluating both sides, the female coupler had the least friction. The goal of reducing friction in order to obtain accurate test data in experiments, lead the team to utilize the female connector side to couple with the accumulator. This motivated the design of a coupler shaft that would fit into the female connector and simply couple the clutch and the accumulator. The coupler shaft is provided below in Figure 38. The keyway is cut to match the keyway on the input side of the clutch, and the flat is to ensure the set screw of the Lovejoy adapter has a firm surface to rest on.

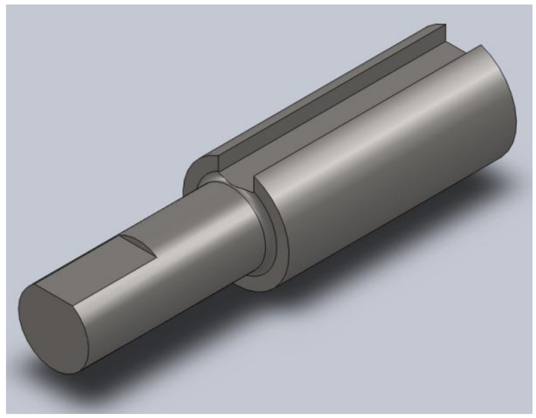

Figure 38: Coupler Shaft

The LoveJoy couplings were chosen to connect shaft due to the wide range of metric and U.S. bore sizes available and the flexibility to compensate for misalignments. The couplings are two steel hubs that are connected to a rubber spider that can deform to provide the flexibility in order to compensate for errors in alignment or mounting. Two sets of these couplings were required in order to connect the motor to the clutch and connect the clutch to the accumulator.

Figure 39: LoveJoy Coupling

Now that all the mechanical components of the system have been designed or chosen, a final CAD assembly was created in SolidWorks 2009, which can be seen in Figure 40. The CAD model was used to verify all the parts fit together and would fit on the plate. Detailed drawings of each component can be reviewed in Appendix K: Part Drawings.

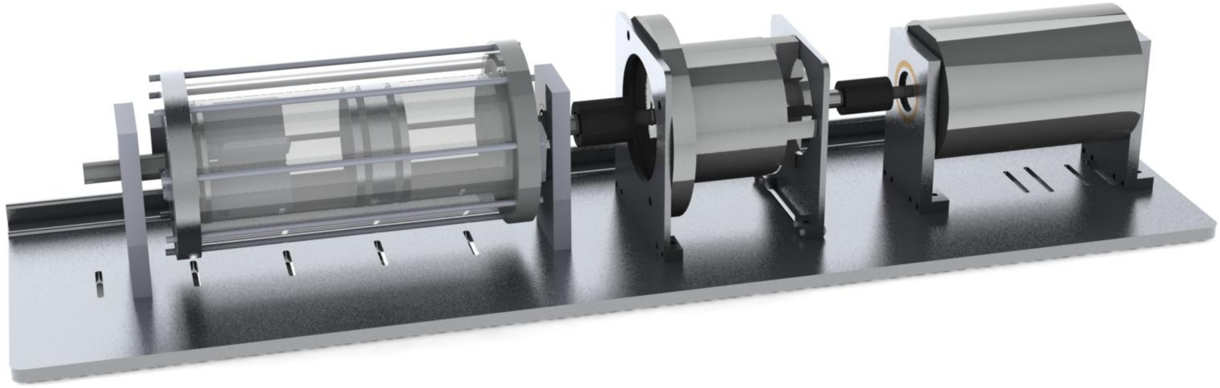

Figure 40: Final CAD Assembly

3.16. DAQ Selection

One of the critical aspects of the system is the DAQ selection; several data measurements are required for experimental purposes as well as verifying the unique properties of this accumulator. The four onboard pressure sensors, two on each end cap and two strain gauges presented the biggest challenge in terms of complexity since they are rotating with the flywheel. There were multiple methods to transmit data off the unit including electro-mechanical and wireless connections. Each of the previously stated means of transferring data along with the remaining forms of data were all weighted against was cost, performance, power consumption, reliability, size, installation and setup. A summary of the components, their placement, and a brief description of their function can be seen in Table 4.

Table 4: Sensor Function

Sensor	Placement	Function
Strain gauges	Acrylic chamber	Measure strain, verify FEA
Gas side pressure sensors	Gas end cap	Measure pressure
Oil side pressure sensors	Oil side end cap	Measure pressure
Inline pressure sensor	In hydraulic line	Provide third data point to verify pressure distribution
Load cell	Mounted to motor	Measure torque applied by the motor
Rotary encoder	Mounted to lovejoy coupling	Measure angular velocity
Web cam	Placed in front of unit	Measure the piston location to find the volume of the fluid

A visual of the overall DAQ system can be seen in Figure 41. The six onboard sensors are connected to the analog to digital (ADC) converter, which is received by another XBee acting as a receiver, connected via USB to a computer running LabVIEW. Mounted to the motor is a torque arm with the load attached to the end. The excitation voltage to the pressure sensor and load cell is recorded as well. The ratio of the output voltage to the supply is taken, to make the measurements insensitive to voltage supply variations. Thirdly there is a rotary encoder, made from an acrylic disc, which passes through an optical interrupter to generate a pulse train. These previous three items are connected to a NI USB-6008 USB DAQ card. Lastly there is a webcam, connected to a computer running LabVIEW which processes the images to find the length of the hydraulic volume.

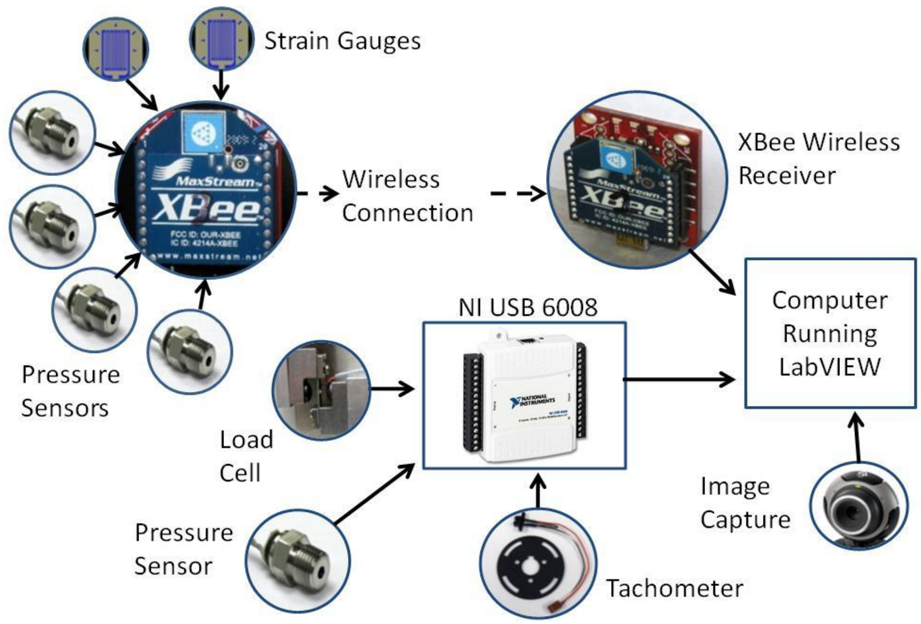

Figure 41: DAQ Flowchart

3.16.1. Acquiring Data from a Rotating Body

One of the most difficult aspects of the data acquisition system was finding a reliable method for acquiring data off of the spinning accumulator. The two modes that were researched were slip rings and wireless. Within wireless, there were additional applicable options of microcontrollers and wireless modules. Once a method was chosen, means to powering the unit was investigated.

Slip Rings

A slip ring is simply a series of wire rings with a wiper making contact, allowing an electrical connection even though the physical connection is rotating. One of the best examples of a slip ring in everyday use is in a car steering wheel; they allow electrical signals to pass through while rotating. Precision slip rings are available with 0.1Ω noise per revolution; however these proved to be too expensive to use. If a slip ring were used, then there would be no need to mount a power source to the end cap, and having to balance the mass accordingly. The slip ring which appeared to suit the needs of the project, an over shaft design with 8 circuits cost roughly $3,000 from Michigan Scientific. To save cost a used slip ring which was an end of shaft design and only had 6 circuits could be had for $300 (the normal cost is $600). Thus a slip ring within the budget would not suit the needs of the system. Slip rings can be purchased cheaply (around

$30) if the speed they are rotating at is below 500RPM, once this speed is passed the only devices that fit the needs of the project are precision instruments, and this precision makes them expensive. Since this electro-mechanical connection would not suit the needs of the project at the right price, wireless alternatives were investigated.

Wireless Sensors

While wireless sensors do exist, they are quite expensive, not only is the sensor costly, but the receiver is a cost as well. Since the wireless transmitter is included in each sensor, the packaging of the device tends to be much larger than their wired counterparts. The wired sensors tend to be bulky, and the wireless sensors are about twice this size. One wireless pressure sensor from Electrochem is about 2 inches long [**28**], whereas the current pressure sensors are about 0.5 inches long. These pressure sensors transmit over the standard WiFi spectrum used in wireless laptops, and are also compatible with the ZigBee standard. While these sensors would be useful in remote applications, the size of the devices is much too large for an object rotating at 3,000 RPM.

Microcontrollers

Another possible method for the data acquisition system is attaching a microcontroller to one of the end caps of the tube to perform on-board analog to digital conversion of the voltage signals received from the pressure sensors and strain gauges. This digital data will be sent to either a slip ring mounted at one end of the shaft, which will then transmit it to a computer, or the data can be sent from the microcontroller to a wireless data transmitter mounted on the cap of the tube. In the case of the wireless method, the data will be received by a receiver off board and then transmitted to the computer.

The requirements of the microcontroller being considered are that it should be extremely small and lightweight, and it should be easy to mount to the cap of the acrylic tube. Problems could surface relating to the functioning of the clock of the microcontroller at 3,000 rpm, and also relating to transmitting wireless data accurately at such a high angular velocity.

Two microcontrollers were considered: the Baby Orangutan B-48 and an Arduino microcontroller. The Baby Orangutan B-48 is a conveniently small microcontroller, measuring just 1.2in x 0.7in, or 3.05cm x 1.78cm. It does not have an LCD screen or any switches and so its light weight will not pose a problem when it comes to static balancing of the accumulator. It has 18 user I/O lines and an operating voltage range of 5-13.5V [**29**].

Figure 42: The Baby Orangutan B-48 Microcontroller [29**]**

An Arduino microcontroller was the second option considered. The Arduino mini, based on the ATmega168, ,the smallest Arduino offered, has 14 Digital I/O pins and 8 analog inputs. In order to make the Arduino wireless, an XBee shield will need to be used. The XBee module consists of a transmitter and receiver. The receiver would be connected to the computer and act as a serial port. The Arduino operates at a maximum of 9V, so a voltage reduction would be needed since the sensors are likely to be greater than 10V input. The pro mini Arduino is about the same size as the mini, but does not have any headers attached allowing for a lower profile mounting.

Table 3 below compares the specifications of the Pololu Baby Orangutan B-48 and the Arduino Mini for the purpose of selection.

Table 5: Comparison of Microcontrollers

	Pololu Baby Orangutan B-48	**Arduino Mini**
Operating Voltage	5-13.5V	5V
Input Voltage	5-15V	7-9V
Digital I/O Pins	16	14
Analog Input Pins	8	8
DC Current per I/O Pin	40mA	40mA
Flash Memory	4KB	16KB
Clock Speed	20MHz	16MHz

Dimensions	3.05cm x 1.78cm	3.3cm x 1.78cm
Weight	1.5g	< 2g
Price	$37	$44

Wireless Modules

The primary candidate for the wireless transmitter and receiver was the XBee Series 1 Chip Antenna. The antenna allows a maximum range of 122m, which is more than what is required for the application. It also comes with 6, 10-bit ADC input pins and 8 digital I/O pins, and a built-in antenna which allows for compact installation onto the tube cap. It is priced at $23 per module. Figure 34 shows a picture of the chip antenna wireless module from XBee.

Figure 43: XBee Wireless Antenna[30]

Since these modules have 6 analog to digital (ADC) conversion pins and are compact and light, they are a better choice over the microcontrollers. They also do not require programming unlike the microcontrollers, which need to be setup to perform ADC conversions and transmit data. The wireless system can be expanded on by adding more modules, or by using a microcontroller to perform more ADC conversions and they have low power consumption. Therefore, these XBee units were selected as intermediaries between the sensors and the off-board computer.

Powering Unit

An obstacle was determining a method of powering the wireless system without introducing unnecessary mass that would be difficult to package. It appears a battery would be the simplest way to power the system; however every additional object attached to the flywheel must be counterbalanced. Some common battery dimensions and characteristics are presented in Table 6. The power draw of all the sensors and microcontroller will have to be added in order to determine the lifespan of the battery. For all the 3V batteries, it would take at least four batteries to have 10V or more of supply to power everything. For a rough calculation an Arduino draws about 40mA, and XBee wireless module about 40-50mA, the pressure sensors about 10mA (40mA total) and about 30mA for a strain gauge (assuming 10V supply and 350Ω strain gauge). This means there will be about a 40 + 50 + 40+ 30 = 160mA consumption. This means most of the small watch batteries would be depleted in less than an hour, so a larger battery would be more appropriate. A battery such as a 9V would supply ample voltage, although a 3.3V regulator for the XBee is required as well as another regulator for any other circuitry to account for the voltage of the battery decreasing.

Table 6: Battery Specs

Battery name	Dimensions	Voltage (V)	Capacity (mA)	Cost $ea (jameco)
Cr2032	0.787 in (thin)	3	180	1.25
DL2032	0.787 in (thin)	3	180	1.49
CR2325	0.906 in (thin)	3	165	1.79
CR123A	D0.67 X H1.36 in	3	1300	2.75
DL2450	0.97 in (thin)	3	500	2.25
AA rechargeable	D0.57 X H2 in	1.2	2500	2.95 (sparkfun)
A76	D11.6 X H5.4 (mm)	1.5	~150ma	1.95
9V	H48.5X L26.5X W17.5	9	45.6	~3

The choices to extract data from the rotating system were narrowed down to the XBee unit, with or without micro controller, or a slip ring. Since the slip ring which was affordable would not quite suit the needs of the project, it was decided on using an XBee unit. Since there were six ADC ports being used, the XBee is ideal since the device can convert the sensor outputs to a digital readout and transmit them wirelessly to a base station. Also in the future a microcontroller or additional XBee could be added to the system, making it modular. Also with not using a slip ring, any frictional losses caused by the slip ring are eliminated. Since the pressure sensors can be balanced by a 9V battery, the XBee, sensors, and circuitry can be powered off voltage regulators attached to the battery. The circuitry and XBee units weigh so little (only a few ounces) the weight can almost be ignored for balancing as well. Now that there is an apparatus to transmit data from the rotating body, the sensors on the device can be selected.

3.16.2 Sensors on Wireless Module

Data from a total of six sensors need to be transmitted via the wireless module: two strain gauges and four pressure transducers. The specific strain gauges and pressure sensors chosen for this application are further discussed in this section.

Strain Gauges

A strain gauge is typically a strip of wire arranged in a zigzag pattern [**31**] that changes resistance depending on how much the wire is deformed. Strain gauges can be arranged with a single strain gauge, two, or four in a system. Typically the strain gauge or gauges are arranged in a Wheatstone bridge, which acts as a voltage divider. When two or more strain gauges are used, the accuracy is increased since the strain is being measured from both sides of the material and increases the voltage differential. This voltage difference has to be amplified since it is typically less than 1V. The amplification can be performed with 3 op-amps or an instrumentation amplifier which tends to have a higher accuracy than multiple op-amps, partially due to the fact the internal resistance is uniform across the op-amps. An instrumentation amplifier also requires less circuitry. There are many varieties of strain gauges, the main difference being the resistance of the gauge itself. Most gauges' resistances are above 350Ω. Also, the gauge factor or the sensitivity to strain is an important factor to consider and is expressed by:

$$GF = \frac{\Delta R/R}{\Delta L/L} = \frac{\Delta R/R}{\varepsilon} \qquad \text{(Eq. 8)}$$

where ΔR = change in strain of the gauge, R= resistance of undeformed gauge, and ε = strain, most gauges have a GF of around 2[**32**]. Thus, by knowing the voltage applied to the bridge, the output voltage of the bridge, and the gauge factor, we can find the strain [**33**]. Some aspects of the circuitry, such as the Wheatstone bridge and amplification, can be simulated in LabVIEW without the need for physical components. This simplifies the complexity by the ability to wire the strain gauge directly into the data acquisition equipment.

A device is needed that measures the strain in the walls of the acrylic tube, which does not affect the strain measurements itself. The expected maximum tangential and radial strains are 5.607×10^{-3} and 5.146×10^{-4}. The most commonly used strain gauge is the bonded metallic gauge [**34**]. In this application, a strain gauge that measures bending strain is required. Therefore, the best type of strain gauge for this application is one that rejects axial strain and compensates for temperature. It should be most sensitive to bending strain. The sensitivity of strain measurement of the gauges being considered is about 2.0 mV/V @ 1000 μE.

Pressure Sensors

It is highly desirable to verify the pressure profile of the fluid, to determine if the system is functioning properly and compare to computational results. This can be accomplished with pressure transducers. The most likely type of sensor to be used is a gauge pressure sensor where pressure is measured relative to atmospheric pressure at a given location. An absolute pressure sensor would be acceptable as well but not necessary since this type measures pressure from absolute zero pressure. The sensor should be able to measure pressure accurately and function up to the operational pressure of the device. Diaphragm transducers that are very small would be advantageous, and threaded ones are even better since they would be easy to install and remove.

Multiple factors are to be considered when choosing an appropriate pressure sensor to monitor the pressure on the inner walls of the acrylic cylinder. The specific guidelines to be considered when choosing the pressure sensor for this application can be seen in Table 7. The pressure sensor should be mounted in such a way that the centripetal acceleration does not alter the measurements of the sensor. Since the minimum and maximum pressure in the chamber is 0 psi and 500 psi, respectively, a gauge pressure sensor would be suitable, since the system is not running at less than atmospheric pressure. The most critical considerations were the sensors should be small, lightweight, and accurate.

Table 7: Pressure Sensor Guidelines

Sensor	Expected Values
Type of sensor:	Gauge or Absolute
Sensor Pressure Range	0-500 Psi (500 Psi max expected)
Supply Voltage	0-10v
Mount Type	Threaded or Flush Mount
Operating Temperature	0-50C
Size	As small as possible

When finally choosing the pressure sensors, Omega makes small lightweight pressure sensors, but they are cost prohibitive since the system requires four on the accumulator. Unfortunately the cost for each of the lightweight pressure sensors is $400 each. The 85 series from Measurement Specialties are reasonably priced, accurate and repeatable, and compact. This series of pressure sensors is available in either a weld fit, which require the sensor to be pressed in with a back plate to hold it in, or with a pipe thread. ¼ NPT pipe thread sensors were purchased since the mounting holes could be easily drilled and tapped to this pipe thread size. The supplier also offers sensors with a 1/8 NPT pipe thread, however the lowest range is 0 to 1000 psi, which is twice the range the system demands. The specifications of the pressure sensors can be seen in Table 8.

Table 8: Pressure Sensor Specifications

Specification	Value	Units
Model Number	85-500A-4C	n/a
Cost (ea)	76.85	$
Range	0-500	Psia
Media Compatibility	Liquids and gases compatible with 316L stainless steel	n/a
Output	0-100	mV
Supply Current	1.5	mA
Weight	24	grams
Pressure non –linearity	±0.1	%Span
Pressure Hysteresis	±0.02	%Span
Temperature Error - Span	±0.75	%Span
Temperature Error - Offset	±0.5	%Span
Thermal Hysteresis – Span	±0.05	%Span
Thermal Hysteresis – Offset	±0.05	%Span
Long Term Stability – Span	±0.1	%Span
Long Term Stability – Offset	±0.1	%Span
Pressure Overload	1500	Psia

At a cost of $76.85 [**35**] these sensors were reasonably priced for their size and performance. These pressure sensors meet or exceed all of the requirements of the system. The sensor can be seen below in Figure 44. The gauge style pressure sensors were originally ordered but were on two month backorder; thus, the absolute pressure version of the sensors were ordered since they were the same price and same performance. The only downfall being the max measurable pressure of the system is now 485.3 psig. These pressure sensors require a 1.5mA power supply, which can be supplied with an op-amp circuit powered by the battery. The circuit inside the pressure sensor is a full wave Wheatstone bridge, which outputs 0-100 mV ratiometric. The output is amplified to 3.3 V with a gain of 33, via an instrumentation amplifier. The voltage of 3.3V is chosen since this is the maximum voltage the XBee units can handle for ADC conversion. The sensors are also compatible with the oil used in the system. On the gas side of the end caps, there will be two pressure sensors to see if there is any pressure non-linearity, and three pressure sensors will be used on the oil side, two on the end cap and one after the rotary union to verify the parabolic pressure distribution of the oil side.

Figure 44: MSP Pressure Sensor [36]

3.16.3. Other Measurable Data

In addition to the measurements being transmitted wirelessly, additional data is collected to find angular velocity and piston position.

Angular Velocity

In order to determine the total energy density of the system, the kinetic energy stored as rotational motion, must be calculated. Since this is similar to a flywheel the energy density of a flywheel is $E_{flyweel} = \frac{1}{2} I\omega^2$, where $E_{flywheel}$ is the energy stored in the flywheel, I is the inertia, and ω is the angular velocity. Once the energy stored is known, the total energy density can be verified, as well as how much rotating the system improved the energy density. In order to find the angular velocity of the system, either a rotary encoder or tachometer must be used.

The DAQ card supplied to the group is a NI-USB 6008, which has an onboard falling edge counter. Since this card does not have a hardware based counter, an extremely accurate measurement of the pulse count train cannot be generated. The card can only record how many pulses happened, but not at which frequency they happen. In order to overcome this pitfall, either an analog voltage could be output to the USB DAQ card, or a software timed frequency counter could be built.

Normally a rotary encoder would be purchased; the different types were discussed above in the flow meter section. These pulses would be recorded by a hardware timed counter card, which would generate a pulse train. This gives the angular position in steps, in order to find velocity and acceleration, these results must be differentiated with respect to time twice, once to find velocity, and twice to find acceleration. Since this system only requires an angular velocity, one option investigated was a frequency to voltage chip.

The LM2917 is a 14 pin DIP package, which converts a frequency to a voltage by using a charge pump to charge up a capacitor. By choosing an appropriate charging resistor and capacitor combination, the output ratio of volts per revolution can be controlled. In this circuit, a sensor such as an optical interrupter or Hall Effect sensor would output a pulse when an object passes by them. The increasing trend of these pulses would increase the output voltage of the chip. This analog output voltage would be connected to the analog in on the DAQ card. An optical interrupter is to be interfaced with this integrated circuit (IC), rather than a hall effect sensor since the optical interrupter outputs a clean 5V signal, and the optical interrupter was supplied free of charge to the group. A magnet on each of the tie rods was considered with a Hall Effect sensor counting the pulses; however, the magnets would need to be firmly attached, and a filtering circuit may be required. Unfortunately, the LM2917 chip has poor documentation with regards to interfacing with an optical interrupter, thus making it difficult to build a circuit. Also in this setup, a digital signal is converted to analog, then back to digital again, increasing the error. Thus, due to the difficulty of implementing this circuit, it was forsaken for the implementation of another device.

Since the optical interrupter can output a clean 0-5V signal, the counter on the DAQ card was used. Using the NI developer zone, a LabVIEW program was discovered, which reads in the number of pulses over a set period of time, then divides it by that time, results in a frequency. By multiplying this frequency by 60 and dividing by the number of pulses per revolution, the RPMs of the system can be determined. The longer the sampling time, the more accurate the measurement will be, the shorter the sample time the better the response time will be. A disk with four slots in it was laser cut to generate the pulses for the tachometer LabVIEW virtual instrument (VI). Four pulses per revolution is a maximum frequency of 200 Hz, which according to the Nyquist criterion the data must be sampled at twice the frequency or 400 Hz in this case. Since the maximum frequency of the counter is 5MHz, the system should be able to acquire data fast enough.

The disk was manufactured to fit over the shaft and keyway, as well as mount to the love joy coupling drilling and tapping holes into the coupling. The disc was sized to fit within the 3 inch wide bearing mount, thus giving the outer diameter. Next the by measuring the depth of the slot in the optical interrupter, the minimum width of the slot could be determined. Coupled with the outer diameter this yielded a maximum outer radius. The disc was manufactured with an outer wall on the slot to add some strength as well as prevent the disc from destroying the sensor in case the two collided. The slots were made an equal distance apart, creating a equidistant pulses at a constant angular velocity. Since the disk was thin, and had no bosses or extrusion, the fastest and easiest way to manufacture it was with a laser cutter. A piece of 3/32 inch thick acrylic was used for stock since it is inexpensive, easily cut with the laser cutter, and a readily available size that would pass freely through the sensor. The gap on the sensor was 0.122 inches, which 1/8 inch thick acrylic would not pass through without modification. The clear acrylic was lightly sanded then spray painted flat black to prevent any light from passing through. The assembly where the disc would be attached was modeled in CAD, the image of which can be seen on the left side of Figure 45. The finished laser cut disk with optical interrupter can be seen in Figure 45.

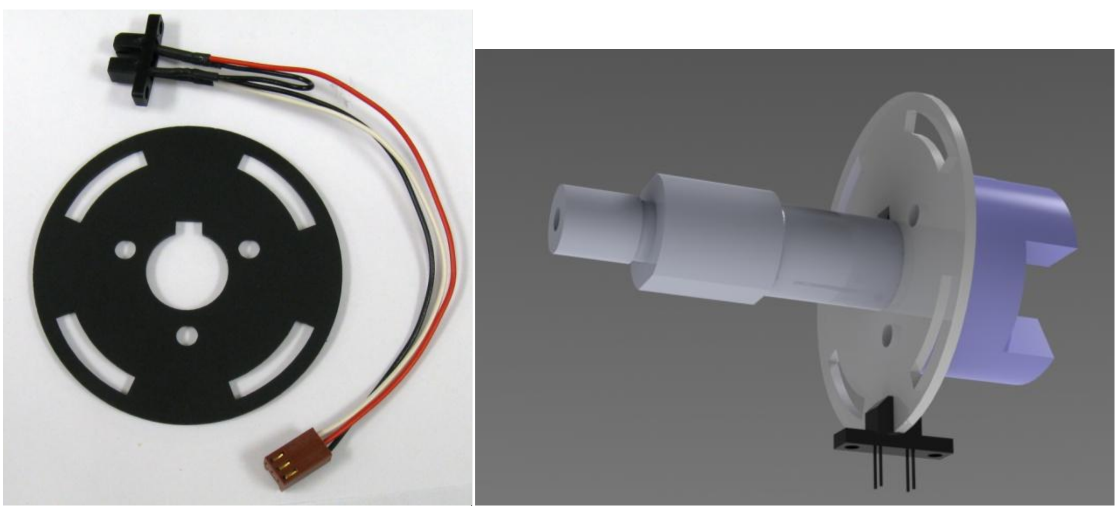

Figure 45: Rotary Encoder Manufactured and CAD Model

Piston Position

In this system, the group desired to measure the volume of fluid in the system, there were two main ideas considered in order to determine this. One method is to measure the flow rate in and out of the system. Second, the piston position can be measured in order to determine the volume. For the flow rate, a flow meter was considered, both off the shelf and a cheaper option created from a pump modified to act as a flow meter. For the piston location, a LVDT (linear variable displacement transformer), magnetic linear potentiometer, and image acquisition system were considered.

If the flow rate into and out of the system is known, then the volume of the oil can be determined by adding up all the fluid entering the system and subtracting the fluid leaving the system with respect to time. Since the cost of buying a positive displacement flow meter off the shelf is at least $1000, it was decided that a hydraulic motor with a shaft encoder attached to it will be used to calculate the flow rates, which will reduce the cost.

A 12V hydraulic motor with the encoder attached is installed in such a way that it obstructs all the fluid passing it. When the motor is forced to rotate due to fluid flow, the encoder will translate the rotational motion (from angular position) of the shaft into electrical signals in the form of either analog or digital code. There are two main types of rotary encoders: absolute and incremental. Thus by counting the revolutions of the motor shaft, flow rate can be calculated. Using the flow rate and inner diameter of the chamber, the volume of fluid entering can be calculated over a period of time. This can then be used to actively calculate the position of the piston.

The problem with this method is that an accurate flow meter is expensive, but on the other hand a cheaply constructed one could be very inaccurate. The concept of a flow meter is shown in Figure 46.

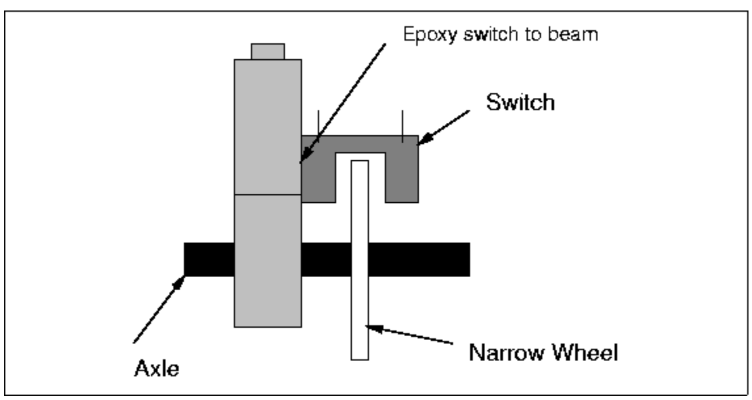

Figure 46: Rotary Shaft Encoder

Since flow meters are expensive, and adapting a pump to function as a flow meter would not result in accurate and repeatable measurements, the other avenue of determining volume was pursued, by measuring piston position. The three methods to accurately measure this position were using an LVDT, magnetic linear potentiometer, or image capture system.

An LVDT, or linear variable differential transformer, is an accurate way to measure position. An LVDT is three coils wrapped around a center bore in which a ferrous core passes through. An AC excitation voltage is applied to the center core, and the AC output from the two secondary coils to the left and right of the center primary core is measured. By subtracting the two outputs, a linear voltage is recorded which indicates position [**37**]. Since the sliding core does not make electrical contact with the three cores, it is virtually frictionless, and sealable. This results in a long and repeatable lifespan. Unfortunately, the downfalls of this system are a high cost (roughly $400 [**38**]) and packaging issues as it must fit into the shaft, but leave enough room for nitrogen gas to fill the chamber, and it requires a connection to the cylinder. As shown below in Figure 47, attempting to fit the LVDT into the shaft while trying to minimize the shaft diameter would present a challenge.

Figure 47: LVDT [38**]**

Since there would be major obstacles in packaging and cost of the LVDT, a magnetic linear potentiometer was investigated. The theory behind the magnetic linear potentiometer was to attach individual magnets or magnetic strips to the piston. These magnets would cause a change in resistance in the potentiometer, and by applying a voltage or current with knowing ohms law, V=IR, where V is voltage, I is current, and R is resistance, the output would be proportional to the change in the resistance. These devices are simply a potentiometer strip laid out in a straight line with a wiper embedded below the surface. Since the device is inexpensive ($22.95 [**39**]), the magneto pot by Spectra Symbol was purchased to be experimented with, the device can be seen below in Figure 48. Using strong rare earth magnets it was determined the device had a high amount of friction as the magnet pulls the wiper across the resistive strip. The magnets could barely slide the wiper from one inch away through air, let alone 0.75 inches of acrylic. It was determined this device would not be reliable enough for the system, thus a vision system was investigated.

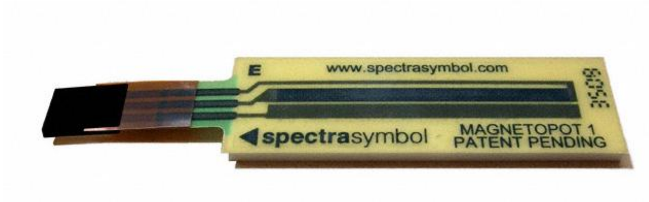

Figure 48: Magneto pot [39**]**

The method by which the piston position will be measured is a vision detection system utilizing a NI Vision Assistant through the use of a commonly available webcam. Using the Vision Assistant, the camera can be placed in any location and register data as long as a calibration step is performed before data is generated. The program allows for sequences of frames to be analyzed. The biggest difference between webcams and other cameras is the image quality and the effects that lighting have on the picture.

The first camera used in the project had an image resolution of only 320x240 pixels with a sampling rate of 10 frames per second (fps). The camera was not able to display colors very well and required careful lighting schemes in order to differentiate components like the end caps and piston in the image. The webcam that is currently used in the project is a Logitech S 7500 that has a maximum picture resolution of 640x480 pixels and a sampling rate of 15 fps. This camera handled the glare and effects of lighting better than the first camera and has a color boost option. Differentiating between components was fairly easier, but would require further processing.

The program utilizes a perspective grid calibration step that converts pixels into real measurements. A grid with dots at a known distance of 25.4 mm (1 in) needs to be placed near the object in question, and a parallel axis must be defined to complete the calibration. Given the known distances from the dots, the programs singles the dots out and calibrates the image. Once the calibration step is complete, the images are processed by first applying a color threshold, which converts the image into a bitmap. Different low pass and edge detection filters can be used to further enhance the differences in the image. Then an edge detector is applied to the bitmap to draw a rectangle. The length of this rectangle is then averaged from the end cap to the piston and displayed by the program. Using these methods, the camera is able to reference a known distance and track the displacement of the piston.

The accuracy of the optical measurement system is dependent on the quality of the picture, the filters, and the operations that Vision Assistant employs. Through testing, the system has an error ranging from 5% to 2% with respect to other measurements.

The image acquisition system was decided on since it was inexpensive, as LabVIEW was already installed on the computer, and off the shelf webcam is inexpensive (around $30-$50). The flow meter for an accurate off the shelf one was too costly, the fabricated version may not be accurate enough, an LVDT is costly and had packaging issues, and the magnetic linear potentiometer had frictional issues.

4. Testing Methodology

In order to compute the energy density of the accumulator, the mass and energy stored in the system must be known. The mass is measured beforehand, thus the energy stored as a gas and as a flywheel must be computed and added together. Energy stored in the gas will be measured as follows:

The pressure sensors will also provide part of the equation to solve for the energy stored as a gas. By treating the gas as isothermal, then only the change in volume and the initial pressure are required to compute the energy stored as a gas. Since the cylinder and piston geometry are known, by measuring the length of the hydraulic volume, the total volume of the fluid may be found. Armed with the pressure and volume, the energy stored in the gas can be computed.

For the second component of the energy stored in the flywheel, the angular velocity must be known. For this measurement an optical interrupter will be used. In addition, the angular velocity can be compared to the pressure sensor data to correlate angular velocity with pressure distribution. Thirdly, the angular velocity will be used to determine the frictional loses in the system which will be achieved by spinning the system up to a preset velocity, then observing the decrease in speed with respect to time. The friction can then be computed from the resulting data. Also by knowing the torque applied to the system, the losses can be computed by comparing it with the angular velocity. The torque in the system will be measured using a load cell attached to a torque arm.

With the ability to measure energy density, through various sensors, there are two additional strain gauges on board, mounted in the axial and radial direction in order to verify the FEA and hand calculations. The calibration and set up procedure for all these tests is as follows:

XBee Modules

The XBee 802.15.4 modules are used to transmit pressure sensor data, as well as strain measurements, from the rotating system to the computer off-board. One module is mounted to the fluid side end cap, and the other module is connected to a computer via a USB port.

The modules require 3.3V for their operation. A voltage reference also needs to be provided, which indicates to the device the maximum voltage value that it should be able to transmit. The reference voltage was set to 3.3V to allow a higher resolution for maximum accuracy when reading pressure and strain data. Finally, the ground pin is hooked up on the transmitter.

Each module has two rows of 12 pins each. Since the spacing between the pins is too small to mount the module on a standard printed circuit board, breakout boards were purchased that are designed especially for the XBee modules. Wires are then soldered onto the board to provide access to the corresponding pin. An example of the XBee being used to read values from a sensor is shown in the schematic in Figure 49.

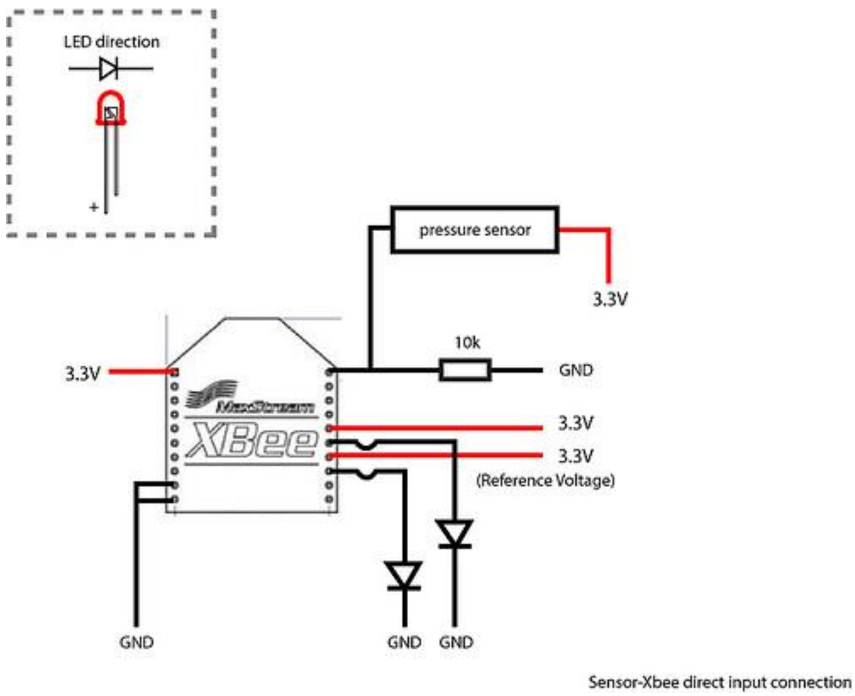

Figure 49: XBee Sensor Schematic

Since the modules had to gather analog voltage data from 4 pressure sensors and 2 strain gauges, all 6 of the analog to digital converters available on the device were used. ADC0 and ADC1 are connected to the pressure sensors on the fluid side, and ADC4 and ADC5 are connected to the pressure sensors on the gas side of the accumulator. ADC2 and ADC3 are wired to the two strain gauges that measure axial and radial strain. The modules are protected from any surges in voltage by a voltage regulator, which is connected between the 9V battery and the module. Data streaming begins as soon as the transmitting module receives power.

The software X-CTU needs to be downloaded in order to program the XBee's to perform analog to digital conversions. This is available free of cost from the Digi website. In addition, the FTDI driver needs to be installed in order for the computer to recognize and communicate with the receiving module. A screenshot of the X-CTU interface with hexadecimal data is shown in Figure 50Figure 51.

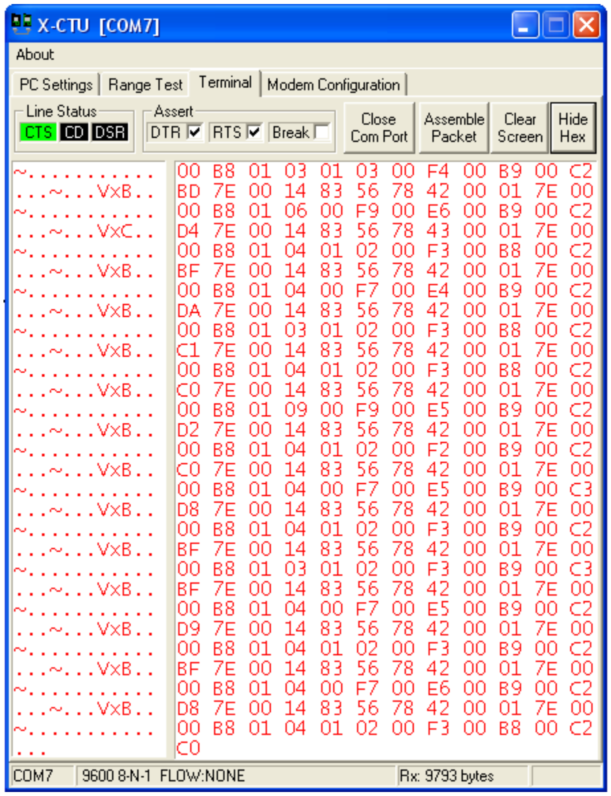

Figure 50: X-CTU Interface

The configuration commands used in the software to program the transmitter are shown in Table 9.

Table 9: Configuration Commands for XBee Modules

Command	Transmitter	Receiver	Description
ATDL	5678	1234	Address of each unit
ATMY	1234	5678	Address of unit to send to
ATID	3333	3333	PAN ID (should be same)
ATIU	1	N/A	Set to receive of UART
ATIA	5678	N/A	
ATD0	N/A	2	Set pin 0 to analog input
ATD1	N/A	2	Set pin 1 to analog input
ATD2	N/A	2	Set pin 2 to analog input
ATD3	N/A	2	Set pin 3 to analog input
ATD4	N/A	2	Set pin 4 to analog input
ATD5	N/A	2	Set pin 5 to analog input
ATIT	N/A	2	Samples before transmission
ATIR	N/A	14	Sample rate (in hex)
ATWR	No value	No value	Write to non-volatile memory

Several points must be noted when using these settings to configure the modules. First, the sample rate maximum is 1 kHz for one pin, or for all 6 pins, 1000/6 = 167 Hz for each pin. The samples before transmission is limited by the buffer limit of 93 bytes for the XBee. Since these are 10 bit samples, each sample is two bytes resulting in a maximum of 46 samples able to be sent on one transmission. For all six channels this means a maximum of seven samples can be sent for each transmission. On the receiver the command that causes the device to send data is ATIU, where the transmitter will automatically send the API packets as a hexadecimal string. Once the commands are entered, ATWR must be sent to write the settings to non-volatile memory. Without this command, all changes will be lost.

The hexadecimal string is received at the USB port as serial data. A LabVIEW program is used to parse the string and convert it to a decimal value. Screenshots of the program are shown in Figure 51 and Figure 52.

The baud rate is selected on the front panel, as well as the COM port at which data is received by the receiving module. Depending on the baud rate, which should be selected to match the baud rate of the modules, the number of bits per second received is determined.

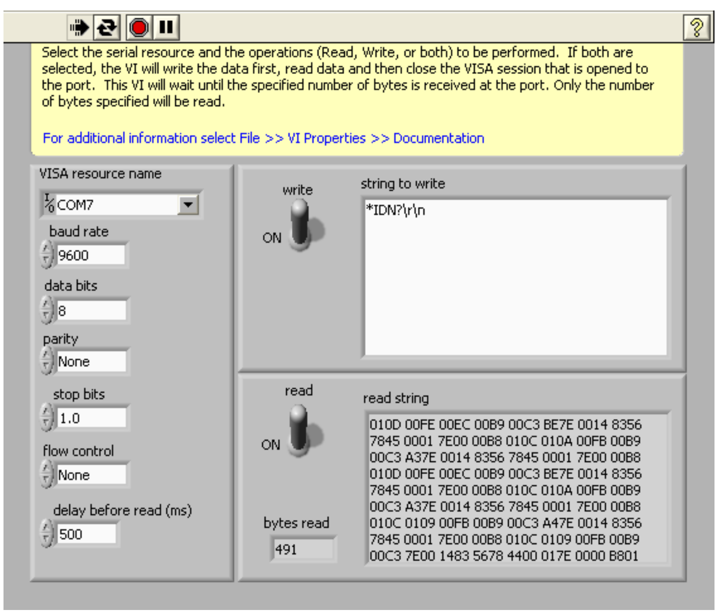

Figure 51: LabVIEW Front Panel for XBee

The string of hexadecimal data received is checked for the delimiter ‘7E’. After every instance of this hexadecimal byte, the 6 different desired measurements are extracted from the string and separated into columns. This is done by saving each string received into an array and using a counter to arrive at the desired 6 bytes.

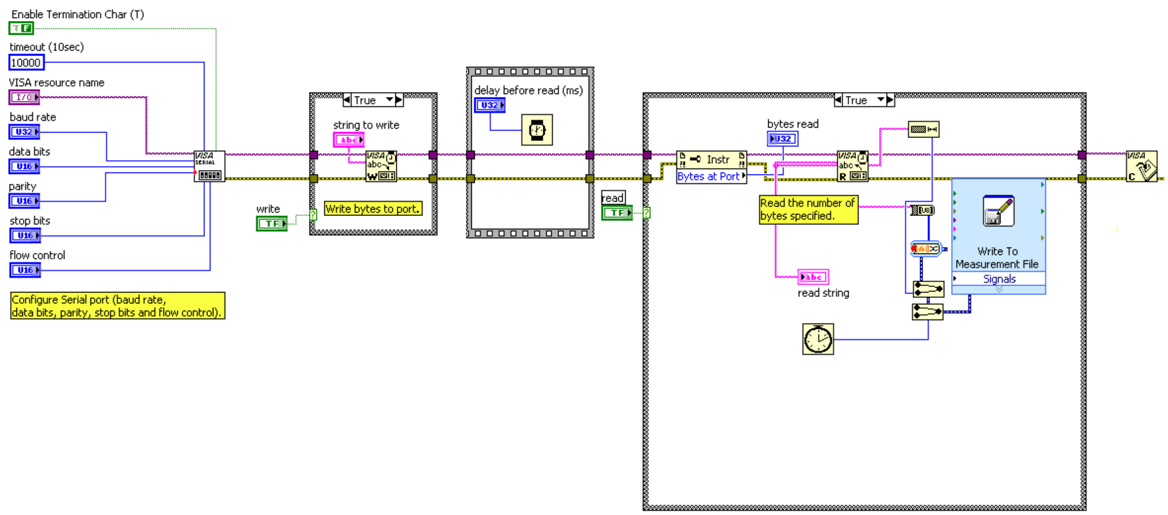

Figure 52: LabVIEW Block Diagram for XBee

Each byte is written to a different column in an excel spreadsheet. An example of a serial string received by the computer is:

7E 00 00 B8 01 0C 01 0A 00 FB 00 B9 00 C3 A3

The data is then adjusted based on the 10 bit capability of the ADC. Since the maximum value of the hexadecimal byte that is received is 1024, the data is divided by this value and adjusted on a 3.3V scale to obtain the analog voltage initially received by the transmitter. Therefore final values are obtained for pressure and strain.

Pressure Sensors

For calibrating the pressure sensors, the system is first pre-charged to a set value, then the hydraulic fluid is pumped in. The valve is closed, and the pressure at the mechanical pressure transducer in the hydraulic line is recorded. In a static environment, with no fluid being added or removed, and the accumulator not rotating, the pressure across all five pressure sensors should be the same. The voltages at this corresponding pressure are recorded. This step is repeated five times at varying pressures in order to obtain the slope of the pressure sensor in relationship to the pressure. This will also reveal the dc offset of each sensor. Adjusting for this offset and slope, pressure readings may commence.

The onboard pressure sensors require a VI, which reads in the values from the XBee and stores them to an excel file. The strings in this file must be parsed, as they are in a standard format, so the pressure readings may be separated. The strings are transmitted as hexadecimal; therefore, a conversion to binary is required. After this binary conversion, the voltage can be related to pressure via a conversion factor. After calibration, the slope and dc offset may be used to read the proper pressure readings of the sensors.

The voltage ratio of the pressure sensor output compared to the supply voltage was applied for the pressure senor that was in the hydraulic line. The VI for this pressure sensor can be seen in Figure 53 and the block diagram in Figure 54.

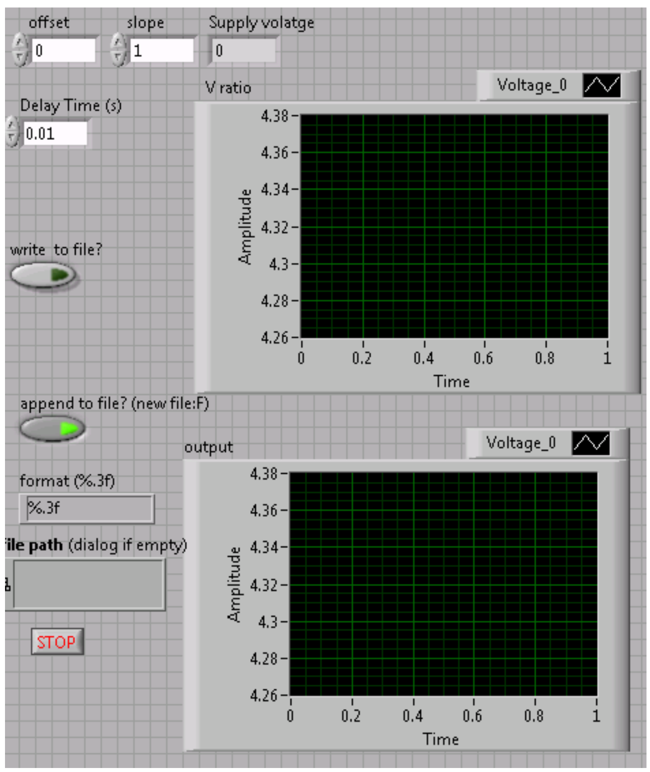

Figure 53: Pressure Sensor VI

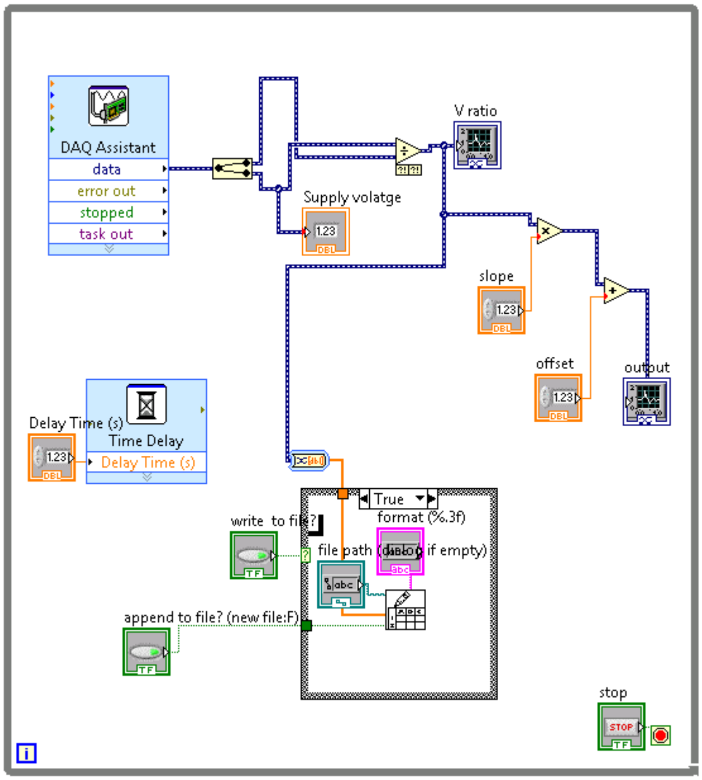

Figure 54: Pressure Sensor Block Diagram

Strain Gauges

The strain gauges are used to verify the strain values predicted by the finite element analysis model. The maximum value for predicted strain on the outer wall of the acrylic chamber is 3 μ-strain in the radial direction. Two strain gauges are used; one mounted in the radial direction at the point of maximum external strain, and the other in the axial direction at a similar location.

The strain gauges used have a gauge factor of 2.1, and an internal resistance of 120Ω. They are configured using a quarter wave Wheatstone bridge. The change in temperature during operation is negligible; thus, a full wave bridge that compensates for changes in temperature is not required. The schematic for the strain gauge set up is shown in Figure 55.

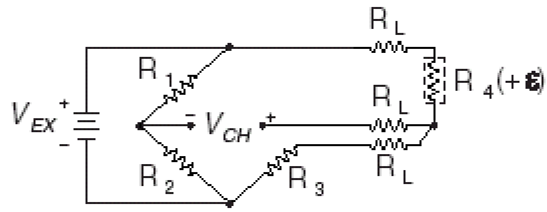

Figure 55: Quarter Bridge Configuration

The gain of the output of the strain gauges is set up such that the maximum possible output corresponds to a radial strain of 6 μ-strain. The voltage readings from the output of the strain gauge can be used to find strain from the formula:

$$strain\ (\varepsilon) = \frac{-4V_r}{GF(1+2V_r)} \times \left(1 + \frac{R_L}{Rg}\right) \qquad \text{(Eq. 9)}$$

Where:

$$V_r = \left(\frac{V_{CH}(\text{strained}) - V_{CH}(\text{unstrained})}{V_{EX}}\right) \qquad \text{(Eq. 10)}$$

V_r is the voltage ratio that is used in the voltage to strain conversion equations

GF is the gauge factor

R_L is the lead resistance

R_g is the nominal gauge resistance

V_{CH} is the measured signal voltage

V_{EX} is the excitation voltage

Therefore, the voltage obtained from the strain gauge via the wireless modules is directly substituted in the formulas above to get the corresponding strain value.

Tachometer

To determine the angular velocity of the system, and optical interrupter has a disc with slots cut, rotate in between the sensor, each slot generates a pulse which is counted by the counter on the DAQ. Since there is no hardware timer on the card, the number of pulses is read in over a given period of time, counted by the software, and this number of pulses is divided by the time to find the frequency. To physically connect the device, the sensor must be placed so the disc slides between it easily. A 5-volt power source must be connected to it. To test if the sensor is working, when the sensor is blocked it should output 5V, and 0V when open. The LabVIEW

VI will record the RPM with respect to time. The number of pulses is set at 4, corresponding to the number of slots in the disc. By decreasing the time a faster response to velocity changes will be observed, but the accuracy will decrease. Thus, a time of 2-seconds is chosen to trade of between accuracy and response time. After choosing a file save directory, the file will be saved to the directory in two columns whenever write to file is enabled. The User VI and block diagram can be seen in Figure 56 and Figure 57.

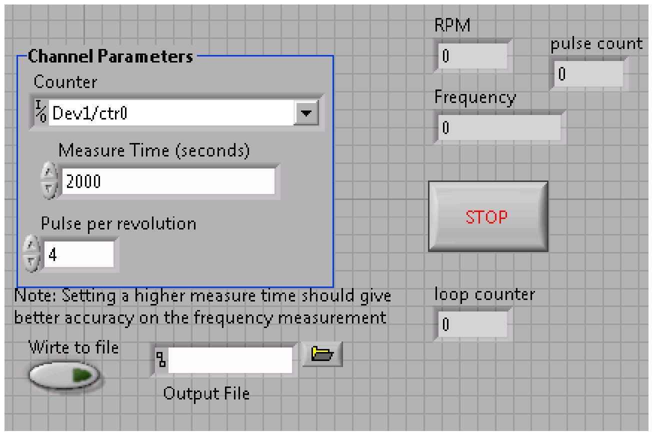

Figure 56: Tachometer VI

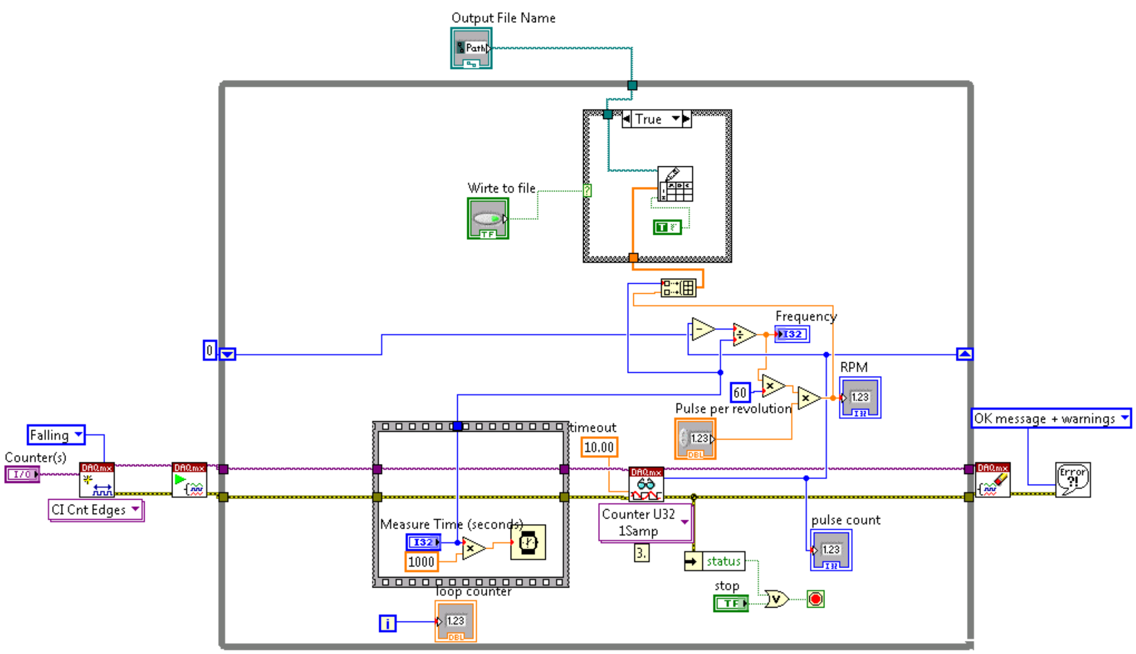

Figure 57: Tachometer Block Diagram

Instrumentation Amplifier

The instrumentation amplifiers are an integral part of the DAQ; they increase the resolution of the measurements by increasing the range. A gain of 33 is applied to the 0 to 100mV output of each pressure transducer to bring the range to 0 to 3.3V. There are three dual channel amplifiers, which were used to minimize the size of the circuits (3 were needed onboard rather than 6). Gain set resistors of 1% tolerance were used to reduce uncertainty. The output of the strain gauge at the maximum strain was computed and scaled, with a resistor of 390Ω, and 20Ω for the axial and radial strain. The instrumentation amplifier gain can be easily changed by changing the gain set resistor. If the voltage output is around 7-8V, then the pressure sensor or current source is not connected. The output of the instrumentation amplifier should not exceed 3.3V, as this could damage the microcontroller. The 200 kHz INA126 dual channel instrumentation amplifier is fast enough to respond to changes as the XBee can sample at 1 kHz maximum.

Load Cell

The load cell specified previously is a full-bridge thin-beam type, which essentially is a beam that is able to be in compression or tension. The strain gauge based load cell has a Wheatstone bridge configuration attached to one surface at the center. If a positive and negative power source is applied to the load cell, the output also can be read in positive or negative, and thus a direction can be established. The group decided to give a 5 V source based on the load cell specifications. This gives a read out of 2 mV/V, resulting in a 10 mV output; therefore, an instrumentation amplifier was utilized. To get the proper feedback, the following circuit was implemented (see Figure 58).

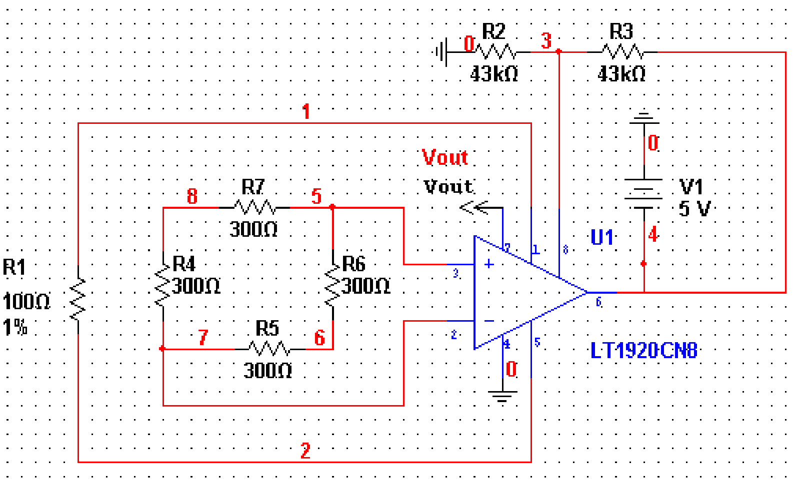

Figure 58: Load Cell Circuit Diagram

An output wire and a reference ground wire are attached to the positive input of the AI1 channel and ground of the USB DAQ card, respectively. Since the power source cannot reliably provide a constant 5 volts, the positive and negative leads were also connected and read in LabVIEW. The positive source was attached to the AI0 channel of the DAQ card, and the negative source was grounded. Now the DAQ card can interface with LabVIEW and perform the necessary calculations to find the torque. The front panel of the VI is shown in Figure 59.

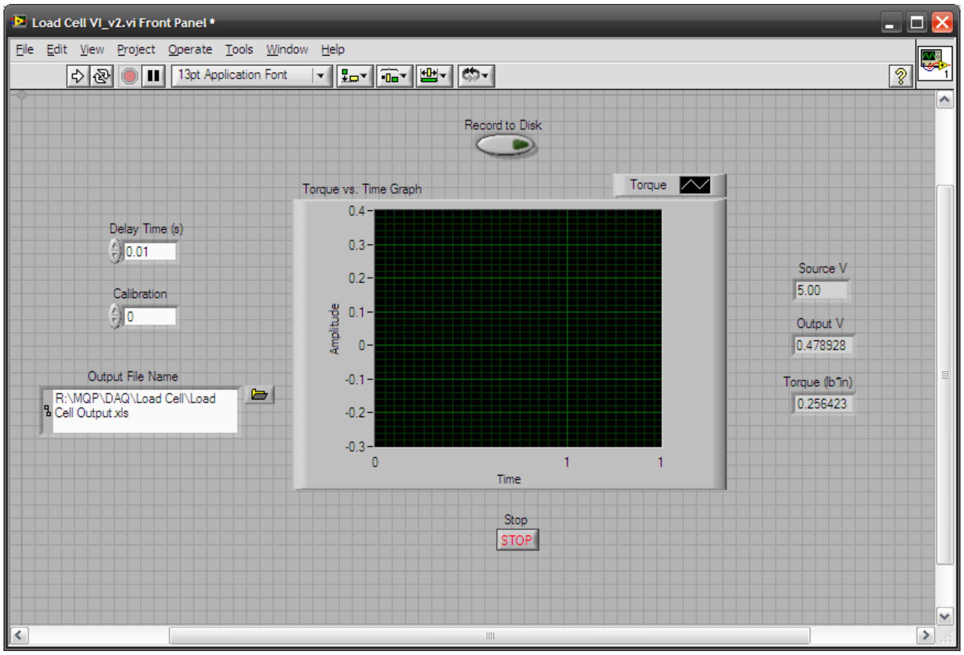

Figure 59: Load Cell VI Front Panel

The front panel is quite simple; the user only has to enter in a calibration factor and an Excel file to output data to. The delay time can also be changed, but the default setting of 0.01 seconds was found to be sufficient in identifying the peak torque. All other values, as seen on to the right of the graph, are outputs for easy reference. The graph allows the user to get real time feedback, so they are able to see the calculated torque during operation.

The block diagram looks more complex than it is (see Figure 60). The VI starts on the left side where the two analog inputs are read into LabVIEW. The output voltage is calibrated first, and then a ratio of the output voltage to the source voltage is taken. This ratio is multiplied by the maximum 5 lbf of the load cell. At this point, the force exerted on the torque arm is known, which is then multiplied by the distance of 3.25 inches to obtain the torque. Each calculation step is recorded to an Excel file for easy manipulation. The most important graph comparison is the torque versus time. The peak value in the graph is the maximum torque of the motor.

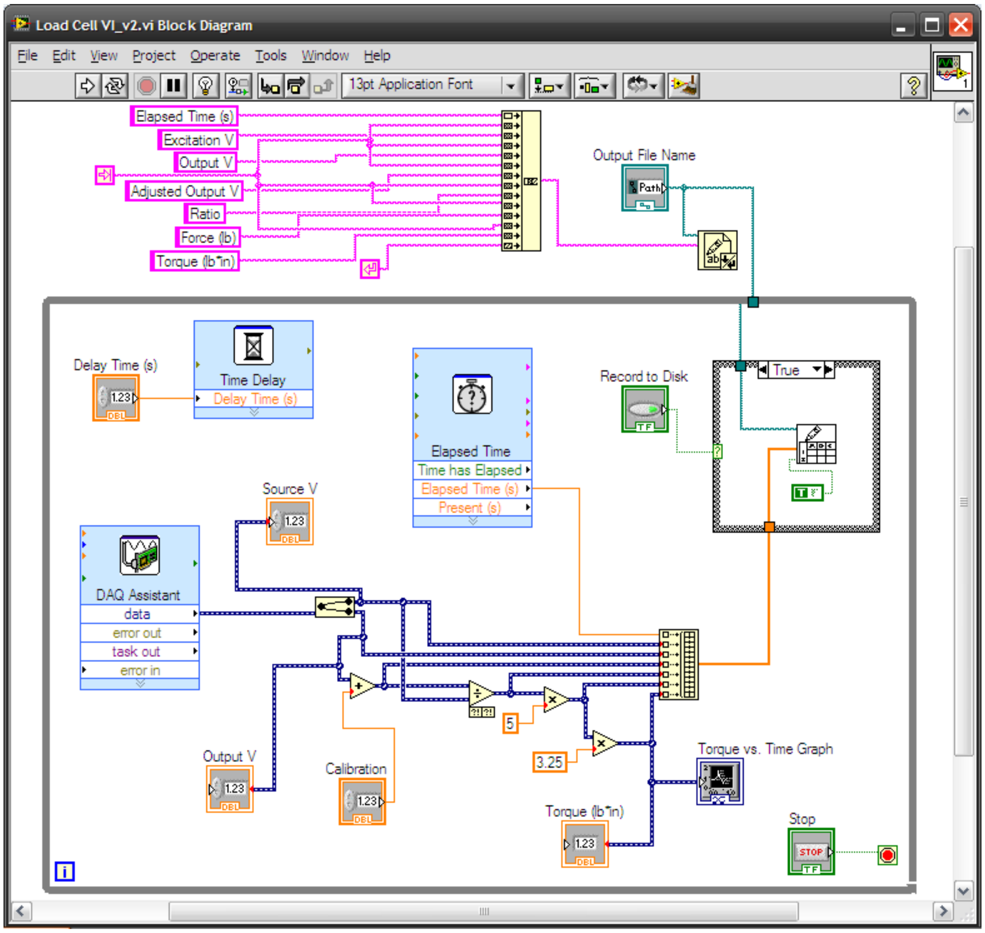

Figure 60: Load Cell VI Block Diagram

Vision System

The idea of using NI's vision assistant and LabVIEW to monitor the piston position was synthesized due to the possibility of having an external sensor to measure the movement of the piston during a test on an already cramped system. The concept behind using the vision system was to identify features of the flywheel-accumulator that could be used to measure the movement of the piston and record the change as close to real-time as possible.

The configuration used in the project involves the use of a Logitech S 7500 webcam with a maximum resolution of 640x480 image capture at 15 frames per second (fps). The camera is interfaced with a computer via USB and is configured to NI Vision Assistant that can acquire and process images. The Vision Assistant can acquire a single image or a sequence of frames to be used in the process image option via a script. It has the capability to write scripts to analyze images with respect to properties such as color or geometry. These scripts could then be utilized to build a LabVIEW VI.

The first step in calibrating the piston position measurement is to acquire a snapshot and then calibrate the figure using a perspective grid calibration shown in Figure 61. This step identifies the grid dots and isolates them from the original image using a color threshold operation.

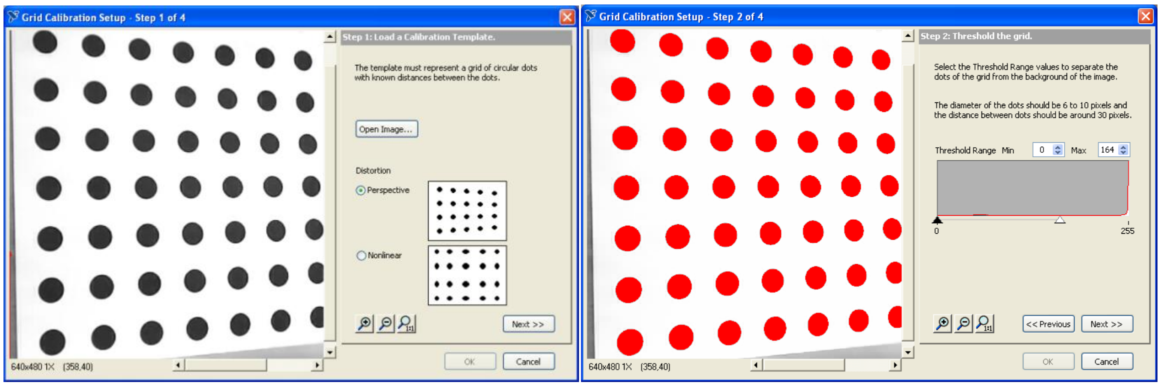

Figure 61: Grid Calibration

Next, the program converts the pixels into real-world distances via the known distances between the dots (24.5 mm) in a box that is defined by the user. An axis of origin that is parallel to the components in the image must also be defined in order to finish the calibration process.

Once the calibration step is completed, Vision Assistant can apply operations that will isolate features, such as the end caps and the piston in order to determine the piston position. The color threshold function isolates a certain color range in RGB format. It isolates the colors and generates an 8-bit image that can be further processed. Figure 62 depicts how the operation takes the original image isolates the color ranges and creates a new image. The figure depicts how the color threshold is able to isolate the black o-ring in the gas side end cap and the U-seal of the piston.

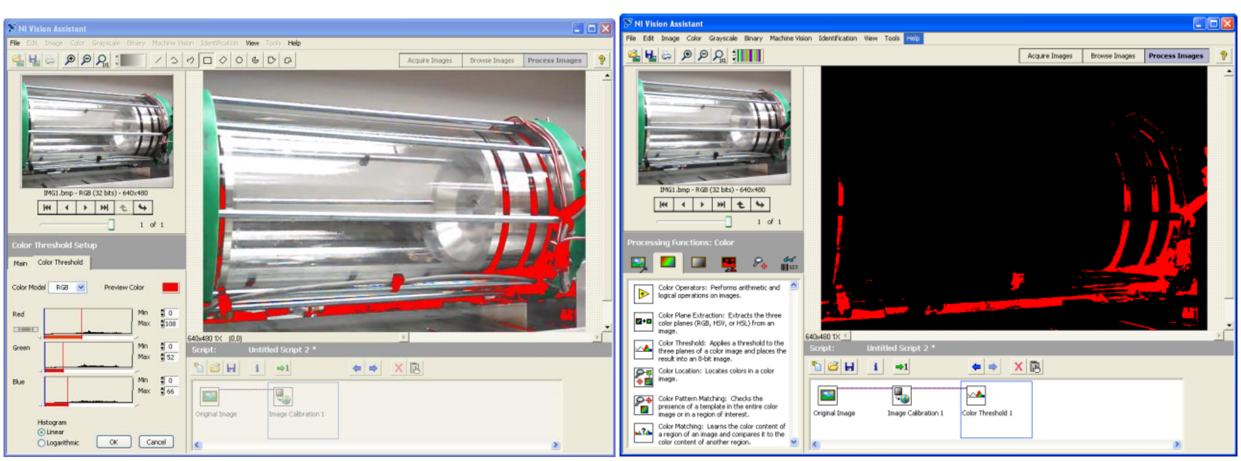

Figure 62: Color Threshold Operation

The new image can then go through two different filters to clean up any noise caused by lighting and unwanted shadows. A low pass filter is used to eliminate any outlying shadow or unwanted features leaving the edges of the seals that can be used as reference points. The second filter is an edge detection filter that separate edges and eliminates solid regions. Figure 63 displays how the filters manipulate the 8-bit image.

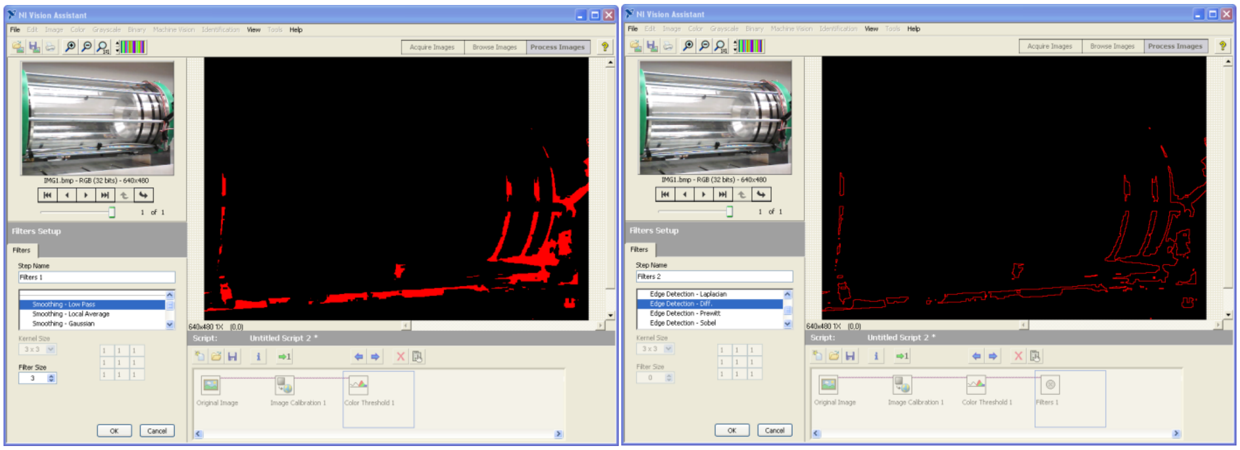

Figure 63: Filter Operations

The final step to setting up the Vision Assistant is to apply a clamp operation of the edges that can be utilized to measure the distance the piston travels. The clamp operation defines a box of interest and the function measures the average distance from the outer lines that exist in the region. Drawing the box so one of the end cap seals is an edge and the other edge is at the furthest position where furthest u seal can travel will allow the program to always measure the same distance. Figure 64 provided below shows this setup.

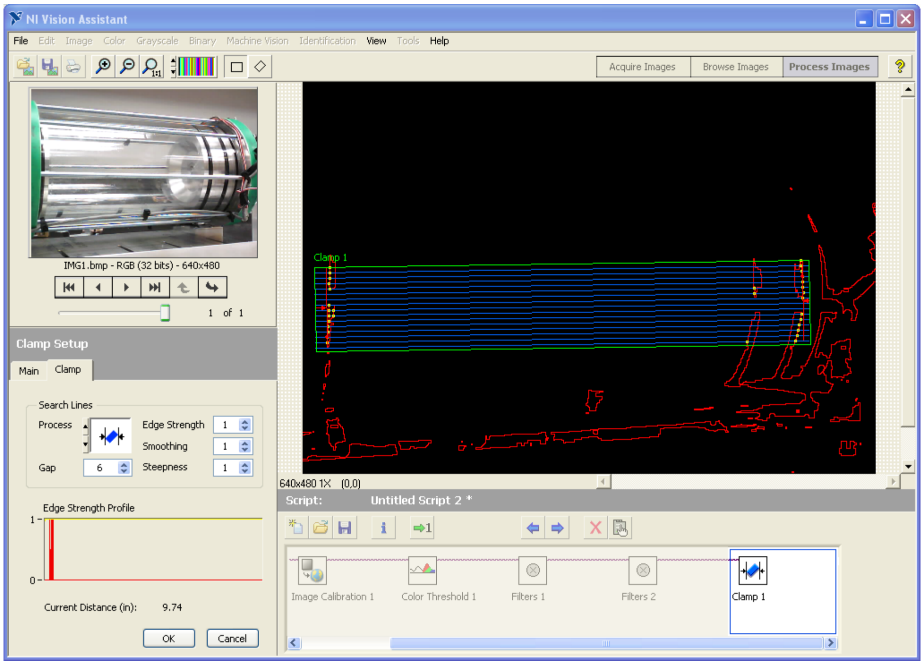

Figure 64: Clamping Function

The clamping function also allows the user to define properties of the types of edges it is searching for based on edge strength, smoothing, gap, and steepness.

With the Vision Assistant script complete, a LabVIEW VI can be created based on the script. Creating the VI requires the user to define the controls and indicators desired in the VI. Once all the parameters are filled, LabVIEW creates the VI that can analyze images and record data, which can be viewed in Appendix O: Vision System LabVIEW VI.

5. Results

Unfortunately, the group was unable to record any pressure sensor readings. Additionally, the circuitry for the strain gages was not complete, and the tachometer was not reading the necessary voltage. The only reportable results the team obtained were for the torque of the motor.

Torque Results

The torque was calculated per the torque arm and load cell combination. The three following runs were consecutive outputs from LabVIEW to Excel.

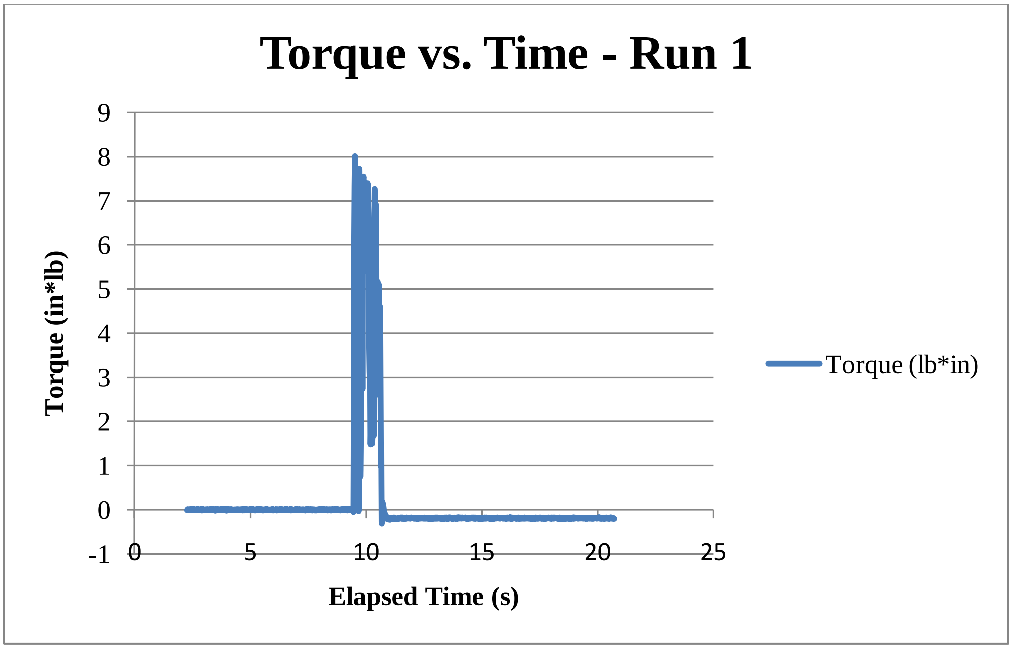

Figure 65: Torque Measurement – Run 1

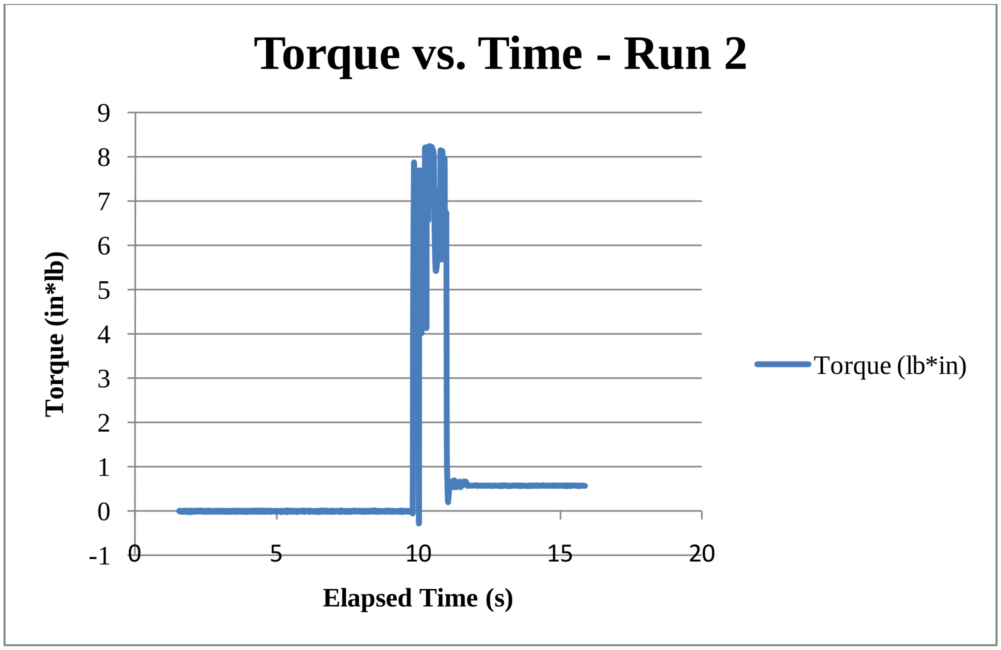

Figure 66: Torque Measurement – Run 2

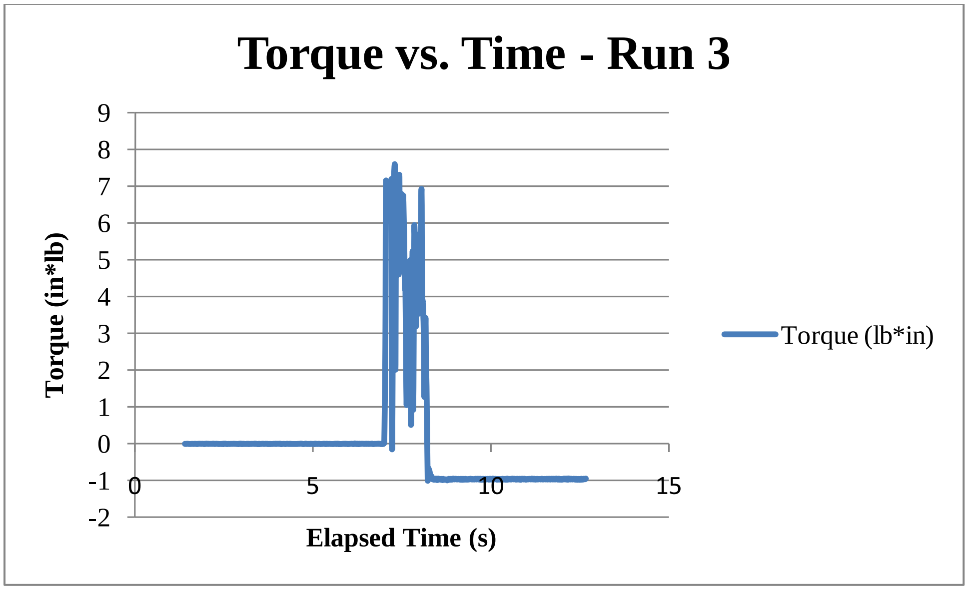

Figure 67: Torque Measurement – Run 3

The first run registered a maximum torque of 7.951 in*lb. The second and third had a maximum of 8.242 and 7.55 in*lb, respectively.

6. Discussion

Due to a combination of issues with our data acquisition system, the team was unable to collect results from the pressure sensors, strain gages, tachometer, and video capture. Three out of the five pressure sensors were damaged unexpectedly from being secured to the accumulator during demonstration. The strain gages were mounted, but not connected to the wireless XBees because the team felt time was better spent on the pressure sensors. Additionally, the strain gages were mounted on the outer circumference of the cylinder, which according to the FEA model where the chamber experiences about 1 to 2 μ-strain. The team felt that this small strain would be difficult to register given the small values of strain. The tachometer was not reading the necessary voltage due to problems interfacing with the DAQ card. When disconnected from the card the expected output voltages would be correct, but when the tachometer was connected to the card it would register unexpected output voltages. Lastly, the video capture worked to an extent, but could not be applied without the other components in unison. The images would need to be acquired and then inputted individually into the LabVIEW VI for analysis. The only preliminarily data that was collected was for the torque measurement.

Torque Measurement

The torque results do not match the analytical value of 13.701 in*lb at maximum operating conditions. There is error in either the data collection method or natural elements are affecting it. Natural elements may include the friction in the motor mounts and/or the motor may have exhibited power loss. Although the motor support structure was designed to have a free running fit, there is still noticeable friction when rotated by hand. The motor also could not be running at its full potential. Further testing would need to be done to find the true reasoning for the difference in values.

Each test seemed to imply good repeatability, but further improvements could be made to reduce noise. It would be beneficial to have a better calibration technique. The load cell could be calibrated by applying a known force and comparing actual to the output in the VI. Also, shielded wire would block the 60 Hz atmosphere better, which would in turn reduce the noise in the data.

7. Conclusion

No formal conclusion could be made about the energy density and the pressure distribution of the gas and oil sides. The only notable data was the torque measurements for the motor. If we were able to work the problems out, the group is confident that our original goal could be achieved.

This MQP project required knowledge of design, manufacturing, testing, and many aspects of engineering that the team was not introduced to in coursework. Therefore, the flywheel-accumulator taught us a lot about hydraulics and the interaction between different energy systems. Unfortunately, the full goal of this project was not reached because each stage of the prototype process took longer than expected, which left little time at the end for testing. On the other hand, the system performed adequately given the operational ranges that it was designed to handle. Hopefully, Professor Van de Ven or other students will take our work and continue the concept in hopes of proving the increased energy density and parabolic distribution.

The first possible place for future work would be to create a baffle design. The baffles would ideally prevent fluid swirl, which is a cause for frictional loses. The team had initial baffle designs, but was unable to bring any to a full working scale. The challenge with this is that the baffles must retract and expand as the piston moves side to side.

Since our project was only a proof of concept, others could apply the idea of the flywheel-accumulator to a regenerative braking system to better test the feasibility of its use in hybrid vehicle applications. The flywheel-accumulator could even be applied to other hydraulic systems to increase the energy storage density of accumulators in general.

References

[1] J. D. Van de Ven, "Increasing Hydraulic Energy Storage Capacity: Flywheel-Accumulator," *International Society of Fluid Power*, pp. 41-50, 2009.

[2] H. Ibrahim, A. Ilinca, and J. Perron, "Energy storage systems - Characteristics and comparisons," Quebec, Canada, Jan 2009.

[3] J. S. Cundiff, *Fluid Power Circuits and Controls: Fundamentals and Applications*. Blacksburg: CRC Press LLC, 2001.

[4] RoyMech. (2007, February) RoyMech. [Online]. http://www.roymech.co.uk/Related/Electrics/Electrics_Direct_Current.html

[5] Tobul Accumulator, Inc. Tobul Accumulator Web site. [Online]. http://www.tobul.com/index.php?option=com_content&task=view&id=13&Itemid=27

[6] Ed Godin. Industrial Equipment News Web site. [Online]. http://www.ien.com/article/hydraulic-accumulators-boost/122463

[7] Department of the Army, "Hydraulics," Washington, DC, 1997.

[8] J Van de Ven, M Olson, and P Li, "Development of a Hydro-Mechanical Hydraulic Hybrid Drive Train with Independent Wheel Torque Control for an Urban Passenger Vehicle," in *International Fluid Power Exposition*, Las Vegas, 2008, pp. 1-2.

[9] Perry Y Li, James D Van de Ven, and Caleb Sancken, "Open Accumulator Concept for Compact Fluid Power Energy Storage," in *ASME 2007 International Mechanical Engineering Congress and R&D Exposition*, Seattle, 2007, pp. 1-4.

[10] J. G. Bitterly, "Flywheel Technology: Past, Present, and 21st Century Projections," *IEEE Aerospace and Electronic Systems MAgazine*, vol. 13, no. 8, pp. 13-14, 1998.

[11] Y., Gay, S. E., Ehsani, M., Thelen, R. F., and Hebner, R. E. Gao, "Flywheel Electric Motor /Generator Characterization for Hybrid Vehicles," in *IEEE Vehicular Technology Conference*, 2003, p. 3332.

[12] R., Beno, J., and Walls, A. Hebner, "Flywheel Batteries Come Around Again," *IEEE Spectrum*, vol. 39, no. 4, pp. 46-51, 2002.

[13] H. Moosavi-Rad, "BVIF-Integrated Hybrid Bus," *Proceedings of the Institution of Mechanical Engineers. Part D, Journal of Automobile Engineering*, pp. 95-101, 1995.

[14] J. T. Wagner, "Energy Storage Flywheels Using Fluid Transfer to Vary Moments of Inertia," 5086664, 1992.

[15] Oliver W.J. Burstall, "Variable Inertia Flywheel," 6883399.

[16] Granta Material Intelligence. (2009, Sep) Polycarbonate Properties. CES Edupack2009.

[17] Robert L. Norton, *Machine Design: An Integrated Approach*.: Prentice Hall, 2009.

[18] Granta Material Intelligence. (2009, Sep) Acrylic. CES Edupack2009.

[19] Norton,.: Prentice Hall, 2009.

[20] Valley Seal. (2009, Oct) O-rings. [Online]. http://www.valleyseal.com/o-rings.htm

[21] Precision Associates Inc. (2009, Oct) Multiseals. [Online]. http://catalog.precisionassoc.com/product/precision-associates-inc-multiseals/multiseals

[22] Hercules. (2009) Sealing Products: Catalog Offerings pp 105. Catalog.

[23] Hercules. (2009) Sealing Products: Catalog Offerings pp 63. Catalog.

[24] Simply Bearings. 62042Z Shielded Ball Bearing. [Online]. http://simplybearings.co.uk/shop/product_info.php?products_id=1496

[25] Super Swivels. Super Swivels. [Online]. http://www.superswivels.com/InlineSwivels.html

[26] Rotary Systems Inc. Rotary Systems Inc. [Online]. http://www.rotarysystems.com/series-008

[27] Omega. (2010, Feb) Full-Bridge Thin Beam Load Cells. [Online]. http://www.omega.com/Pressure/pdf/LCL.pdf

[28] Electro chem. (Oct, 2009) Wireless Pressure Sensor. [Online]. http://www.electrochemsolutions.com/pdf/PS1.pdf

[29] Robots in Search. Baby Orangutan B-48 Robot Controller. [Online]. http://robotsinsearch.com/baby-orangutan-robot-controller-p-244.html

[30] Digi. [Online]. http://www.digi.com/products/wireless/point-multipoint/xbee-pro-series1-module.jsp

[31] RDP group. (2009, Oct) How it Works - LVDT. [Online]. http://www.rdpe.com/ex/hiw-lvdt.htm

[32] National Instruments. (2009, Sep) Measuring Strain with Strain Gages. [Online]. http://zone.ni.com/devzone/cda/tut/p/id.3642

[33] Answers.com. (2009, Sep) Strain Gauge. [Online]. http://answers.com/topic/strain-gauge#gauge_factor

[34] National Instruments. (2009, Oct) Choosing the Right Strain Gauge for Your Application. [Online]. http://zone.ni.com/devzone/cda/tut/p/id/3092?nipkw=strain%20gauge&nisrc=Google&niurl=&ninet=search&nicam=DAQ%20&nigrp=Sensor%20-%20Strain%20Gauge

[35] Digikey. (2010, Jan) Pressure Sensors. [Online]. http://search.digikey.com/scripts/DkSearch/dksus.dll?vendor=0&keywords=msp6920

[36] Measurement Specialties. Measurement Specialties. [Online]. http://www.meas-spec.com/pressure-sensors.aspx

[37] Applied Measurements Ltd. (2009, Oct) How LVDTs Work - Operating Principles. [Online]. http://www.lvdt.co.uk/howtheywork.html

[3 Omega. (2009, Oct) Omega.com. [Online]. http://www.omega.com/pptst/LD620.html

8]
[3 Digikey. (2010, Jan) Digikey Magnetopot. [Online].
9] http://search.digikey.com/scripts/DkSearch/dksus.dll?Detail&name=905-1032-ND

[4 Arduino. Arduino Hardware. [Online]. http://arduino.cc/en/Main/Hardware
0]

[4 Simply Bearings. 62042Z Shielded Ball Bearing. [Online].
1] http://simplybearings.co.uk/shop/product_info.php?products_id=1496

[4 Simply Beairngs. 62042Z Shielded Ball Bearing. [Online].
2] http://simplybearings.co.uk/shop/product_info.php?products_id=1496

[4 Granta Material Intelligence. (2009, Sep) Polycarbonate Properties. CES Edupack2009.
3]

[4 United States Army, "U.S. Field Manual Fm 5-499 (Hydraulics)," 2007.
4]

[4 Hydrotrole USA. Accumulators. [Online]. http://www.accumulators-
5] hyd.com/accumulators/Accumulators.htm

[4 Parts Geek. [Online]. http://www.partsgeek.com/gbproducts/YN/C85-CFW-
6] I3045.html?utm_source=google&utm_medium=ff&utm_term=01+2001+Porsche+911+

[4 Wikipedia. Centrifugal Governor. [Online]. http://en.wikipedia.org/wiki/Centrifugal_governor
7]

Nomenclature

Word	**Description**
ADC	Analog to digital
ANSYS	FEA program
CAD	Computer Aided Design
FEA	Finite Element Analysis
NI	National Instruments
XBee	Wireless microcontroller

Symbol	Description
a_n	Normal acceleration
A_t	Tensile area
d	Bolt diameter
$E_{flywheel}$	Energy stored in a flywheel
E_{gas}	Energy stored in a gas
E_{stored}	Energy stored
F	Force
F_b	Balance force
F_i	Preload force
g	Gravity
I_{fluid}	Inertia of the fluid
$I_{flywheel}$	Inertia of the accumulator with no fluid
I_{total}	Total inertia
K_i	Coefficient of friction
Ksi	1000 psi
L	Length
l_g	Length of gas volume
l_h	Length of hydraulic volume
M_b	Mass of the 9v battery
M_s	Mass of the pressure sensor
N_a	Actual safety factor
N_s	Desired safety factor
P	Power
P(r)	Pressure as a function of radius
P_1	Initial Pressure
P_{max}	Maximum pressure
P_s	System pressure
R	Compression factor
r_0	Outer radius
r_1	Distance from center to first pressure sensor

r_2	Distance from center to second pressure sensor
r_b	Distance from center to battery
r_i	Inner radius
S_p	Proof strength
t	Thickness of acrylic
T_i	Preload torque
V	Volume
V_f	Final volume
V_i	Initial volume
V_{sp}	Modified proof strength
V_{st}	Modified tensile strength
ΔL	Change in length
ΔP	Pressure differential from center to edge
ε	Strain
ε_r	Radial strain
ε_t	Tangential strain
ρ	Density
σ'	Von Mises stresses
σ'_{max}	Maximum Von Mises stresses
$\sigma_{1,2,3}$	Principle stresses
σ_{ap}	Axial stress from pressure
σ_{rf}	Radial stress from flywheel
σ_{rp}	Radial stress from pressure
σ_{tf}	Tangential stress from flywheel
σ_{tp}	Tangential stress from pressure
ω	Angular velocity
ω_{max}	Maximum angular velocity

Appendix A: Analytical Chamber Stress & Strain

Stresses in an Acrylic Thick Walled Cyclinder with 6in. OD/t = 1"

Yield Strength — Weight Density — Gravity

$S_y := 6.038\,ksi$ $\quad \gamma := 73.737846\,\dfrac{lbf}{ft^3}$ $\quad g = 32.174\,\dfrac{ft}{s^2}$

Poisson's Ratio — Elastic Modulus

$\nu := 0.35$ $\quad E := 425\,ksi$

Dimensions of the cylinder — **Working Pressure** — **Desired Safety Factor** — **Angular Velocity**

$t := .75\,in$ $\quad r_0 := 3\,in$ $\quad p_i := 500\,psi$ $\quad N_s := 2.5$ $\quad \omega := 3000\,rpm$

Inner Radius

$r_i := r_0 - t = 2.25\,in$

Generic Equations

Pressure Induced Stresses

Axial Stress

$$\sigma_{ap}(p_i) = \frac{p_i \cdot r_i^2}{r_0^2 - r_i^2}$$

Tangential Stress

$$\sigma_{tp}(p_i) = \frac{r_i^2 \cdot p_i}{r_0^2 - r_i^2} \cdot \left(1 + \frac{r_0^2}{r^2}\right)$$

Radial Stress

$$\sigma_{rp}(p_i) = \frac{r_i^2 \cdot p_i}{r_0^2 - r_i^2} \cdot \left(1 - \frac{r_0^2}{r^2}\right)$$

Flywheel Stresses

Tangential Stress

$$\sigma_{tf} = \frac{\gamma}{g} \cdot \omega^2 \cdot \left(\frac{3 + \nu}{8}\right) \cdot \left(r_i^2 + r_0^2 + \frac{r_i^2 \cdot r_0^2}{r^2} - \frac{1 + 3 \cdot \nu}{3 + \nu} \cdot r^2\right)$$

Radial Stress

$$\sigma_{rf} = \frac{\gamma}{g}\omega^2\cdot\left(\frac{3+\nu}{8}\right)\cdot\left(r_i^{\,2} + r_0^{\,2} - \frac{r_i^{\,2}\cdot r_0^{\,2}}{r^2} - \frac{1+3\cdot\nu}{3+\nu}\cdot r^2\right)$$

Anaylsis of the Stresses at the Outer Diameter

$$r := r_0 = 3\cdot in$$

Pressure Induced Stresses

Axial Stress

$$\sigma_{ap}(p_i) := \frac{p_i\cdot r_i^{\,2}}{r_0^{\,2} - r_i^{\,2}}$$

Tangential Stress

$$\sigma_{tp}(p_i) := \frac{r_i^{\,2}\cdot p_i}{r_0^{\,2} - r_i^{\,2}}\cdot\left(1 + \frac{r_0^{\,2}}{r^2}\right)$$

Radial Stress

$$\sigma_{rp}(p_i) := \frac{r_i^{\,2}\cdot p_i}{r_0^{\,2} - r_i^{\,2}}\cdot\left(1 - \frac{r_0^{\,2}}{r^2}\right)$$

Flywheel Stresses

Tangential Stress

$$\sigma_{tf} := \frac{\gamma}{g}\cdot\omega^2\cdot\left(\frac{3+\nu}{8}\right)\cdot\left(r_i^{\,2} + r_0^{\,2} + \frac{r_i^{\,2}\cdot r_0^{\,2}}{r^2} - \frac{1+3\cdot\nu}{3+\nu}\cdot r^2\right) = 62.203\,psi$$

Radial Stress

$$\sigma_{rf} := \frac{\gamma}{g}\omega^2\cdot\left(\frac{3+\nu}{8}\right)\cdot\left(r_i^{\,2} + r_0^{\,2} - \frac{r_i^{\,2}\cdot r_0^{\,2}}{r^2} - \frac{1+3\cdot\nu}{3+\nu}\cdot r^2\right) = 15.953\,psi$$

Stresses on the Cylinder due to Working Pressure

$\sigma_{ap}(p_i) = 0.643\,ksi$ $\quad$ $\sigma_{tp}(p_i) = 1.286\,ksi$ $\quad$ $\sigma_{rp}(p_i) = 0\cdot psi$

Principal Stresses

$\sigma_1 := \sigma_{tp}(p_i) + \sigma_{tf} = 1.348\,ksi$ $\quad$ $\sigma_2 := \sigma_{ap}(p_i) = 0.643\,ksi$ $\quad$ $\sigma_3 := \sigma_{rp}(p_i) + \sigma_{rf} = 15.953\,psi$

Von Mises Stress

$$\sigma' := \sqrt{\sigma_1^2 + \sigma_2^2 + \sigma_3^2 - \sigma_1 \cdot \sigma_2 - \sigma_2 \cdot \sigma_3 - \sigma_1 \cdot \sigma_3} = 1.154\,\mathrm{ksi}$$

Maximum Allowable Stress

$$\sigma'_{max} := \frac{S_y}{N_s} = 2.415\,\mathrm{ksi}$$

Actual Safety Factor

$$N_a := \frac{S_y}{\sigma'} = 5.231$$

$$\text{Solution} := \left| \begin{array}{l} \text{return "Safe" if } \sigma'_{max} > \sigma' \\ \text{"Fail" otherwise} \end{array} \right.$$

Solution = "Safe"

Strain Analysis

Tangential Strain

$$\sigma = E \cdot \varepsilon$$

$$\varepsilon_t := \frac{\sigma_1}{E} = 3.172 \times 10^{-3}$$

Radial Strain

$$\sigma = E \cdot \varepsilon$$

$$\varepsilon_r := \frac{\sigma_3}{E} = 3.754 \times 10^{-5}$$

$$\varepsilon = \frac{\Delta L}{L}$$

Circumference of Interest

$$L_t := 2 \cdot \pi \cdot r = 18.85\,\mathrm{in}$$

Radius of the Interest

$$L_r := r = 3 \cdot \mathrm{in}$$

$$\Delta L_t := \varepsilon_t \cdot L_t = 0.06\,\mathrm{in}$$

$$\Delta L_r := \varepsilon_r \cdot L_r = 1.126 \times 10^{-4} \cdot \mathrm{in}$$

$$r' := \frac{\Delta L_t}{2 \cdot \pi} = 9.515 \times 10^{-3} \cdot \mathrm{in}$$

Analysis of the Stresses at the Inner Diameter

$r := r_i = 2.25\,in$

Pressure Induced Stresses

Axial Stress

$$\sigma_{ap}(p_i) := \frac{p_i \cdot r_i^2}{r_0^2 - r_i^2}$$

Tangential Stress

$$\sigma_{tp}(p_i) := \frac{r_i^2 \cdot p_i}{r_0^2 - r_i^2} \cdot \left(1 + \frac{r_0^2}{r^2}\right)$$

Radial Stress

$$\sigma_{rp}(p_i) := \frac{r_i^2 \cdot p_i}{r_0^2 - r_i^2} \cdot \left(1 - \frac{r_0^2}{r^2}\right)$$

Flywheel Stresses

Tangential Stress

$$\sigma_{tf} := \frac{\gamma}{g} \cdot \omega^2 \cdot \left(\frac{3 + \nu}{8}\right) \cdot \left(r_i^2 + r_0^2 + \frac{r_i^2 \cdot r_0^2}{r^2} - \frac{1 + 3 \cdot \nu}{3 + \nu} \cdot r^2\right) = 91.196\,psi$$

Radial Stress

$$\sigma_{rf} := \frac{\gamma}{g} \omega^2 \cdot \left(\frac{3 + \nu}{8}\right) \cdot \left(r_i^2 + r_0^2 - \frac{r_i^2 \cdot r_0^2}{r^2} - \frac{1 + 3 \cdot \nu}{3 + \nu} \cdot r^2\right) = 8.974\,psi$$

Stresses on the Cylinder due to Working Pressure

$\sigma_{ap}(p_i) = 0.643\,ksi$ $\quad$ $\sigma_{tp}(p_i) = 1.786\,ksi$ $\quad$ $\sigma_{rp}(p_i) = -500\,psi$

Principal Stresses

$\sigma_1 := \sigma_{tp}(p_i) + \sigma_{tf} = 1.877\,ksi$ $\quad$ $\sigma_2 := \sigma_{ap}(p_i) = 0.643\,ksi$ $\quad$ $\sigma_3 := \sigma_{rp}(p_i) + \sigma_{rf} = -491.026\,psi$

Von Mises Stress

$$\sigma' := \sqrt{\sigma_1^{\,2} + \sigma_2^{\,2} + \sigma_3^{\,2} - \sigma_1 \cdot \sigma_2 - \sigma_2 \cdot \sigma_3 - \sigma_1 \cdot \sigma_3} = 2.051 \cdot \text{ksi} \qquad \sigma' = 14.143\,\text{MPa}$$

Maximum Allowable Stress

$$\sigma'_{max} := \frac{S_y}{N_s} = 2.415\,\text{ksi}$$

Actual Safety Factor

$$N_a := \frac{S_y}{\sigma'} = 2.943$$

$$\text{Solution} := \left| \begin{array}{l} \text{return "Safe" if } \sigma'_{max} > \sigma' \\ \text{"Fail" otherwise} \end{array} \right.$$

Solution = "Safe"

Strain Analysis

Tangential Strain

$$\sigma = E \cdot \varepsilon$$

$$\varepsilon_t := \frac{\sigma_1}{E} = 4.416 \times 10^{-3}$$

Radial Strain

$$\sigma = E \cdot \varepsilon$$

$$\varepsilon_r := \frac{\sigma_3}{E} = -1.155 \times 10^{-3}$$

$$\varepsilon = \frac{\Delta L}{L}$$

Half of the Circumference of Interest

$$L_t := \pi \cdot r = 7.069\,\text{in}$$

Radius of Interest

$$L_r := r = 2.25\,\text{in}$$

$$\Delta L_t := \varepsilon_t \cdot L_t = 0.031\,\text{in}$$

$$\Delta L_r := \varepsilon_r \cdot L_r = -2.6 \times 10^{-3} \cdot \text{in}$$

$$r' := \frac{\Delta L_t}{2 \cdot \pi} = 4.968 \times 10^{-3} \cdot \text{in}$$

Appendix B: Acrylic Material Properties

09/30/2009 10:55 FAX 515 265 0710 SPARTECH TOWNSEND 002

Jeff

Typical Properties			Cast Acrylic Tubing (ASTM-D-5436)	Cast Acrylic Rods (ASTM-D-5436)
Mechanical Properties				
Specific Gravity	ASTM-D-792		1.19	1.19
Tensile Strength	ASTM-D-638			
Yield		psi	11,250	11,250
Elongation, Rupture		%	6.4	6.4
Modulus of Elasticity		psi	450,000	450,000
Flexural Strength	ASTM-D-790			
(Rupture)		psi	15,250	15,250
Modulus of Elasticity		psi	475,000	475,000
Compressive Strength	ASTM-D-695			
(Yield)		psi	18,000	18,000
Modulus of Elasticity		psi	440.000	440,000
Compressive Deformation (Under Load)	ASTM-D-621			
4000 PSI 122F,24hr		%	0.75	0.75
Sheer Strength	ASTM-D-732	psi	9,000	9,000
Impact Strength				
Izod Milled Notch	ASTM-D-256	ft. lbs/in. of notch	.0375*	.0375*
Falling Steel Ball, 0.5lb. (Breakage drop height (ft.)			18	18
Rockwell Hardness	ASTM-D-785		M98*	M98*
Barcol Hardness	ASTM-D-2583		50*	50*
Residual Shrinkage (Internal Strain)	ASTM-D-4802			
Townsend		%	2.2	2.2
Optical Properties				
Refractive Index	ASTM-D-542		1.49	1.49
Luminous Transmittance (As Cast)	ASTM-D-1003			
Total		%	92	92
Haze			<0.5	<0.5
Yellowness Index	ASTM-D-1925		0.5	
After 1000 hrs. Accelerated Weathering	ASTM-D-1449			
Total		%	92	
Haze			<0.5	
Effect Of Accelerated Weathering-On Appearance	ASTM-D-1449			
Crazing / Discoloration / Warping			none	
Ultraviolet Transmission @ 320nm		%	0	>80
Taber Abrasion (500g, ca. wheel, 100 rev.) ANSI Z26.1	ASTM-D-1044		14	
Mar Resistance	ASTM-D-637		29	
Thermal Properties				
Hot Forming Temperature		deg. Fahrenheit	320 **	320 **
Deflection Temperature under load	ASTM-D-648			
(Heat Distortion Temp.)				
66 psi			230*	230*
264 psi		deg. Fahrenheit	203*	203*
Maximum Recommended Continuous Service Temp.		deg. Fahrenheit	180	180
		deg. Fahrenheit	0.000042	0.000042
Coefficient of Linear Thermal Expansion	ASTM-D-696	in./in./deg. F	1.3	1.3
Coefficient of Thermal Conductivity	Cento-Fitch[4]	BTU/(Hr.) (Sq.Ft.) (deg. F/in.)	0.65	0.65
Water Absorption	26 day immersion	%	0.2	0.2
	24 hour immersion	%	1.2*	1.2*
Flammability (Burning Rate) UL94HB	ASTM-D-635	In./min.	830*	830*
Self-ignition Temperature	ASTM-D-1929	deg. Fahrenheit	0.35	0.35
Specific Heat @ 77°F	DuPont 900 (Therm.An. Cal.)[4]	BTU/(Lb.) (deg. F)	27**	27**
Smoke Density	ASTM-D-2843	%		
Electrical Properties				
Dielectric Strength	ASTM-D149	volts/mil.	430**	
Short Time Test		(1/8" thickness)		
Dielectric Constant	ASTM-D150	-		ADDITIONAL DATA CODES AND APPROVALS ARE AVAILABLE UPON REQUEST.
60 Cycles			3.5	
1,000 Cycles			3.2	
1,000,000 Cycles			2.7	
Dissipation Factor	ASTM-D150	-		Asterisked (*) values will change with thickness. Difference in length and width, as measured at room temperature, before and after heating above 300 deg. F. ** Varies with thickness.
60 Cycles			0.06	
1,000 Cycles			0.04	
1,000,000 Cycles			0.02	
Power Factor	ASTM-D150	-		
60 Cycles			0.06	
1,000 Cycles			0.04	
1,000,000 Cycles			0.02	
Loss Factor	ASTM-D150	-		
60 Cycles			0.21	
1,000 Cycles			0.13	
1,000,000 Cycles			0.06	
Arc Resistance	ASTM-D495	-	No Tracking	
Volume	ASTM-D257	ohm-cm.	1.6x1016	
Surface Resistivity	ASTM-D257	ohms	1.9x1015	

Appendix C: System Pressure Model

Fluidic Flywheel System Pressure Model

Input Variables

Maximum Pressure
Assume: Pump can continuously output

$$P_{max} := 250 \cdot psi$$

Cylinder Dimensions

Inner Chamber radius of accumulator

Assume: 6 in diam pipe with 3/4 in walls

$$r_0 := 2.25 in$$

Assume: Length of accumulator is 12 in and piston thickness is 1/2 in

Estimate: Piston position

Axial length of gas volume

$$l_g := 5.5 in$$

Find hydraulic fluid volume length from gas length and accum length

Axial length of hydraulic fluid volume

$$l_h := 8.5 in - l_g = 3 \cdot in$$

Density

Density of fluid

$$\rho := 876 \cdot \frac{kg}{m^3}$$

Angular Velocity

$$\omega := 3000 rpm$$

Precharge Pressure

Assume: precharge is 1/2 max pressure

$$P_{charge} := 0.5 P_{max} = 125 \cdot psi$$

Pressure Equations

Gas Pressure

$$P_{gas} = P_{charge} \cdot \left(\frac{l_g + l_h}{l_g} \right)$$

System Sressure

$$P_s = P_{gas} - \frac{\rho \cdot \omega^2 \cdot (r_0)^2}{4}$$

Pressure as a function of radius

$$P(r) = \frac{\rho \cdot \omega^2 \cdot r^2}{2} + P_s$$

Max Pressure at walls

$$P(r_0)$$

Difference in Pressure

$$\Delta P = P(r_0) - P_s$$

Calculation

Gas Pressure

$$P_{gas} := P_{charge} \cdot \left(\frac{l_g + l_h}{l_g} \right) \qquad P_{gas} = 193.182 psi$$

System Sressure

$$P_s := P_{gas} - \frac{\rho \cdot \omega^2 \cdot (r_0)^2}{4} = 182.943 psi$$

Pressure as a function of radius

$$P(r) := \left(\frac{\rho \cdot \omega^2 \cdot r^2}{2} + P_s \right)$$

Max Pressure at walls

$$P(r_0) = 203.421 psi$$

Difference in Pressure

$$\Delta P := P(r_0) - P_s = 20.478 psi$$

Pressure Profile Graph

$r := 0in, 0.001r_0 .. r_0$

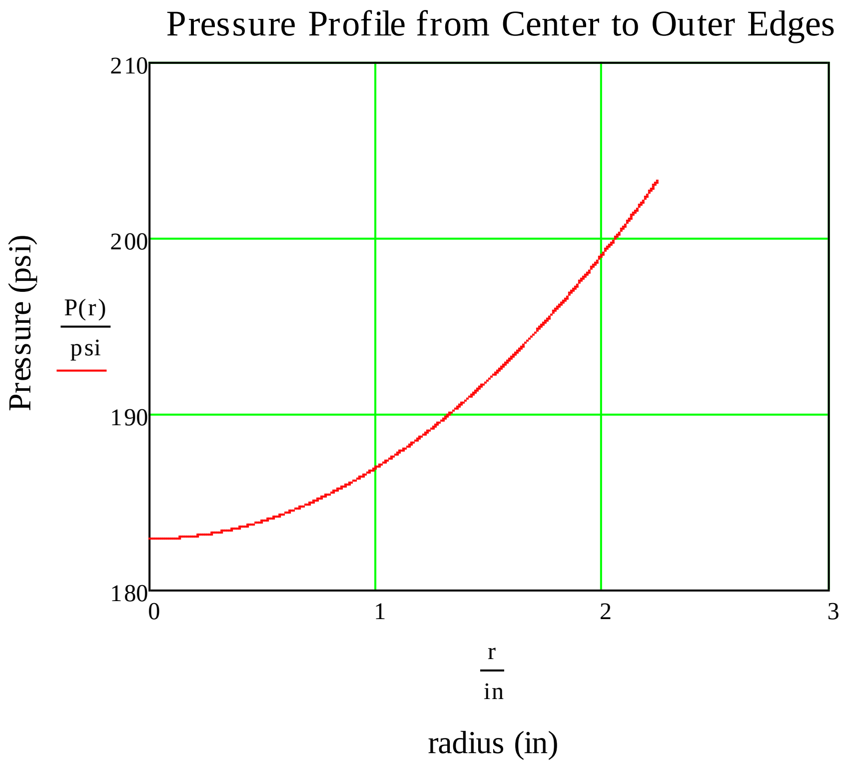

Appendix D: Chamber Selection Tables

Analysis of Pressure Chamber (7" OD x 1")												
Angular Velocity	**Working Pressure (psi)**											
	600			**500**			**400**			**300**		
ω (rpm)	**Safety Factor**	**ΔP (psi)**	**Radial Strain (in)**	**Safety Factor**	**ΔP (psi)**	**Radial Strain (in)**	**Safety Factor**	**ΔP (psi)**	**Radial Strain (in)**	**Safety Factor**	**ΔP (psi)**	**Radial Strain (in)**
1000	2.831	2.809	0.011	3.394	2.809	9.149*10^-3	4.236	2.809	7.335*10^-3	5.634	2.809	5.522*10^-3
1500	2.814	6.32	0.011	3.369	6.32	9.249*10^-3	4.196	6.32	7.436*10^-3	5.564	6.32	5.622*10^-3
2000	2.789	11.236	0.011	3.333	11.236	9.39*10^-3	4.142	11.236	7.576*10^-3	5.467	11.236	5.763*10^-3
2500	2.758	17.557	0.011	3.289	17.557	9.571*10^-3	4.073	17.557	7.757*10^-3	5.347	17.557	5.944*10^-3
3000	2.72	25.281	0.012	3.235	25.281	9.792*10^-3	3.991	25.281	7.978*10^-3	5.206	25.281	6.165*10^-3
3500	2.677	34.411	0.012	3.174	34.411	0.01	3.898	34.411	8.24*10^-3	5.047	34.411	6.426*10^-3
4000	2.628	44.945	0.012	3.106	44.945	0.01	3.794	44.945	8.541*10^-3	4.874	44.945	6.727*10^-3

Analysis of Pressure Chamber (7" OD x 3/4")												
Angular Velocity	**Working Pressure (psi)**											
	600			**500**			**400**			**300**		
ω (rpm)	**Safety Factor**	**ΔP (psi)**	**Radial Strain (in)**	**Safety Factor**	**ΔP (psi)**	**Radial Strain (in)**	**Safety Factor**	**ΔP (psi)**	**Radial Strain (in)**	**Safety Factor**	**ΔP (psi)**	**Radial Strain (in)**
1000	2.214	3.399	0.016	2.655	3.399	0.014	3.315	3.399	0.011	4.411	3.399	8.295*10^-3
1500	2.204	7.648	0.017	2.64	7.648	0.014	3.291	7.648	0.011	4.368	7.648	8.407*10^-3
2000	2.188	13.596	0.017	2.618	13.596	0.014	3.257	13.596	0.011	4.309	13.596	8.565*10^-3
2500	2.169	21.243	0.017	2.59	21.243	0.014	3.214	21.243	0.012	4.234	21.243	8.768*10^-3
3000	2.146	30.591	0.017	2.557	30.591	0.014	3.163	30.591	0.012	4.146	30.591	9.016*10^-3
3500	2.119	41.637	0.018	2.519	41.637	0.015	3.105	41.637	0.012	4.045	41.637	9.308*10^-3
4000	2.089	54.383	0.018	2.476	54.383	0.015	3.039	54.383	0.012	3.933	54.383	9.646*10^-3

Analysis of Pressure Chamber (6" OD x 1")												
Angular Velocity	**Working Pressure (psi)**											
	600			**500**			**400**			**300**		
ω (rpm)	**Safety Factor**	**ΔP (psi)**	**Radial Strain (in)**	**Safety Factor**	**ΔP (psi)**	**Radial Strain (in)**	**Safety Factor**	**ΔP (psi)**	**Radial Strain (in)**	**Safety Factor**	**ΔP (psi)**	**Radial Strain (in)**
1000	3.214	1.798	7.388*10^-3	3.854	1.798	6.164*10^-3	4.811	1.798	4.941*10^-3	6.401	1.798	3.717*10^-3
1500	3.197	4.045	7.446*10^-3	3.83	4.045	6.223*10^-3	4.773	4.045	4.999*10^-3	6.335	4.045	3.776*10^-3
2000	3.174	7.191	7.528*10^-3	3.796	7.191	6.304*10^-3	4.721	7.191	5.081*10^-3	6.243	7.191	3.857*10^-3
2500	3.144	11.236	7.633*10^-3	3.753	11.236	6.41*10^-3	4.656	11.236	5.186*10^-3	6.128	11.236	3.962*10^-3
3000	3.108	16.18	7.761*10^-3	3.703	16.18	6.538*10^-3	4.577	16.18	5.314*10^-3	5.992	16.18	4.091*10^-3
3500	3.067	22.023	7.913*10^-3	3.644	22.023	6.69*10-3	4.487	22.023	5.466*10^-3	5.838	22.023	4.243*10^-3
4000	3.02	28.765	8.088*10^-3	3.578	28.765	6.865*10^-3	4.387	28.765	5.641*10^-3	5.668	28.765	4.418*10^-3

Analysis of Pressure Chamber (6" OD x 3/4")												
Angular Velocity	**Working Pressure (psi)**											
	600			**500**			**400**			**300**		
ω (rpm)	**Safety Factor**	**ΔP (psi)**	**Radial Strain (in)**	**Safety Factor**	**ΔP (psi)**	**Radial Strain (in)**	**Safety Factor**	**ΔP (psi)**	**Radial Strain (in)**	**Safety Factor**	**ΔP (psi)**	**Radial Strain (in)**
1000	2.533	2.275	0.011	3.038	2.275	9.507*10^-3	3.794	2.275	7.617*10^-3	5.05	2.275	5.726*10^-3
1500	2.523	5.119	0.011	3.023	5.119	9.574*10^-3	3.77	5.119	7.684*10^-3	5.008	5.119	5.793*10^-3
2000	2.508	9.101	0.012	3.002	9.101	9.668*10^-3	3.738	9.101	7.778*10^-3	4.951	9.101	5.887*10^-3
2500	2.49	14.221	0.012	2.976	14.221	9.789*10^-3	3.697	14.221	7.898*10^-3	4.879	14.221	6.008*10^-3
3000	2.467	20.478	0.012	2.943	20.478	9.937*10^-3	3.647	20.478	8.046*10^-3	4.792	20.478	6.155*10^-3
3500	2.441	27.873	0.012	2.906	27.873	0.01	3.59	27.873	8.22*10^-3	4.694	27.873	6.329*10^-3
4000	2.412	36.405	0.012	2.864	36.405	0.01	3.526	36.405	8.421*10^-3	4.584	36.405	6.531*10^-3

Failure Modes	
	Safety
	Low ΔP

Appendix E: Bolt Preload Calculation

Flywheel Accumulator

Preload Torque for End Cap Tie Rods

1/4-20 Zinc Plated Bolts Grade 2 UNC

Known Values:

Tensile Area	Coefficient of Friction	Bolt Diameter	Proof Strength
$A_t := 0.032\,in^2$	$K_i := 0.22$	$d := 0.25\,in$	$S_p := 55\,ksi$

Preload Force:

$$F_i := 0.9\,S_p \cdot A_t = 1.584 \times 10^3\,lbf$$

Preload Torque:

$$T_i := K_i \cdot F_i \cdot d = 87.12\,in \cdot lbf$$

Appendix F: Bolt Loading

Tie Rod Loading

Known Values

Tensile Area

$A_t := 0.032\,in^2$

Coefficient of Friction

$K_i := 0.2$

Bolt Diameter

$d := 0.25\,in$

Proof Strength

$S_p := 55\,ksi$

Number of Bolts

$n := 8$

Young's Modulus (Al)

$E := 71\,GPa = 1.03 \times 10^4 \cdot ksi$

Aluminum Constants

$b := 0.6381$

$A := 0.7967$

Preload Force

$$F_i := 0.9\,S_p \cdot A_t = 1.584 \times 10^3 \cdot lbf$$

Bolt Loading

Length of Clamp Zone

$l_t := 13.19\,in$

Stiffness of the Bolt

$$k_b := \frac{1}{\left(\frac{l_t}{A_t \cdot E}\right)} = 2.498 \times 10^4 \cdot \frac{lbf}{in}$$

Stiffness of the End Caps

$$k_m := d \cdot E \cdot A \cdot e^{b \cdot \left(\frac{d}{l_t}\right)} = 2.076 \times 10^6 \cdot \frac{lbf}{in}$$

Stiffness Constant

$$C := \frac{k_b}{k_m + k_b} = 0.012$$

Portion of Loads in Bolt and Material

$P_b := C \cdot F_i = 18.836\,lbf$

$P_b = 83.785\,N$

$P_m := (1 - C) \cdot F_i = 1.565 \times 10^3 \cdot lbf$

Appendix G: Shaft Calculations

Units: $ksi := 10^3 psi$

Safety Factor $N := 1.7$

Material: Steel 1018 carbon

$S_y := 44ksi$ $S_{ut} := 60ksi$ $S'_e := 0.5S_{ut}$

$\omega := 314.159\frac{rad}{s}$

Offset: $r_s := 0.125in$

Fillet: $r_f := 0.0625in$

$d_{in} := 0.2in$ $d_{hex} := 0.96in$ $r_{in} := \frac{d_{in}}{2}$

Max fluid volume: $V_c := 0.0023456m^3$

Lengths: $L_{hex} := 1in$ $L_2 := 1.5in$ $L := L_{hex} + L_2 = 2.5in$

$x := 0, 0.01L..L$ $S(x,z) := if(x \geq z, 1, 0)$

Masses: $m_a := 3.5lb + 3.5lb + 6lb + 2lb + 2lb = 7.711kg$

$m_f := 879\frac{kg}{m^3}V_c = 2.062kg$ $m := m_a + m_f = 9.773kg$

Acceleration: $a_c := \omega^2 r_s = 313.359\frac{m}{s^2}$

Reaction Forces: $F_s := m a_c = 3.062\times 10^3 N$ $R := \frac{F_s}{2} = 1.531\times 10^3 N$

Moment and Torque: $M_a := R L_{hex} = 38.893J$ $T_{max} := 0$

Load $C_{load} := 1$ (Bending)

Size $C_{size}(d) := 0.869\left(\frac{d}{in}\right)^{-0.097}$ (Diameter between 0.3 and 10 in)

Surface $A_s := 2.7$ $b'_s := -0.265$ (Machined)

$$C_{surf} := A_s\left(\frac{S_{ut}}{ksi}\right)^{b'_s} \qquad C_{surf} = 0.912$$

Temperature $C_{temp} := 1$

Reliability $C_{reliab} := 0.814$ (R = 99%)

$$S_e(d) := C_{load}\, C_{size}(d)\, C_{surf}\, C_{temp}\, C_{reliab}\, S'_e$$

$$Frac(d) := \frac{d_{hex}}{d}$$

$$A(d) := \frac{Frac(d) - 1.2}{1.5 - 1.2}(0.93836 - 0.97098) + 0.97098$$

$$b(d) := \frac{Frac(d) - 1.2}{1.5 - 1.2}(-0.25759 + 0.21796) - 0.21796$$

$$K_t(d) := A(d)\left(\frac{r_f}{d}\right)^{b(d)}$$

Guess $d := 1in$

Given $$S_e(d) = \frac{M_a\left(\frac{d}{2}\right)}{\frac{\pi}{4}\left[\left(\frac{d}{2}\right)^4 - r_{in}^{\,4}\right]} N\,K_t(d)$$

$d := Find(d)$ $\qquad$ $d = 0.8in$

$Frac(d) = 1.2$

$A(d) = 0.971$ $\qquad$ $b(d) = -0.218$

$K_t(d) = 1.693$

Check:

Guess $d := 1in$

Given $$d = \left[\frac{32N}{\pi}\left(K_t(d)\,\frac{M_a}{S_e(d)}\right)\right]^{\frac{1}{3}}$$

$d := Find(d)$ $\qquad$ $d = 0.799in$

Appendix H: Tolerance Charts

From: SKF Bearing Catalog

Table 12
Shaft Bearing-Seat Diameters (Values in Inches)

Bearing Bore Diameter	Inches		g6 Shaft Dia.		Fit in 0.0001"	h6 Shaft Dia.		Fit in 0.0001"	h5 Shaft Dia.		Fit in 0.0001"	j5 Shaft Dia.		Fit in 0.0001"	j6 Shaft Dia.		Fit in 0.0001"	k5 Shaft Dia.		Fit in 0.0001"
mm	Max.	Min.	Max.	Min.		Max.	Min.		Max.	Min.		Max.	Min.		Max.	Min.		Max.	Min.	
4	0.1575	0.1572	0.1573	0.1570	5L 1T	0.1575	0.1572	3L 3T	0.1575	0.1573	2L 3T	0.1576	0.1574	1L 4T	0.1577	0.1574	1L 5T	0.1577	0.1575	0T 5T
5	0.1969	0.1966	0.1967	0.1964		0.1969	0.1966		0.1969	0.1967		0.1970	0.1968		0.1971	0.1968		0.1971	0.1969	
6	0.2362	0.2359	0.2360	0.2357		0.2362	0.2359		0.2362	0.2360		0.2363	0.2361		0.2364	0.2361		0.2364	0.2362	
7	0.2756	0.2753	0.2754	0.2750	6L 1T	0.2756	0.2752	4L 3T	0.2756	0.2754	2L 3T	0.2758	0.2755	1L 5T	0.2759	0.2755	1L 6T	0.2759	0.2756	0T 6T
8	0.3150	0.3147	0.3148	0.3144		0.3150	0.3146		0.3150	0.3148		0.3152	0.3149		0.3153	0.3149		0.3153	0.3150	
9	0.3543	0.3540	0.3541	0.3537		0.3543	0.3539		0.3543	0.3541		0.3545	0.3542		0.3546	0.3542		0.3546	0.3543	
10	0.3937	0.3934	0.3935	0.3931		0.3937	0.3933		0.3937	0.3935		0.3939	0.3936		0.3940	0.3936		0.3940	0.3937	
12	0.4724	0.4721	0.4722	0.4717	7L 1T	0.4724	0.4720	4L 3T	0.4724	0.4721	3L 3T	0.4726	0.4723	1L 5T	0.4727	0.4723	1L 6T	0.4728	0.4724	0T 7T
15	0.5906	0.5903	0.5904	0.5899		0.5906	0.5902		0.5906	0.5903		0.5908	0.5905		0.5909	0.5905		0.5910	0.5906	
17	0.6693	0.6690	0.6691	0.6686		0.6693	0.6689		0.6693	0.6690		0.6695	0.6692		0.6696	0.6692		0.6697	0.6693	
20	0.7874	0.7870	0.7871	0.7866	8L 1T	0.7874	0.7869	5L 4T	0.7874	0.7870	4L 4T	0.7876	0.7872	2L 6T	0.7878	0.7872	2L 8T	0.7878	0.7875	1T 8T
25	0.9843	0.9839	0.9840	0.9835		0.9843	0.9838		0.9843	0.9839		0.9845	0.9841		0.9847	0.9841		0.9847	0.9844	
30	1.1811	1.1807	1.1808	1.1803		1.1811	1.1806		1.1811	1.1807		1.1813	1.1809		1.1815	1.1809		1.1815	1.1812	
35	1.3780	1.3775	1.3776	1.3770	10L 1T	1.3780	1.3774	6L 5T	1.3780	1.3776	4L 5T	1.3782	1.3778	2L 7T	1.3784	1.3778	2L 9T	1.3785	1.3781	1T 10T
40	1.5748	1.5743	1.5744	1.5738		1.5748	1.5742		1.5748	1.5744		1.5750	1.5746		1.5752	1.5746		1.5753	1.5749	
45	1.7717	1.7712	1.7713	1.7707		1.7717	1.7711		1.7717	1.7713		1.7719	1.7716		1.7721	1.7715		1.7722	1.7718	
50	1.9685	1.9680	1.9681	1.9675		1.9685	1.9679		1.9685	1.9681		1.9687	1.9683		1.9689	1.9683		1.9690	1.9686	
55	2.1654	2.1648	2.1650	2.1643	11L 2T	2.1654	2.1647	7L 6T	2.1654	2.1649	5L 6T	2.1656	2.1651	3L 8T	2.1658	2.1651	3L 11T	2.1660	2.1655	1T 12T
60	2.3622	2.3616	2.3618	2.3611		2.3622	2.3615		2.3622	2.3617		2.3624	2.3619		2.3626	2.3619		2.3628	2.3623	
65	2.5591	2.5585	2.5587	2.5580		2.5591	2.5584		2.5591	2.5586		2.5593	2.5588		2.5595	2.5588		2.5597	2.5592	
70	2.7559	2.7553	2.7555	2.7548		2.7559	2.7552		2.7559	2.7554		2.7561	2.7556		2.7563	2.7556		2.7565	2.7560	
75	2.9528	2.9522	2.9524	2.9517		2.9528	2.9521		2.9528	2.9523		2.9530	2.9525		2.9532	2.9525		2.9534	2.9529	
80	3.1496	3.1490	3.1492	3.1485		3.1496	3.1489		3.1496	3.1491		3.1498	3.1493		3.1500	3.1493		3.1502	3.1497	
85	3.3465	3.3457	3.3460	3.3452	13L 3T	3.3465	3.3456	9L 8T	3.3465	3.3459	6L 8T	3.3467	3.3461	4L 10T	3.3470	3.3461	4L 13T	3.3472	3.3466	1T 15T
90	3.5433	3.5425	3.5428	3.5420		3.5433	3.5424		3.5433	3.5427		3.5435	3.5429		3.5438	3.5429		3.5440	3.5434	
95	3.7402	3.7394	3.7397	3.7389		3.7402	3.7393		3.7402	3.7396		3.7404	3.7398		3.7407	3.7398		3.7409	3.7403	
100	3.9370	3.9362	3.9365	3.9357		3.9370	3.9361		3.9370	3.9364		3.9372	3.9366		3.9375	3.9366		3.9377	3.9371	
105	4.1339	4.1331	4.1334	4.1326		4.1339	4.1330		4.1339	4.1333		4.1341	4.1335		4.1344	4.1335		4.1346	4.1340	
110	4.3307	4.3299	4.3302	4.3294		4.3307	4.3298		4.3307	4.3301		4.3309	4.3303		4.3312	4.3303		4.3314	4.3308	
115	4.5276	4.5268	4.5271	4.5263		4.5276	4.5267		4.5276	4.5270		4.5278	4.5272		4.5281	4.5272		4.5283	4.5277	
120	4.7244	4.7236	4.7239	4.7231		4.7244	4.7235		4.7244	4.7238		4.7246	4.7240		4.7249	4.7240		4.7251	4.7245	
125	4.9213	4.9203	4.9207	4.9198	15L 4T	4.9213	4.9203	10L 10T	4.9213	4.9206	7L 10T	4.9216	4.9209	4L 13T	4.9219	4.9209	4L 16T	4.9221	4.9214	1T 18T
130	5.1181	5.1171	5.1175	5.1166		5.1181	5.1171		5.1181	5.1174		5.1184	5.1177		5.1187	5.1177		5.1189	5.1182	
140	5.5118	5.5108	5.5112	5.5103		5.5118	5.5108		5.5118	5.5111		5.5121	5.5114		5.5124	5.5114		5.5126	5.5119	
150	5.9055	5.9045	5.9049	5.9040		5.9055	5.9045		5.9055	5.9048		5.9058	5.9051		5.9061	5.9051		5.9063	5.9056	
160	6.2992	6.2982	6.2986	6.2977		6.2992	6.2982		6.2992	6.2985		6.2995	6.2988		6.2998	6.2988		6.3000	6.2993	
170	6.6929	6.6919	6.6923	6.6914		6.6929	6.6919		6.6929	6.6922		6.6932	6.6925		6.6935	6.6925		6.6937	6.6930	
180	7.0866	7.0856	7.0860	7.0851		7.0866	7.0856		7.0866	7.0859		7.0869	7.0862		7.0872	7.0862		7.0874	7.0867	
190	7.4803	7.4791	7.4797	7.4786	17L 6T	7.4803	7.4792	11L 12T	7.4803	7.4795	8L 12T	7.4806	7.4798	5L 15T	7.4809	7.4798	5L 18T	7.4812	7.4805	2T 21T
200	7.8740	7.8728	7.8734	7.9823		7.8740	7.3729		7.8740	7.8732		7.8743	7.3735		7.8746	7.8735		7.8749	7.8742	
220	8.6614	8.6602	8.6608	8.6597		8.6614	8.6600		8.6614	8.6606		8.6617	8.6609		8.6620	8.6609		8.6623	8.6616	
240	9.4488	9.4476	9.4482	9.4471		9.4492	9.4477		9.4488	9.4480		9.4491	9.4483		9.4494	9.4483		9.4497	9.4490	
250	9.8425	9.8413	9.8419	9.8408		9.8425	9.8414		9.8425	9.8417		9.8428	9.8420		9.8431	9.8420		9.8434	9.8427	
260	10.2362	10.2348	10.2355	10.2343	19L 7T	10.2362	10.2349	13L 14T	10.2362	10.2353	9L 14T	10.2365	10.2356	6L 17T	10.2368	10.2356	6L 20T	10.2373	10.2364	2T 25T
280	11.0236	11.0222	11.0229	11.0217		11.0236	11.0223		11.0236	11.0225		11.0239	11.0230		11.0241	11.0230		11.0247	11.0238	
300	11.8110	11.8096	11.8103	11.8091		11.8110	11.8097		11.8110	11.8101		11.8113	11.8104		11.8116	11.8104		11.8121	11.8112	
310	12.2047	12.2033	12.2040	12.2028		12.2047	12.2034		12.2047	12.2038		12.2050	12.2041		12.2053	12.2041		12.2058	12.2049	
320	12.5984	12.5968	12.5977	12.5963	21L 9T	12.5084	12.5970	14L 16T	12.5984	12.5974	10L 16T	12.5987	12.5977	7L *19T	12.5991	12.5977	7L 23T	12.5995	12.5986	2T 27T
340	13.3858	13.3842	13.3851	13.3837		13.3858	13.3844		13.3858	13.3848		13.3861	13.3851		13.3865	13.3851		13.3869	13.3860	
350	13.7795	13.7779	13.7788	13.7774		13.7795	13.7781		13.7794	13.7785		13.7798	13.7788		13.7802	13.7788		13.7806	13.7797	
360	14.1732	14.1716	14.1725	14.1711		14.1732	14.1718		14.1732	14.1722		14.1735	14.1725		14.1739	14.1725		14.1743	14.1734	
380	14.9606	14.9590	14.9599	14.9585		14.9616	14.9592		14.9616	14.9596		14.9609	14.9599		14.9613	14.9599		14.9617	14.9608	
400	15.7480	15.7464	15.7473	15.7459		15.7480	15.7466		15.7480	15.7464		15.7483	15.7473		15.7487	15.7473		15.7491	15.7482	
420	16.5354	16.5336	16.5346	16.5330	24L 10T	16.5354	16.5338	16L 18T	16.5354	16.5343	11L 18T	16.5357	16.5346	8L 21T	16.5362	16.5346	8L 26T	16.5367	16.5356	2T 31T
440	17.3228	17.3210	17.3220	17.3186		17.3226	17.3212		17.3228	17.3217		17.3231	17.3220		17.3236	17.3220		17.3241	17.3230	
460	18.1102	18.1084	18.1094	18.1080		18.1102	18.1086		18.1102	18.1091		18.1105	18.1094		18.1110	18.1094		18.1115	18.1104	
480	18.8976	18.8958	18.8968	18.8952		18.8976	18.8960		18.8976	18.8965		18.8979	18.8968		18.8984	18.8968		18.8989	18.8978	
500	19.6850	19.6832	19.6842	19.6826		19.6850	19.6834		19.6850	19.6839		19.6853	19.6842		19.6858	19.6842		19.6863	19.6852	
530	20.8661	20.8641	20.8652	20.8635	26L 11T	20.8661	20.8644	17L 20T							20.8670	20.8652	9L 29T	20.8673	20.8661	0T 32T
560	22.0472	22.0452	22.0463	22.0446		22.0472	22.0455								22.0481	22.0461		22.0484	22.0472	
600	23.6220	23.6200	23.6211	23.6194		23.6220	23.6203								23.6229	23.6211		23.6232	23.6220	
630	24.8031	24.8011	24.8022	24.8005		24.8031	24.8614								24.8040	24.8012		24.8063	24.8031	
660	25.9843	25.9813	25.9834	25.9814	29L 21T	25.9833	25.9823	20L 30T							25.9853	25.9833	10L 40T	25.9857	25.9843	0T 44T
670	26.3780	26.3750	26.3771	27.3751		26.3780	26.3760								26.3790	26.3770		26.3794	26.3780	
710	27.9528	27.9498	27.9519	27.9499		27.9528	27.9508								27.9538	27.9518		27.9542	27.9528	
750	29.5276	29.5246	29.5267	29.5247		29.5276	29.5256								29.5316	29.5266		29.5290	29.5276	
780	30.7087	30.7057	30.7078	30.7058		30.7087	20.7067								30.7127	30.7077		30.7101	30.7087	
800	31.4961	31.4931	31.4952	31.4932		31.4962	31.4941								31.5001	31.4961		31.4975	31.4961	
850	33.4646	33.4607	33.4636	33.4614	32L 29T	33.4645	33.4624	22L 39T							33.4657	33.4635	11L 50T	33.4662	33.4646	0T 55T
900	35.4331	35.4292	35.4321	35.4299		35.4331	35.4309								35.4342	35.4320		35.4347	35.4331	
950	37.4016	37.3977	37.4006	37.3984		37.4016	37.3994								37.4066	35.4005		37.4032	37.4016	
1000	39.3701	39.3662	39.3691	39.3669		39.3701	39.3679								39.3751	39.3690		39.3717	39.3701	
1060	41.7323	41.7274	41.7312	41.7286	37L 38T	41.7323	41.7297	26L 49T							41.7385	41.7310	13L 62T	41.7341	41.7323	0T 67T
1120	44.0945	44.0896	44.0934	44.0908		44.0945	44.0919								44.1007	44.0937		44.0963	44.0946	
1180	46.4567	46.4518	46.4556	46.4530		46.4227	46.4541								46.4629	46.4554		46.4585	46.4567	
1250	49.2126	49.2077	49.2115	49.2089		49.2126	49.2100								49.2188	49.2113		49.2144	49.2126	

Table 12 (Continued)
Shaft Bearing-Seat Diameters (Values in Inches)

Brg. Bore Dia.	k6 Shaft Dia.		Fit in 0.0001"	m5 Shaft Dia.		Fit in 0.0001"	m6 Shaft Dia.		Fit in 0.0001"	n6 Shaft Dia.		Fit in 0.0001"	p6 Shaft Dia.		Fit in 0.0001"	r6 Shaft Dia.		Fit in 0.0001"	r7 Shaft Dia.		Fit in 0.0001"
	Max.	Min.		Max.	Min.		Max.	Min.		Max.	Min.		Max.	Min.		Max.	Min.		Max.	Min.	
4	0.1579	0.1575	0T 7T	0.1579	0.1577	2T 7T	0.1580	0.1577	2T 8T	0.1581	0.1578	3T 9T									
5	0.1973	0.1969		0.1973	0.1971		0.1974	0.1971		0.1975	0.1972										
6	0.2363	0.2362		0.2363	0.2364		0.2364	0.2364		0.2365	0.2366										
7	0.2760	0.2756	0T 7T	0.2761	0.2758	2T 9T	0.2762	0.2758	2T 9T	0.2763	0.2760	4T 10T									
8	0.3155	0.3150		0.3156	0.3152		0.3157	0.3152		0.3157	0.3154										
9	0.3547	0.3543		0.3548	0.3545		0.3549	0.3545		0.3550	0.3552										
10	0.3941	0.3937		0.3942	0.3938		0.3943	0.3939		0.3944	0.3946										
12	0.4729	0.4724	0T 8T	0.4730	0.4727	3T 9T	0.4731	0.4727	3T 10T	0.4733	0.4729	5T 12T									
15	0.5911	0.5906		0.5912	0.5908		0.5913	0.5909		0.5915	0.5911										
17	0.6698	0.6693		0.6699	0.6696		0.6700	0.6696		0.6702	0.6692										
20	0.7880	0.7875	1T 10T	0.7881	0.7877	3T 11T	0.7882	0.7877	3T 12T	0.7885	0.7880	6T 15T									
25	0.9849	0.9844		0.9850	0.9846		0.9851	0.9846		0.9854	0.9849										
30	1.1817	1.1812		1.1818	1.1814		1.1819	1.1814		1.1822	1.1817										
35	1.3787	1.3781	1T 12T	1.3788	1.3784	4T 13T	1.3790	1.3784	4T 15T	1.3793	1.3787	7T 18T									
40	1.5755	1.5749		1.5756	1.5752		1.5758	1.5752		1.5761	1.5655										
45	1.7724	1.7718		1.7725	1.7721		1.7727	1.7721		1.7730	1.7724										
50	1.9692	1.9686		1.9693	1.9689		1.9695	1.9689		1.9698	1.9692										
55	2.1662	2.1655	1T 14T	2.1664	2.1658	5T 15T	2.1666	2.1658	4T 18T	2.1668	2.1662	8T 21T									
60	2.3630	2.3623		2.3632	2.3627		2.3634	2.3626		2.3637	2.3630										
65	2.5599	2.5592		2.5601	2.5596		2.5603	2.5595		2.5606	2.5599										
70	2.7567	2.7560		2.7569	2.7564		2.7571	2.7563		2.7574	2.7567										
75	2.9536	2.9529		2.9538	2.9533		2.9540	2.9532		2.9543	2.9536										
80	3.1504	3.1497		3.1506	3.1501		3.1508	3.1500		3.1511	3.1504										
85	3.3475	3.3466	1T 18T	3.3476	3.3470	5T 19T	3.3479	3.3470	5T 22T	3.3483	3.3474	9T 26T	3.3488	3.3480	15T 31T						
90	3.5443	3.5434		3.5444	3.5438		3.5447	3.5438		3.5451	3.5442		3.5456	3.5448							
95	3.7412	3.7403		3.7413	3.7407		3.7416	3.7407		3.7420	3.7411		3.7425	3.7417							
100	3.9380	3.9371		3.9381	3.9375		3.9384	3.9375		3.9388	3.9379		3.9393	3.9385							
105	4.1349	4.1340		4.1350	4.1344		4.1353	4.1344		4.1357	4.1348		4.1364	4.1354							
110	4.3317	4.3308		4.3318	4.3312		4.3321	4.3312		4.3325	4.3316		4.3330	4.3322							
115	4.5286	4.5277		4.5287	4.5281		4.5290	4.5281		4.5294	4.5285		4.5299	4.5291							
120	4.7254	4.7245		4.7255	4.7249		4.7258	4.7249		4.7262	4.7253		4.7267	4.7259							
125	4.9224	4.9214	1T 21T	4.9226	4.9219	6T 23T	4.9229	4.9219	6T 26T	4.9233	4.9224	11T 30T	4.9240	4.9230	17T 37T	4.9248	4.9239	26T 45T			
130	5.1192	5.1182		5.1194	5.1187		5.1197	5.1187		5.1201	5.1192		5.1208	5.1198		5.1216	5.1207				
140	5.5129	5.5119		5.5131	5.5124		5.5134	5.5124		5.5138	5.5129		5.5145	5.5135		5.5153	5.5144				
150	5.9066	5.9056		5.9068	5.9061		5.9071	5.9061		5.9075	5.9066		5.9082	5.9072		5.9090	5.9081				
160	6.3003	6.2993		6.3005	6.2998		6.3008	6.2998		6.3012	6.3003		6.3019	6.3009		6.3027	6.3018				
170	6.6940	6.6930		6.6942	6.6935		6.6945	6.6935		6.6949	6.6940		6.6956	6.6946		6.6964	6.6955				
180	7.0877	7.0867		7.0879	7.0872		7.0882	7.0872		7.0886	7.0877		7.0893	7.0883		7.0901	7.0892				
190	7.4817	7.4805	2T 28T	7.4818	7.4810	7T 27T	7.4821	7.4810	7T 30T	7.4827	7.4815	12T 36T	7.4834	7.4823	20T 43T	7.4845	7.4833	30T 54T			
200	7.8754	7.8742		7.8755	7.8747		7.8758	7.8747		7.8764	7.8752		7.8771	7.8760		7.8782	7.8770				
220	8.6628	8.6616		8.6629	8.6621		8.6632	8.6621		8.6638	8.6626		8.6645	8.6634		8.6657	8.6645	31T 55T	8.6664	8.6645	31T 62T
240	9.4502	9.4490		9.4503	9.4495		9.4506	9.4495		9.4512	9.4500		9.4519	9.4508		9.4532	9.4521	33T 56T	9.4539	9.4521	33T 63T
250	9.8439	9.8427		9.8440	9.8432		9.8443	9.8432		9.8449	9.8437		9.8456	9.8445		9.8469	9.8458		9.8476	9.4858	
260	10.2376	10.2364	2T 28T	10.2379	10.2370	8T 31T	10.2382	10.2370	8T 34T	10.2388	10.2375	13T 40T	10.2397	10.2384	22T 49T	10.2412	10.2399	37T 64T	10.2419	10.2399	31T 71T
280	11.0250	11.0238		11.0253	11.0244		11.0256	11.0244		11.0262	11.0249		11.0271	11.0258		11.0286	11.0273		11.0293	11.0273	
300	11.8124	11.8112		11.8127	11.8118		11.8130	11.8118		11.8136	11.8123		11.8145	11.8132		11.8161	11.8149	39T 65T	11.8168	11.8149	39T 73T
310	12.2061	12.2049		12.2064	12.2055		12.2067	12.2055		12.2073	12.2060		12.2082	12.2069		12.2098	12.2086		12.2102	12.2086	
320	12.6000	12.5986	2T 32T	12.6002	12.5992	8T 34T	12.6006	12.5992	8T 38T	12.6013	12.5999	15T 45T	12.6023	12.6008	24T 55T	12.6041	12.6027	43T 73T	12.6049	12.6027	43T 81T
340	13.3874	13.3860		13.3876	13.3866		13.3880	13.3866		13.3887	13.3873		13.3987	13.3882		13.3915	13.3901		13.3923	13.3901	
350	13.7811	13.7797		13.7813	13.7803		13.7817	13.7803		13.7824	13.7810		13.7834	13.7819		13.7852	13.7838		13.7860	13.7838	
360	14.1748	14.1734		14.1750	14.1740		14.1754	14.1740		14.1761	14.1747		14.1771	14.1756		14.1791	14.1777	45T 75T	14.1799	14.1777	45T 83T
380	14.9622	14.9608		14.9624	14.9614		14.9628	14.9614		14.9635	14.9621		14.9645	14.9630		14.9665	14.9651		14.9673	14.9651	
400	15.7496	15.7482		15.7498	15.7488		15.7502	15.7488		15.7509	15.7495		15.7519	15.7504		15.7539	15.7525		15.7547	15.7525	
420	16.5372	16.5356	2T 36T	16.5374	16.5363	9T 38T	16.5379	16.5363	9T 43T	16.5385	16.5370	16T 49T	16.5397	16.5381	27T 61T	16.5419	16.5404	50T 83T	16.5428	16.5404	50T 92T
440	17.3246	17.3230		17.3248	17.3237		17.3253	17.3237		17.3259	17.3244		17.3271	17.3255		17.3293	17.3278		17.3302	17.3278	
460	18.1120	18.1104		18.1122	18.1111		18.1127	18.1111		18.1133	18.1118		18.1145	18.1129		18.1170	18.1154	52T 86T	18.1179	18.1154	52T 95T
480	18.8994	18.8978		18.8996	18.8985		18.9001	18.8985		18.9007	18.8992		18.9019	18.9003		18.9044	18.9028		18.9053	18.9028	
500	19.6873	19.6852		19.6870	19.6859		19.6875	19.6859		19.6881	19.6866		19.6893	19.6877		19.6918	19.6902		19.6927	19.6902	
530	20.8678	20.8661	0T 37T	20.8683	20.8671	10T 42T				20.8696	20.8678	17T 55T	20.8709	20.8692	31T 68T	20.8737	20.8720	59T 96T	20.8746	20.8720	59T 107T
560	22.0489	22.0472		22.0494	22.0482					22.0507	22.0489		22.0520	23.0503		22.0548	23.0531		22.0559	22.0531	
600	23.6237	23.6220		23.6242	23.6230					23.6255	23.6237		23.6268	23.6251		23.6298	23.6281	61T 98T	23.6309	23.6281	61T 109T
630	24.8048	24.8031		24.8053	24.8041					24.8066	24.8048		24.8079	24.8062		24.8109	24.8092		24.8120	24.8092	
660	25.9863	25.9843	0T 50T	25.9869	25.9855	12T 56T				25.9682	25.9663	20T 69T	25.9697	25.9678	35T 84T	25.9932	25.9912	69T 119T	25.9943	25.9912	69T 130T
670	26.3800	26.3780		26.3806	26.3792					26.3819	26.3800		26.3834	26.3815		26.3969	26.3949		26.3880	26.3849	
710	27.9448	27.9528		27.9554	27.9540					27.9567	27.9548		27.9582	27.9563		27.9617	27.9597		27.9626	27.9597	
750	29.5296	29.5276		29.5302	29.5288					29.5315	29.5296		29.5330	29.5311		29.5369	29.5549	73T 123T	29.5380	29.5349	73T 134T
780	30.7101	30.7087		30.7113	30.7099					30.7126	30.7107		30.7141	30.7122		30.7180	30.7160		30.7191	30.7160	
800	31.4982	31.4961		31.4987	31.4973					31.5000	31.4981		31.5015	31.4996		31.5054	31.5034		31.5065	31.5034	
850	33.4668	33.4646	0T 61T	33.4675	33.4659	13T 68T				33.4690	33.4668	22T 83T	33.4706	33.4685	39T 100T	33.4751	33.4729	83T 144T	33.4764	33.4729	83T 157T
900	35.4343	35.4331		35.4360	35.4344					35.4375	35.4343		35.4391	35.4370		35.4436	35.4414		35.4449	35.4414	
950	37.4038	37.4016		37.4045	37.4029					37.4060	37.4038		37.4076	37.4055		37.4125	37.4103	87T 148T	37.4138	37.4103	87T 161T
1000	39.3723	39.3701		39.3730	39.3714					39.3745	37.3723		39.3761	39.3740		39.3810	39.3788		39.3823	39.3788	
1060	41.7349	41.7323	0T 75T	41.7357	41.7339	16T 83T				41.7376	41.7359	26T 101T	41.7396	41.7370	47T 122T	41.7447	41.7421	98T 173T	41.7463	41.7421	98T 189T
1120	44.0971	44.0945		44.0979	44.0961					44.0997	44.0971		44.1017	44.0992		44.1069	44.1043		44.1085	44.1043	
1180	46.4593	46.4567		46.4601	46.4583					46.4619	46.4593		46.4639	46.4614		46.4694	46.4669	102T 177T	46.4710	46.4669	102T 193T
1250	49.2152	49.2126		49.2160	49.2142					49.2178	49.2152		49.2198	49.2173		49.2253	49.2228		49.2270	49.2228	

From: SKF Bearing Catalog

Table 11
Housing Bearing-Seat Diameters (Values in Inches)

Bearing Outside Diameter			F7			G7			H8			H7			H6		
mm	Inches		Housing Bore		Fit in 0.0001"	Housing Bore		Fit in 0.0001"	Housing Bore		Fit in 0.0001"	Housing Bore		Fit in 0.0001"	Housing Bore		Fit in 0.0001"
	Max.	Min.	Min.	Max.		Min.	Max.		Min.	Max.		Min.	Max.		Min.	Max.	
16	0.6299	0.6296	0.6305	0.6312	16L 6L	0.6301	0.6308	12L 2L	0.6299	0.6310	14L 0	0.6299	0.6306	10L 0	0.6299	0.6303	7L 0
19	0.7480	0.7476	0.7486	0.7496	20L 6L	0.7483	0.7491	15L 3L	0.7480	0.7492	17L 0	0.7480	0.7488	12L 0	0.7480	0.7485	9L 0
22	0.8661	0.8657	0.8669	0.8677		0.8664	0.8672		0.8661	0.8673		0.8661	0.8669		0.8661	0.8666	
24	0.9449	0.9445	0.9457	0.9465		0.9452	0.9460		0.9449	0.9461		0.9449	0.9457		0.9449	0.9454	
26	1.0236	1.0232	1.0244	1.0252		1.0239	1.0247		1.0236	1.0248		1.0236	1.0244		1.0236	1.0241	
28	1.1024	1.1020	1.1032	1.1040		1.1027	1.1035		1.1024	1.1036		1.1024	1.1032		1.1024	1.1029	
30	1.1811	1.1807	1.1819	1.1827		1.1814	1.1822		1.1811	1.1823		1.1811	1.1819		1.1811	1.1816	
32	1.2598	1.2594	1.2608	1.2619	24L 10L	1.2602	1.2611	17L 4L	1.2598	1.2613	19L 0	1.2598	1.2608	14L 0	1.2598	1.2604	10L 0
35	1.3780	1.3776	1.3790	1.3800		1.3784	1.3793		1.3780	1.3795		1.3780	1.3790		1.3780	1.3786	
37	1.4567	1.4563	1.4577	1.4587		1.4571	1.4580		1.4567	1.4582		1.4567	1.4577		1.4567	1.4573	
40	1.5748	1.5744	1.5758	1.5768		1.5752	1.5761		1.5748	1.5763		1.5748	1.5758		1.5748	1.5754	
42	1.6535	1.6531	1.6545	1.6555		1.6539	1.6548		1.6535	1.6550		1.6535	1.6545		1.6535	1.6541	
47	1.8504	1.8500	1.8514	1.8524		1.8508	1.8517		1.8504	1.8519		1.8504	1.8514		1.8504	1.8510	
52	2.0472	2.0467	2.0484	2.0496	29L 12L	2.0476	2.0488	21L 4L	2.0472	2.0490	23L 0	2.0472	2.0484	17L 0	2.0472	2.0479	12L 0
55	2.1654	2.1649	2.1666	2.1678		2.1658	2.1670		2.1654	2.1672		2.1654	2.1666		2.1654	2.1661	
62	2.4409	2.4404	2.4421	2.4433		2.4413	2.4425		2.4409	2.4427		2.4409	2.4421		2.4409	2.4416	
72	2.8346	2.8341	2.8358	2.8370		2.8350	2.8362		2.8346	2.8364		2.8346	2.8358		2.8346	2.8353	
80	3.1496	3.1491	3.1508	3.1520		3.1500	3.1512		3.1496	3.1514		3.1496	3.1508		3.1496	3.1503	
85	3.3465	3.3459	3.3479	3.3493	34L 14L	3.3470	3.3484	25L 5L	3.3465	3.3486	27L 0	3.3465	3.3479	20L 0	3.3465	3.3474	15L 0
90	3.5433	3.5427	3.5447	3.5461		3.5438	3.5452		3.5433	3.5454		3.5433	3.5447		3.5433	3.5442	
100	3.9370	3.9364	3.9384	3.9398		3.9375	3.9389		3.9370	3.9391		3.9370	3.9384		3.9370	3.9379	
110	4.3307	4.3301	4.3321	4.3335		4.3312	4.3326		4.3307	4.3328		4.3307	4.3321		4.3307	4.3316	
115	4.5276	4.5270	4.5290	4.5304		4.5281	4.5295		4.5276	4.5297		4.5276	4.5290		4.5276	4.5285	
120	4.7244	4.7238	4.7258	4.7272		4.7249	4.7263		4.7244	4.7265		4.7244	4.7258		4.7244	4.7253	
125	4.9213	4.9206	4.9230	4.9246	40L 17L	4.9219	4.9234	28L 6L	4.9213	4.9238	32L 0	4.9213	4.9229	23L 0	4.9213	4.9223	17L 0
130	5.1181	5.1174	5.1198	5.1214		5.1187	5.1202		5.1181	5.1206		5.1181	5.1197		5.1181	5.1191	
140	5.5118	5.5111	5.5135	5.5151		5.5124	5.5139		5.5118	5.5143		5.5118	5.5134		5.5118	5.5128	
145	5.7087	5.7080	5.7104	5.7120		5.7093	5.7108		5.7087	5.7112		5.7087	5.7103		5.7087	5.7097	
150	5.9055	5.9048	5.9072	5.9088		5.9061	5.9076		5.9055	5.9080		5.9055	5.9071		5.9055	5.9065	
160	6.2992	6.2982	6.3009	6.3025	43L 17L	6.2998	6.3013	31L 6L	6.2992	6.3017	35L 0	6.2992	6.3008	26L 0	6.2992	6.3002	20L 0
170	6.6929	6.6919	6.6946	6.6962		6.6935	6.6950		6.6929	6.6954		6.6929	6.6945		6.6929	6.6939	
180	7.0866	7.0856	7.0883	7.0899		7.0872	7.0887		7.0866	7.0891		7.0866	7.0882		7.0866	7.0876	
190	7.4803	7.4791	7.4823	7.4841	50L 20L	7.4809	7.4827	36L 6L	7.4803	7.4831	40L 0	7.4803	7.4821	30L 0	7.4803	7.4814	23L 0
200	7.8740	7.8728	7.8760	7.8778		7.8746	7.8764		7.8740	7.8768		7.8740	7.8758		7.8740	7.8751	
210	8.2677	8.2665	8.2697	8.2715		8.2683	8.2701		8.2677	8.2705		8.2677	8.2695		8.2677	8.2688	
215	8.4646	8.4634	8.4666	8.4684		8.4652	8.4670		8.4646	8.4674		8.4646	8.4664		8.4646	8.4657	
225	8.8583	8.8571	8.8603	8.8621		8.8589	8.8607		8.8583	8.8611		8.8583	8.8601		8.8583	8.8594	
240	9.4488	9.4476	9.4508	9.4526		9.4494	9.4512		9.4488	9.4516		9.4488	9.4506		9.4488	9.4499	
250	9.8425	9.8413	9.8445	9.8463		9.8431	9.8449		9.8425	9.8453		9.8425	9.8443		9.8425	9.8436	
260	10.2362	10.2348	10.2384	10.2405	57L 22L	10.2369	10.2389	41L 7L	10.2362	10.2394	46L 0	10.2362	10.2382	34L 0	10.2362	10.2375	27L 0
280	11.0236	11.0222	11.0258	11.0279		11.0243	11.0263		11.0236	11.0268		11.0236	11.0256		11.0236	11.0247	
300	11.8110	11.8096	11.8132	11.8153		11.8117	11.8137		11.8110	11.8142		11.8110	11.8130		11.8110	11.8123	
310	12.2047	12.2033	12.2069	12.2090		12.2054	12.2074		12.2047	12.2079		12.2047	12.2067		12.2047	12.2060	
320	12.5984	12.5968	12.6008	12.6031	63L 24L	12.5991	12.6014	46L 7L	12.5984	12.6019	51L 0	12.5984	12.6006	38L 0	12.5984	12.5998	30L 0
340	13.3858	13.3842	13.3882	13.3905		13.3865	13.3888		13.3858	13.3893		13.3858	13.3880		13.3858	13.3872	
360	14.1732	14.1716	14.1756	14.1779		14.1739	14.1762		14.1732	14.1767		14.1732	14.1754		14.1732	14.1746	
380	14.9606	14.9590	14.9630	14.9653		14.9613	14.9636		14.9606	14.9641		14.9606	14.9628		14.9606	14.9620	
400	15.7480	15.7464	15.7504	15.7527		15.7487	15.7510		15.7480	15.7515		15.7480	15.7502		15.7480	15.7494	
420	16.5354	16.5336	16.5381	16.5406	70L 27L	16.5362	16.5387	51L 8L	16.5354	16.5392	56L 0	16.5354	16.5379	43L 0	16.5354	16.5370	34L 0
440	17.3228	17.3210	17.3255	17.3280		17.3236	17.3261		17.3228	17.3266		17.3228	17.3253		17.3228	17.3244	
460	18.1102	18.1084	18.1129	18.1154		18.1110	18.1135		18.1102	18.1140		18.1102	18.1127		18.1102	18.1116	
480	18.8976	18.8958	18.9003	18.9028		18.8984	18.9009		18.8976	18.9014		18.8976	18.9001		18.8976	18.8990	
500	19.6850	19.6832	19.6877	19.6902		19.6858	19.6883		19.6850	19.6888		19.6850	19.6875		19.6850	19.6866	
520	20.4724	20.4704	20.4754	20.4781	77L 30L	20.4733	20.4760	56L 9L	20.4724	20.4767	63L 0	20.4724	20.4752	48L 0	20.4724	20.4741	37L 0
540	21.2598	21.2578	21.2628	21.2655		21.2607	21.2634		21.2598	21.2641		21.2598	21.2626		21.2598	21.2615	
580	22.8346	22.8326	22.8376	22.8403		22.8355	22.8382		22.8346	22.8389		22.8346	22.8374		22.8346	22.8363	
600	23.6220	23.6200	23.6250	23.6277		23.6229	23.6256		23.6220	23.6263		23.6220	23.6248		23.6220	23.6237	
620	24.4094	24.4074	24.4124	24.4151		24.4103	24.4130		24.4094	24.4137		24.4094	24.4122		24.4094	24.4111	
650	25.5906	25.5876	25.5937	25.5969	93L 31L	25.5915	25.5947	71L 9L	25.5906	25.5952	76L 0	25.5906	25.5937	61L 0	25.5906	25.5926	50L 0
670	26.3780	26.3750	26.3811	26.3843		26.3789	26.3821		26.3780	26.3826		26.3780	26.3811		26.3780	26.3800	
680	26.7717	26.7687	26.7748	26.7780		26.7726	26.7758		26.7717	26.7763		26.7717	26.7748		26.7717	26.7737	
700	27.5591	27.5561	27.5622	27.5654		27.5600	27.5632		27.5591	27.5637		27.5591	27.5622		27.5591	27.5611	
720	28.3465	28.3435	28.3496	28.3528		28.3474	28.3506		28.3465	28.3511		28.3465	28.3496		28.3465	28.3485	
750	29.5276	29.5246	29.5307	29.5339		29.5285	29.5317		29.5276	29.5322		29.5276	29.5307		29.5276	29.5296	
780	30.7087	30.7057	30.7118	30.7150		30.7096	30.7128		30.7087	30.7133		30.7087	30.7118		30.7087	30.7107	
790	31.1024	31.0994	31.1055	31.1087		31.1033	31.1065		31.1024	31.1070		31.1024	31.1055		31.1024	31.1044	
820	32.2835	32.2796	32.2869	32.2904	108L 34L	32.2845	32.2881	85L 10L	32.2835	32.2890	94L 0	32.2835	32.2870	74L 0	32.2835	32.2857	61L 0
850	33.4646	33.4607	33.4680	33.4715		33.4656	33.4692		33.4646	33.4701		33.4646	33.4681		33.4646	33.4668	
870	34.2520	34.2481	34.2554	34.2589		34.2530	34.2566		34.2520	34.2575		34.2520	34.2555		34.2520	34.2542	
920	36.2205	36.2166	36.2239	36.2274		36.2215	36.2251		36.2205	36.2260		36.2205	36.2240		36.2205	36.2227	
950	37.4016	37.3977	37.4050	37.4085		37.4026	37.4062		37.4016	37.4071		37.4016	37.4051		37.4016	37.4038	
980	38.5827	38.5788	38.5861	38.5896		38.5837	38.5873		38.5827	38.5882		38.5827	38.5862		38.5827	38.5849	
1000	39.3701	39.3662	39.3735	39.3770		39.3711	39.3747		39.3701	39.3756		39.3701	39.3736		39.3701	39.3715	
1150	45.2756	45.2707	45.2794	45.2836	129L 38L	45.2767	45.2808	101L 11L	45.2756	45.2821	114L 0	45.2756	45.2797	90L 0	45.2756	45.2782	75L 0
1250	49.2126	49.2077	49.2165	49.2206		49.2137	49.2178		49.2126	49.2191		49.2126	49.2167		49.2126	49.2152	
1400	55.1181	55.1118	55.1224	55.1274	156L 43L	55.1193	55.1244	126L 12L	55.1181	55.1258	140L 0	55.1181	55.1230	112L 0	55.1181	55.1212	94L 0
1600	62.9921	62.9858	62.9964	63.0014		62.9933	62.9984		62.9921	62.9998		62.9921	62.9970		62.9921	62.9952	
1800	70.8661	70.8582	70.8708	70.8767	185L 47L	70.8674	70.8733	151L 13L	70.8661	70.8752	170L 0	70.8661	70.8720	138L 0	70.8661	70.8697	115L 0
2000	78.7402	78.7323	78.7449	78.7508		78.7415	78.7474		78.7402	78.7493		78.7402	78.7461		78.7402	78.7438	
2300	90.5512	90.5414	90.5563	90.5632	218L 51L	90.5525	90.5594	180L 13L	90.5512	90.5622	208L 0	90.5512	90.5581	167L 0	90.5512	90.5555	141L 0
2500	98.4252	98.4154	98.4303	98.4372		98.4265	98.4334		98.4252	98.4362		98.4252	98.4321		98.4252	98.4295	

Table 11 (Continued)
Housing Bearing-Seat Diameters (Values in Inches)

Bearing Outside Diameter			J6			J7			K6			K7			M6		
mm	Inches		Housing Bore		Fit in 0.0001"	Housing Bore		Fit in 0.0001"	Housing Bore		Fit in 0.0001"	Housing Bore		Fit in 0.0001"	Housing Bore		Fit in 0.0001"
	Max.	Min.	Min.	Max.		Min.	Max.		Min.	Max.		Min.	Max.		Min.	Max.	
16	0.6299	0.6296	[illegible]	[illegible]	[illegible]	[illegible]	[illegible]	[illegible]	[illegible]	[illegible]	[illegible]	[illegible]	[illegible]	[illegible]	[illegible]	[illegible]	[illegible]
19	0.7480	0.7476	[illegible]	[illegible]	[illegible]	[illegible]	[illegible]	[illegible]	[illegible]	[illegible]	[illegible]	[illegible]	[illegible]	[illegible]	[illegible]	[illegible]	[illegible]
22	0.8661	0.8657	[illegible]	[illegible]		[illegible]	[illegible]		[illegible]	[illegible]		[illegible]	[illegible]		[illegible]	[illegible]	
24	0.9449	0.9445	[illegible]	[illegible]		[illegible]	[illegible]		[illegible]	[illegible]		[illegible]	[illegible]		[illegible]	[illegible]	
26	1.0236	1.0232	[illegible]	[illegible]		[illegible]	[illegible]		[illegible]	[illegible]		[illegible]	[illegible]		[illegible]	[illegible]	
28	1.1024	1.1020	[illegible]	[illegible]		[illegible]	[illegible]		[illegible]	[illegible]		[illegible]	[illegible]		[illegible]	[illegible]	
30	1.1811	1.1807	[illegible]	[illegible]		[illegible]	[illegible]		[illegible]	[illegible]		[illegible]	[illegible]		[illegible]	[illegible]	
32	1.2598	1.2594	[illegible]	[illegible]	[illegible]	[illegible]	[illegible]	[illegible]	[illegible]	[illegible]	[illegible]	[illegible]	[illegible]	[illegible]	[illegible]	[illegible]	[illegible]
35	1.3780	1.3776	[illegible]	[illegible]		[illegible]	[illegible]		[illegible]	[illegible]		[illegible]	[illegible]		[illegible]	[illegible]	
37	1.4567	1.4563	[illegible]	[illegible]		[illegible]	[illegible]		[illegible]	[illegible]		[illegible]	[illegible]		[illegible]	[illegible]	
40	1.5748	1.5744	[illegible]	[illegible]		[illegible]	[illegible]		[illegible]	[illegible]		[illegible]	[illegible]		[illegible]	[illegible]	
42	1.6535	1.6531	[illegible]	[illegible]		[illegible]	[illegible]		[illegible]	[illegible]		[illegible]	[illegible]		[illegible]	[illegible]	
47	1.8504	1.8500	[illegible]	[illegible]		[illegible]	[illegible]		[illegible]	[illegible]		[illegible]	[illegible]		[illegible]	[illegible]	
52	2.0472	2.0467	[illegible]	[illegible]	[illegible]	[illegible]	[illegible]	[illegible]	[illegible]	[illegible]	[illegible]	[illegible]	[illegible]	[illegible]	[illegible]	[illegible]	[illegible]
55	2.1654	2.1649	[illegible]	[illegible]		[illegible]	[illegible]		[illegible]	[illegible]		[illegible]	[illegible]		[illegible]	[illegible]	
62	2.4409	2.4404	[illegible]	[illegible]		[illegible]	[illegible]		[illegible]	[illegible]		[illegible]	[illegible]		[illegible]	[illegible]	
72	2.8346	2.8341	[illegible]	[illegible]		[illegible]	[illegible]		[illegible]	[illegible]		[illegible]	[illegible]		[illegible]	[illegible]	
80	3.1496	3.1491	[illegible]	[illegible]		[illegible]	[illegible]		[illegible]	[illegible]		[illegible]	[illegible]		[illegible]	[illegible]	
85	3.3465	3.3459	[illegible]	[illegible]	[illegible]	[illegible]	[illegible]	[illegible]	[illegible]	[illegible]	[illegible]	[illegible]	[illegible]	[illegible]	[illegible]	[illegible]	[illegible]
90	3.5433	3.5427	[illegible]	[illegible]		[illegible]	[illegible]		[illegible]	[illegible]		[illegible]	[illegible]		[illegible]	[illegible]	
100	3.9370	3.9364	[illegible]	[illegible]		[illegible]	[illegible]		[illegible]	[illegible]		[illegible]	[illegible]		[illegible]	[illegible]	
110	4.3307	4.3301	[illegible]	[illegible]		[illegible]	[illegible]		[illegible]	[illegible]		[illegible]	[illegible]		[illegible]	[illegible]	
115	4.5276	4.5270	[illegible]	[illegible]		[illegible]	[illegible]		[illegible]	[illegible]		[illegible]	[illegible]		[illegible]	[illegible]	
120	4.7244	4.7238	[illegible]	[illegible]		[illegible]	[illegible]		[illegible]	[illegible]		[illegible]	[illegible]		[illegible]	[illegible]	
125	4.9213	4.9206	[illegible]	[illegible]	[illegible]	[illegible]	[illegible]	[illegible]	[illegible]	[illegible]	[illegible]	[illegible]	[illegible]	[illegible]	[illegible]	[illegible]	[illegible]
130	5.1181	5.1174	[illegible]	[illegible]		[illegible]	[illegible]		[illegible]	[illegible]		[illegible]	[illegible]		[illegible]	[illegible]	
140	5.5118	5.5111	[illegible]	[illegible]		[illegible]	[illegible]		[illegible]	[illegible]		[illegible]	[illegible]		[illegible]	[illegible]	
145	5.7087	5.7080	[illegible]	[illegible]		[illegible]	[illegible]		[illegible]	[illegible]		[illegible]	[illegible]		[illegible]	[illegible]	
150	5.9055	5.9048	[illegible]	[illegible]		[illegible]	[illegible]		[illegible]	[illegible]		[illegible]	[illegible]		[illegible]	[illegible]	
160	6.2992	6.2982	[illegible]	[illegible]	[illegible]	[illegible]	[illegible]	[illegible]	[illegible]	[illegible]	[illegible]	[illegible]	[illegible]	[illegible]	[illegible]	[illegible]	[illegible]
170	6.6929	6.6919	[illegible]	[illegible]		[illegible]	[illegible]		[illegible]	[illegible]		[illegible]	[illegible]		[illegible]	[illegible]	
180	7.0866	7.0856	[illegible]	[illegible]		[illegible]	[illegible]		[illegible]	[illegible]		[illegible]	[illegible]		[illegible]	[illegible]	
190	7.4803	7.4791	7.4800	7.4812	21L 3T	7.4797	7.4815	24L 6T	7.4794	7.4805	14L 9T	7.4790	7.4808	17L 13T	7.4788	7.4800	9L 15T
200	7.8740	7.8728	7.8737	7.8749		7.8734	7.8752		7.8731	7.8742		7.8727	7.8745		7.8725	7.8737	
210	8.2677	8.2665	8.2674	8.2686		8.2671	8.2689		8.2668	8.2679		8.2664	8.2682		8.2662	8.2674	
215	8.4646	8.4634	8.4643	8.4655		8.4640	8.4658		8.4637	8.4648		8.4633	8.4651		8.4631	8.4643	
225	8.8583	8.8571	8.8580	8.8592		8.8577	8.8595		8.8574	8.8585		8.8570	8.8588		8.8568	8.8580	
240	9.4488	9.4476	9.4485	9.4497		9.4482	9.4500		9.4479	9.4490		9.4475	9.4493		9.4473	9.4485	
250	9.8425	9.8413	9.8422	9.8434		9.8419	9.8437		9.8416	9.8427		9.8412	9.8430		9.8410	9.8422	
260	10.2362	10.2348	10.2359	10.2372	24L 3T	10.2356	10.2376	28L 6T	10.2351	10.2364	16L 11T	10.2348	10.2368	20L 14T	10.2346	10.2358	10L 16T
280	11.0236	11.0222	11.0233	11.0246		11.0230	11.0250		11.0225	11.0238		11.0222	11.0242		11.0220	11.0232	
300	11.8110	11.8096	11.8107	11.8120		11.8104	11.8124		11.8099	11.8112		11.8096	11.8116		11.8094	11.8106	
310	12.2047	12.2033	12.2044	12.2057		12.2041	12.2061		12.2036	12.2049		12.2033	12.2053		12.2031	12.2043	
320	12.5984	12.5968	12.5981	12.5995	27L 3T	12.5977	12.5999	31L 7T	12.5973	12.5987	19L 11T	12.5968	12.5991	23L 16T	12.5966	12.5980	12L 18T
340	13.3858	13.3842	13.3855	13.3869		13.3851	13.3873		13.3847	13.3861		13.3842	13.3865		13.3840	13.3854	
360	14.1732	14.1716	14.1729	14.1743		14.1725	14.1747		14.1721	14.1735		14.1716	14.1739		14.1714	14.1728	
380	14.9606	14.9590	14.9603	14.9617		14.9599	14.9621		14.9595	14.9609		14.9590	14.9613		14.9588	14.9602	
400	15.7480	15.7464	15.7477	15.7491		15.7473	15.7495		15.7469	15.7483		15.7464	15.7487		15.7462	15.7476	
420	16.5354	16.5336	16.5351	16.5367	31L 3T	16.5346	16.5371	35L 8T	16.5341	16.5357	21L 13T	16.5336	16.5361	25L 18T	16.5334	16.5350	14L 20T
440	17.3228	17.3210	17.3225	17.3241		17.3220	17.3245		17.3215	17.3231		17.3210	17.3235		17.3208	17.3224	
460	18.1102	18.1084	18.1099	18.1115		18.1094	18.1119		18.1089	18.1105		18.1084	18.1109		18.1082	18.1098	
480	18.8976	18.8958	18.8973	18.8989		18.8968	18.8993		18.8963	18.8979		18.8958	18.8983		18.8956	18.8972	
500	19.6850	19.6832	19.6847	19.6863		19.6842	19.6867		19.6837	19.6853		19.6832	19.6857		19.6830	19.6846	
520	20.4724	20.4704	20.4721	20.4739	35L 3T	20.4716	20.4743	39L 9T	20.4707	20.4724	20L 17T	20.4698	20.4724	20L 26T	20.4702	20.4714	10L 22T
540	21.2598	21.2578	21.2595	21.2613		21.2590	21.2617		21.2581	21.2598		21.2572	21.2598		21.2576	21.2588	
580	22.8346	22.8326	22.8342	22.8361		22.8337	22.8365		22.8329	22.8346		22.8318	22.8346		22.8324	22.8336	
600	23.6220	23.6200	23.6217	23.6235		23.6211	23.6239		23.6203	23.6220		23.6192	23.6220		23.6198	23.6210	
620	24.4094	24.4074	24.4091	24.4109		24.4085	24.4113		24.4077	24.4094		24.4064	24.4094		24.4072	24.4084	
650	25.5906	25.5876	25.5902	25.5922	46L 4T	25.5897	25.5928	52L 9T	25.5886	25.5906	30L 20T	25.5875	25.5906	30L 31T	25.5888	25.5894	18L 31T
670	26.3780	26.3750	26.3776	26.3796		26.3771	26.3802		26.3760	26.3780		26.3749	26.3780		26.3762	26.3768	
680	26.7717	26.7687	26.7713	26.7733		26.7708	26.7739		26.7697	26.7717		26.7686	26.7717		26.7699	26.7705	
700	27.5591	27.5560	27.5587	27.5607		27.5582	27.5612		27.5571	27.5591		27.5561	27.5591		27.5573	27.5579	
720	28.3465	28.3435	28.3461	28.3481		28.3456	28.3487		28.3445	28.3465		28.3434	28.3465		28.3447	28.3453	
750	29.5276	29.5246	29.5272	29.5292		29.5267	29.5298		29.5256	29.5276		29.5245	29.5274		29.5258	29.5264	
780	30.7087	30.7057	30.7083	30.7103		30.7078	30.7109		30.7067	30.7087		30.7056	30.7087		30.7069	30.7075	
790	31.1024	31.0994	31.1020	31.1040		31.1015	31.1046		31.1004	31.1024		31.0993	31.1024		31.1006	31.1012	
820	32.2835	32.2796	32.2831	32.2852	57L 4T	32.2825	32.2860	64L 10T	32.2813	32.2835	39L 22T	32.2800	32.2835	39L 35T	32.2800	32.2822	26L 35T
850	33.4646	33.4607	33.4642	33.4663		33.4636	33.4671		33.4624	33.4646		33.4611	33.4646		33.4611	33.4633	
870	34.2520	34.2481	34.2516	34.2537		34.2510	34.2545		34.2498	34.2520		34.2485	34.2530		34.2485	34.2507	
920	36.2205	36.2166	36.2201	36.2222		36.2195	36.2230		36.2183	36.2205		36.2170	36.2205		36.2170	36.2192	
950	37.4016	37.3977	37.4012	37.4033		37.4006	37.4041		37.3994	37.4016		37.3981	37.4016		37.3981	37.4003	
980	38.5827	38.5788	38.5823	38.5844		38.5817	38.5852		38.5805	38.5827		38.5792	38.5827		38.5792	38.5814	
1000	39.3701	39.3662	39.3697	39.3718		39.3691	39.3726		39.3679	39.3701		39.3666	39.3701		39.3666	39.3688	
1150	45.2756	45.2707	45.2752	45.2778	71L 4T	45.2745	45.2786	79L 11T	45.2730	45.2756	49L 26T	45.2715	45.2756	49L 41T	45.2714	45.2740	33L 42T
1250	49.2126	49.2077	49.2122	49.2148		49.2115	49.2156		49.2100	49.2126		49.2085	49.2126		49.2084	49.2110	
1400	55.1181	55.1118	55.1177	55.1208	90L 4T	55.1169	55.1218	100L 12T	55.1150	55.1181	63L 31T	55.1132	55.1181	63L 49T	55.1131	55.1162	44L 50T
1600	62.9921	62.9858	62.9917	62.9948		62.9909	62.9958		62.9890	62.9921		62.9872	62.9921		62.9871	62.9902	
1800	70.8661	70.8582	70.8657	70.8693	111L 4T	70.8647	70.8677	125L 14T	70.8625	70.8661	79L 36T	70.8602	70.8661	79L 59T	70.8602	70.8638	56L 59T
2000	78.7402	78.7323	78.7398	78.7434		78.7389	78.7448		78.7366	78.7402		78.7343	78.7402		78.7343	78.7379	
2300	90.5512	90.5414	90.5508	90.5551	137L 4T	90.5499	90.5558	154L 13T	90.5469	90.5512	98L 43T	90.5443	90.5512	98L 69T	90.5442	90.5485	71L 70T
2500	98.4252	98.4154	98.4248	98.4291		98.4239	98.4298		98.4209	98.4252		98.4183	98.4252		98.4182	98.4225	

Appendix I: PWM Circuit

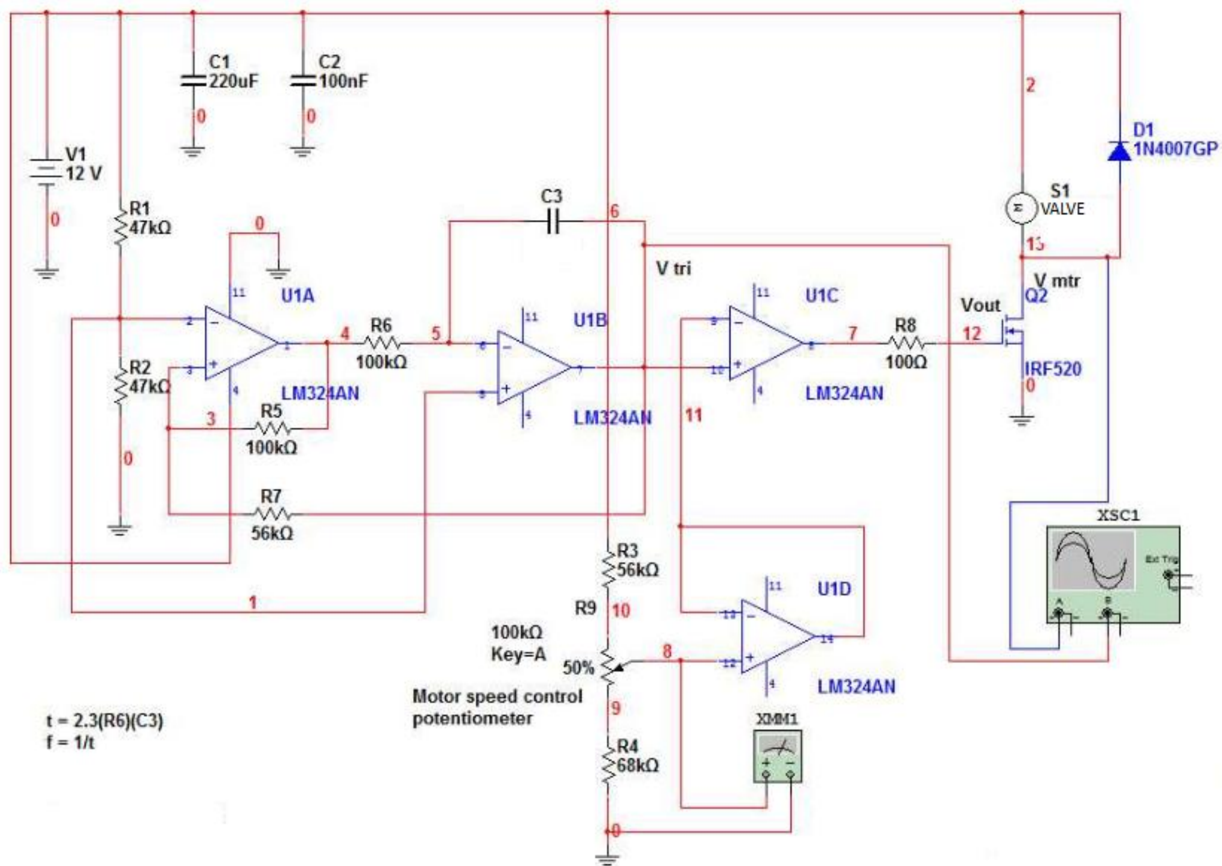

Appendix J: Load Cell Force Calculations

Given Motor Specifications

Power: $P := 559.274904\,W$

Angular Velocity: $\omega := 3450\,rpm = 361.283\,\frac{rad}{s}$

Torque of Motor

Torque: $\tau := \frac{P}{\omega}$

$\tau = 1.548\,J$

$\tau = 13.701\,in \cdot lbf$

Force at Known Length

Radius: $r := 3.25\,in$

Force: $F := \frac{\tau}{r}$

$F = 4.216\,lbf$

Appendix K: Part Drawings

Accumulator

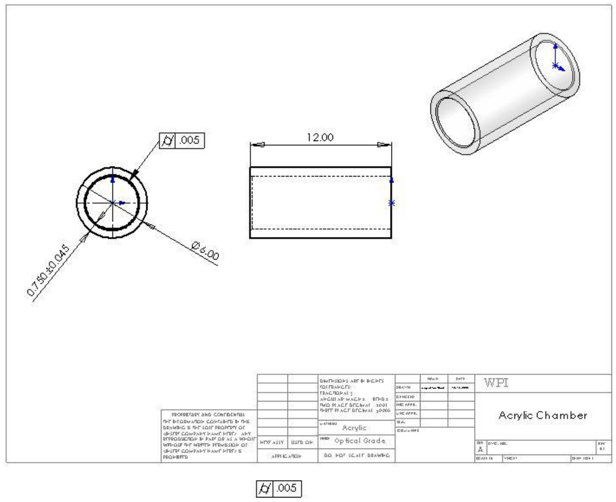

Oil End Cap

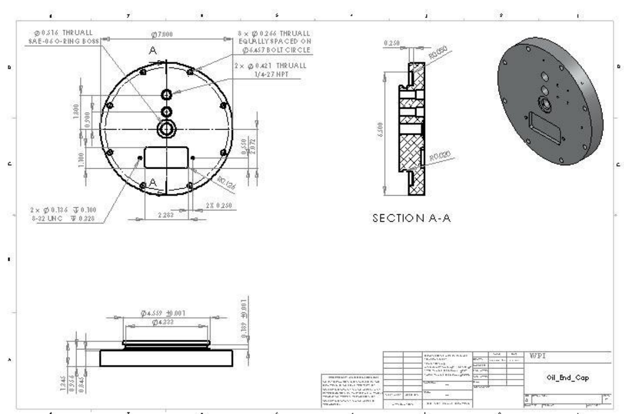

Gas End Cap

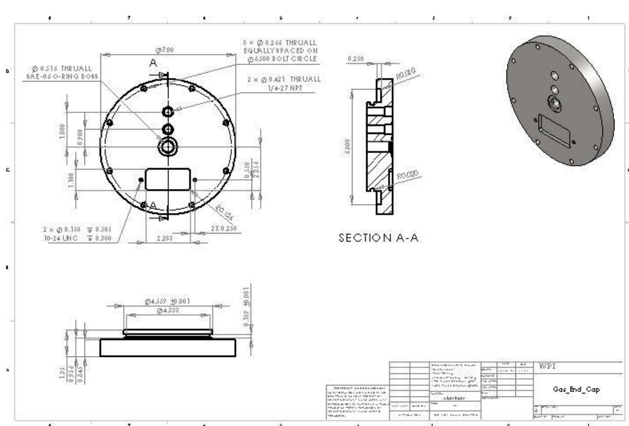

Oil Shaft

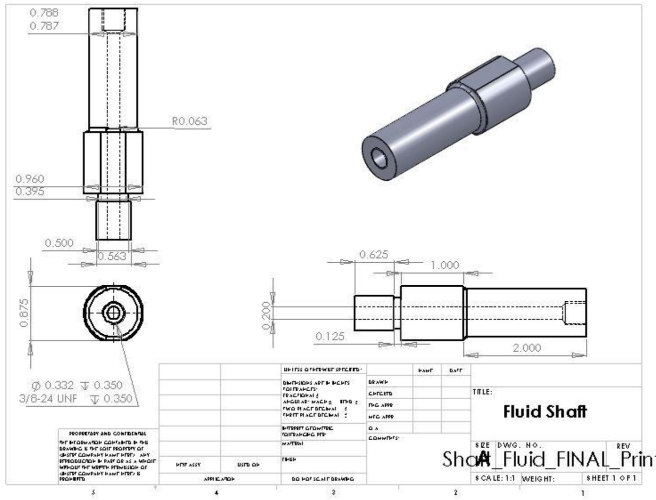

Gas Shaft

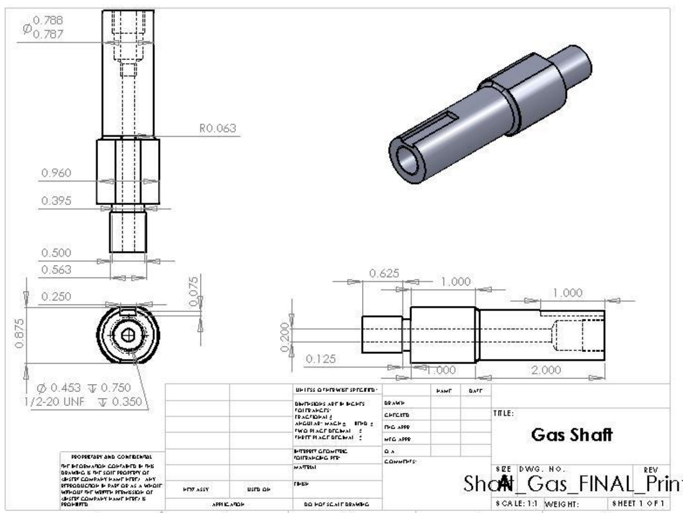

Bearing Mount

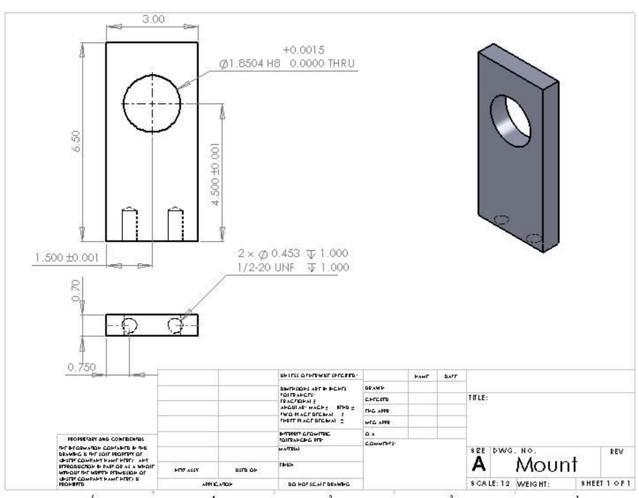

Piston

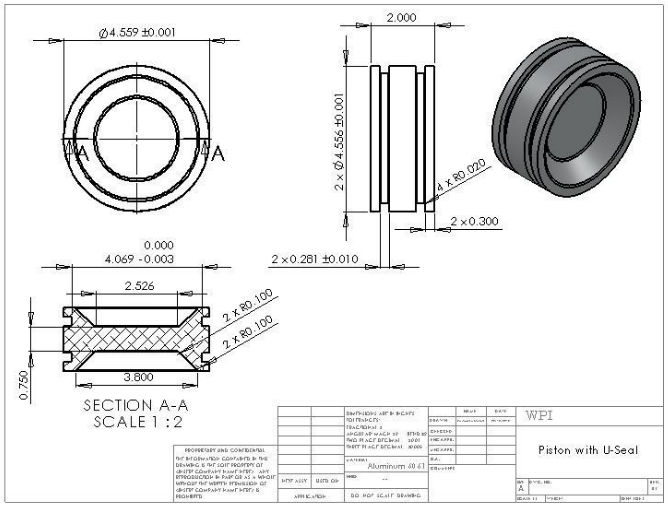

Motor Support

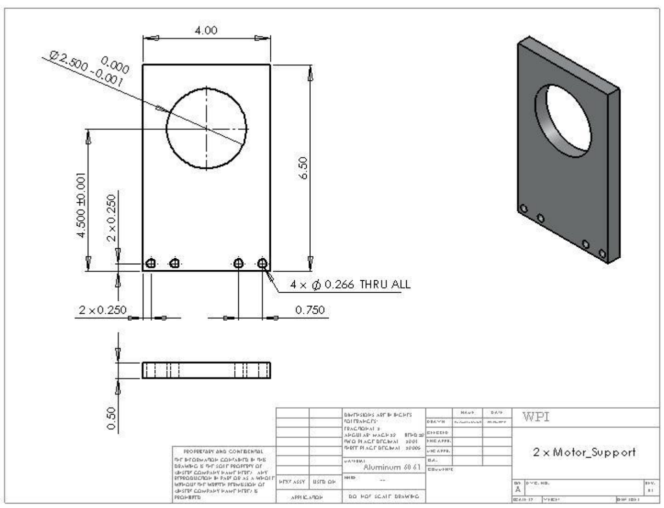

Rotary Encoder

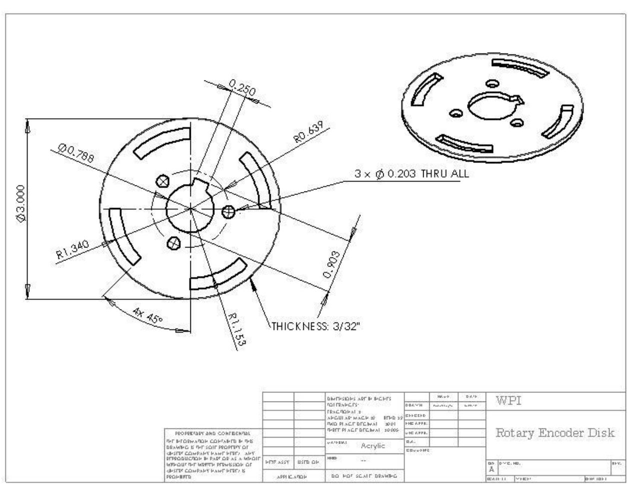

Motor Screw Block

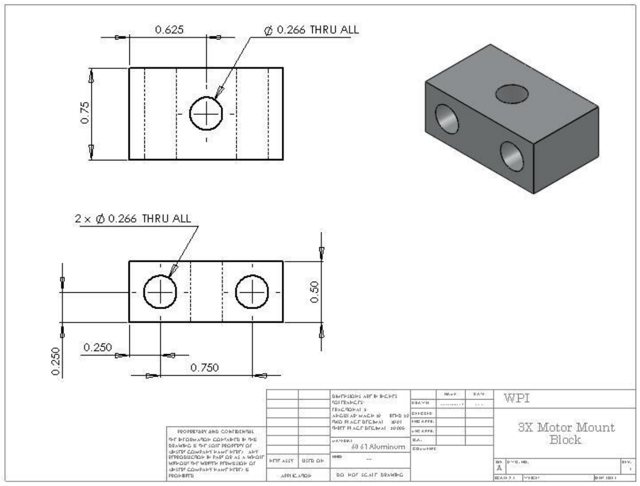

Custom Ring Shaft Side

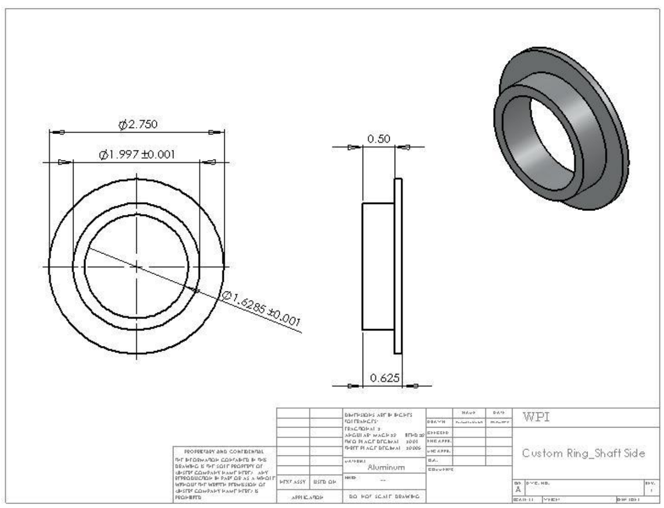

Custom Ring Torque Arm Side

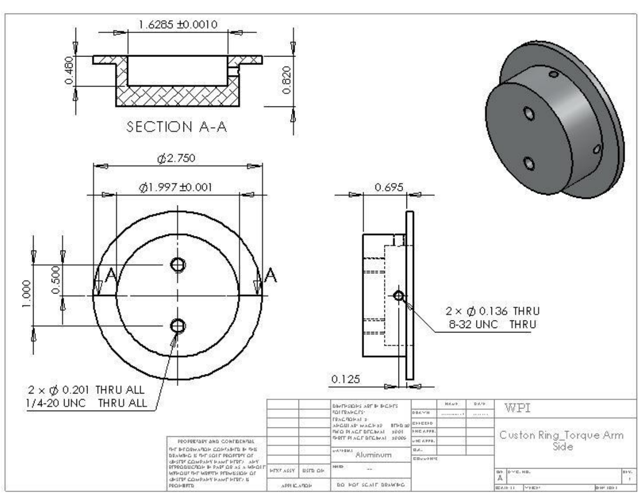

Torque Arm

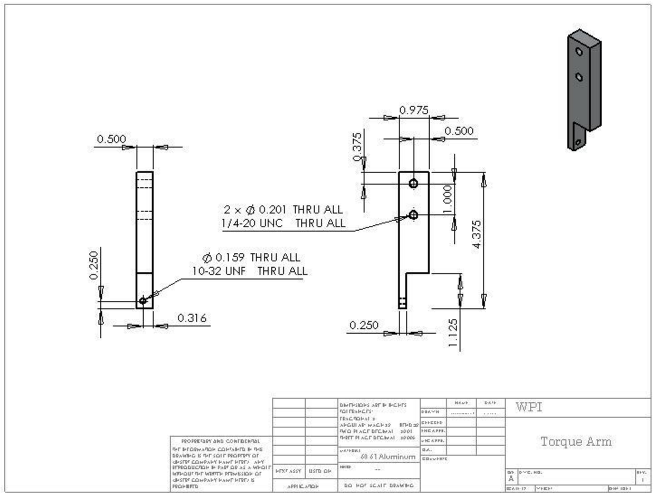

Load Cell Ground

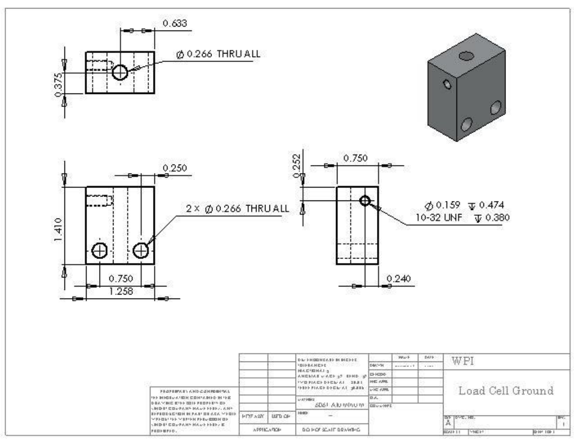

Clutch Front Mount

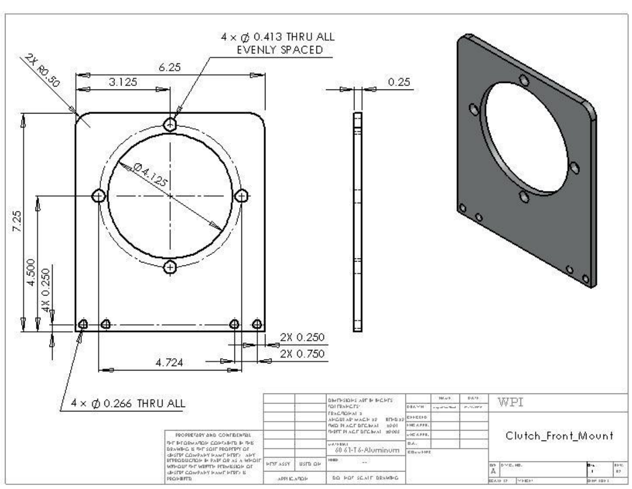

Clutch Back Mount

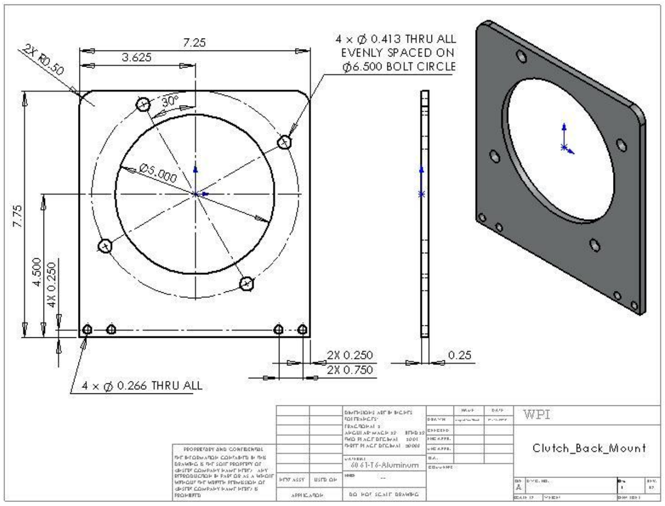

Clutch Support Block

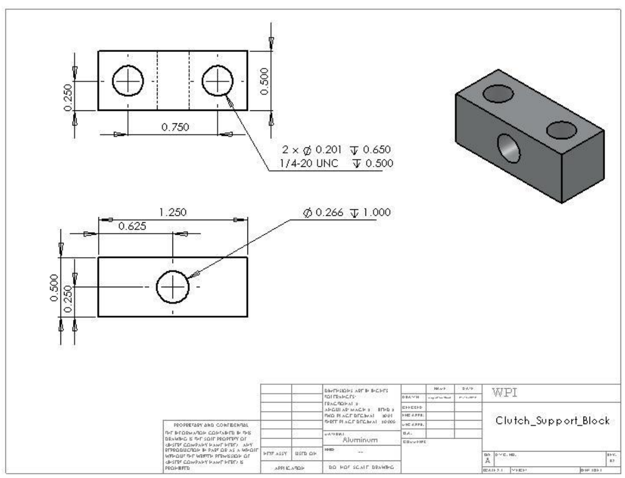

Coupler Shaft

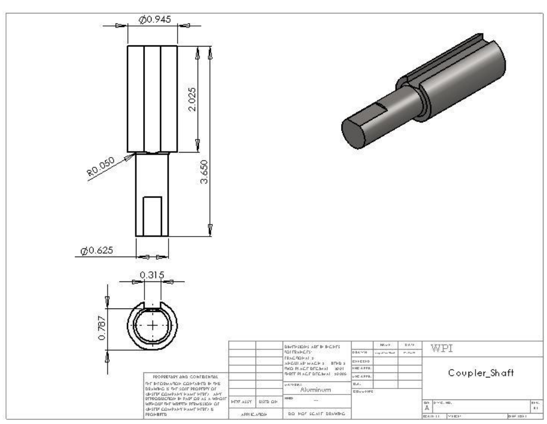

Appendix L: Shaking Force Balancing

Balancing sensors

Knowns $kpsi := 1000\,psi$

Mass sensor $m_s := 24 \cdot 10^{-3} kg$

Mass 9V battery $m_{9v} := 45.6 \cdot 10^{-3} \cdot kg$

Distance from first sensor to center $r_1 := 0.8\,in$

Distance from second sensor to center $r_2 := 2 \cdot r_1$

Density 6061 aluminum $\rho := 2700 \frac{kg}{m^3}$

Mass of material removed for battery and sensors

Volume sensor material removal

$d_1 := 0.519\,in \quad h_1 := 0.455\,in$

$d_2 := 0.421\,in \quad h_2 := 0.545\,in$

$$V_s := \frac{\pi \cdot d_1^2 \cdot h_1}{4} + \frac{\pi \cdot d_2^2 \cdot h_2}{4} \qquad V_s = 0.172\,in^3$$

$$m_{removed} := \rho \cdot V_s \qquad m_{removed} = 7.616 \times 10^{-3}\,kg$$

$$m_t := m_s - m_{removed} \qquad m_t = 0.016\,kg$$

Volume 9v pocket dimensions

$l := 2.03125\,in \quad w := 1.1\,in \quad d := 0.2\,in$

Volume $V_b := l \cdot w \cdot d$ $\qquad V_b = 0.447\,in^3$

mass removed

$$m_r := \rho \cdot V_b \qquad m_r = 0.02\,kg$$

equivalent mass of 9v

$$m_b := m_{9v} - m_r \qquad m_b = 0.026\,kg$$

Shaking force to balance

$$F_b := m_t \cdot (r_1 + r_2) \qquad F_b = 9.988 \times 10^{-4}\,m \cdot kg$$

Since mass of battery and material removed is constant, adjust distance of cent
battery to balance

$$r_b := \frac{F_b}{m_b} \qquad r_b = 1.522\,in$$

Sizing bolts to hold 9V battery in

angular velocity $\omega := 3000\,rpm$

assume worst case scenario, one bolt is withsatnding all the force of the batt

Assume acceleration is zero, so tangential component is zero, leaving only the n acceleration..

$$a_n := r_b \cdot \omega^2 \qquad a_n = 3.817 \times 10^3 \frac{m}{s^2}$$

now to find the force

$$V := m_{9v} \cdot a_n \qquad V = 174.04\,N$$

and finding the stress assuming area is the minor thread diameter

for 6-32 screws

$$d_{r1} := 0.0974\,in \qquad A_1 := \pi \cdot \frac{d_{r1}^2}{4} \qquad A_1 = 7.451 \times 10^{-3} \cdot in^2$$

$$\sigma_1 := \frac{V}{A_1} \qquad \sigma_1 = 5.251\,kpsi$$

for 8-32 screws

$$d_{r2} := 0.1234\,in \qquad A_2 := \pi \cdot \frac{d_{r2}^2}{4} \qquad A_2 = 0.012\,in^2$$

$$\sigma_2 := \frac{V}{A_2} \qquad \sigma_2 = 3.271\,kpsi$$

for 10-24 screws

$$d_{r3} := 0.1359\,in \qquad A_3 := \pi \cdot \frac{d_{r3}^2}{4} \qquad A_3 = 0.015\,in^2$$

$$\sigma_3 := \frac{V}{A_3} \qquad \sigma_3 = 2.697\,kpsi$$

for 1/4-20 screws

$$d_{r4} := 0.185\,in \qquad A_4 := \pi \cdot \frac{d_{r4}^2}{4} \qquad A_4 = 0.027\,in^2$$

$$\sigma_4 := \frac{V}{A_4} \qquad \sigma_4 = 1.456\,kpsi$$

According to Industrial fastener institute (inch fastener standards, 7th ed. 2003. B-8 the s strengths of carbon steel fasteners is approximately 60% of the tensile strength.

according to machinery's handbook for grade 2 tensile strength is 74kpsi and the proof strength 55

tensile $V_{st} := 0.6 \cdot 74 \cdot kpsi$ $V_{st} = 44.4 \cdot kpsi$

proof $V_{sp} := 0.6 \cdot 55 \cdot kpsi$ $V_{sp} = 33 \cdot kpsi$

Thus the safety factor for each screw assuming one is bearing all the load is:

6-32 $N_1 := \frac{V_{sp}}{\sigma_1}$ $N_1 = 6.284$

8-32 $N_2 := \frac{V_{sp}}{\sigma_2}$ $N_2 = 10.087$

10-24 $N_3 := \frac{V_{sp}}{\sigma_3}$ $N_3 = 12.234$

1/4-20 $N_4 := \frac{V_{sp}}{\sigma_4}$ $N_4 = 22.672$

Appendix M: Energy Density Calculations

Energy Density

knowns

length of cylinder — outer radius — inner radius — weight density for acrylic

$l := 12 \cdot in$ $\quad r_0 := 3 \cdot in$ $\quad r_i := 2.5\,in$ $\quad \gamma := 0.04285 \cdot \frac{lb}{in^3}$

angular velocity — length of hydraulic volume — density of DTE 15

$\omega := 3000\,rpm$ $\quad l_h := 5.75\,in$ $\quad \rho := 876 \cdot \frac{kg}{m^3}$ $\quad kJ := 1000\,J$

Inertia of acrylic cylinder

$$I_{flywheel} := \frac{\pi}{2} \cdot \gamma \cdot \left(r_0^{\,4} - r_i^{\,4}\right) \cdot l \qquad I_{flywheel} = 9.913 \times 10^{-3}\,m^2 \cdot kg$$

Inertia of fluid with piston at center

$$I_{fluid} := \frac{\pi \cdot \rho \cdot l_h \cdot r_i^{\,4}}{2} \qquad I_{fluid} = 3.268 \times 10^{-3}\,m^2 \cdot kg$$

$$I_{total} := I_{flywheel} + I_{fluid} \qquad I_{total} = 0.013\,m^2 \cdot kg$$

Energy of flywheel

$$E_{flywheel} := \frac{1}{2} \cdot I_{total} \cdot \omega^2 \qquad E_{flywheel} = 650.414\,J$$

Energy of Gas

Assumptions

Max pressure

$$P_{max} := 500 \cdot psi$$

Precharge pressure

$$P_i := \frac{P_{max}}{2} = 250 \cdot psi$$

Initial volume of gas

$$V_i := \pi \cdot r_i^{\,2} \cdot (l - 0.5\,in) \qquad V_i = 3.7\,L$$

Final volume of gas

$$V_f := \pi \cdot r_i^{\,2} \cdot \left(\frac{l}{2} - \frac{0.5}{2} \cdot in\right) \qquad V_f = 1.85\,L$$

Compression factor

$$R := \frac{V_i}{V_f} \qquad R = 2$$

v_f

Assuming ideal isothermal gas integration of $E_{gas} := \int P\,dV$ reduces to:

$E_{gas} := P_i \cdot V_i \cdot \ln(R)$ $\quad E_{gas} = 4.421\,kJ$

Percentage of storage of flywheel vs potential energy

$$\frac{E_{flywheel}}{E_{gas}} = 0.147$$

total mass $\quad M := 7.711\,kg$

Total energy stored

$E_{stored} := E_{flywheel} + E_{gas}$ $\quad E_{stored} = 5.071\,kJ$

Energy density

for both kinetic and potential

$$E_{d1} := \frac{E_{stored}}{M} \qquad E_{d1} = 0.658\,\frac{kJ}{kg}$$

for gas alone

$$E_{d2} := \frac{E_{gas}}{M} \qquad E_{d2} = 0.573\,\frac{kJ}{kg}$$

increase in energy desnity

$$\frac{E_{gas} + E_{flywheel}}{E_{gas}} = 1.147$$

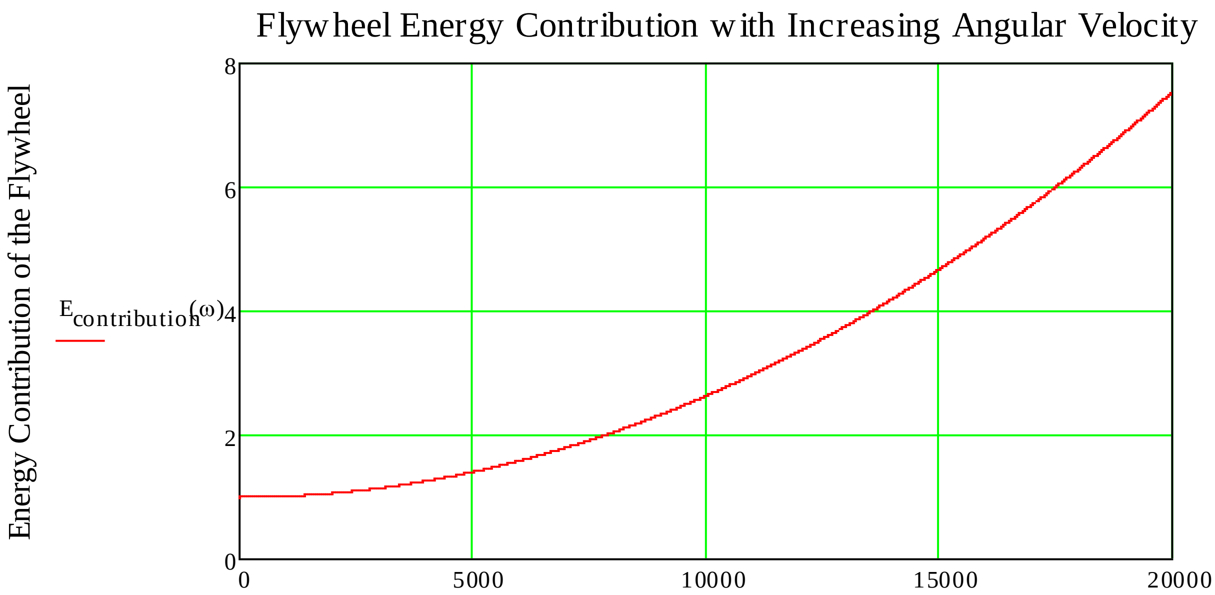

Maximum Energy Density $E_{contribution}(\omega_{max}) = 7.539$ $\frac{\omega}{rpm}$

Angular Velocity, RPM

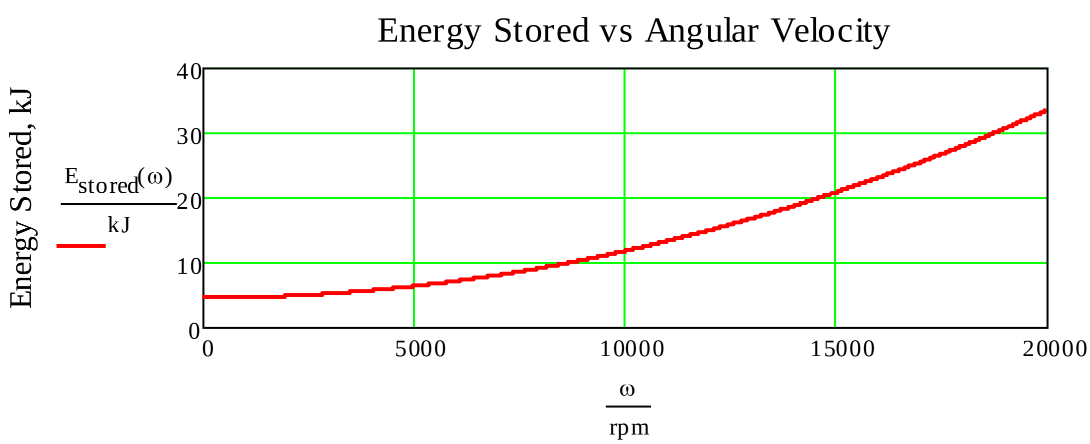

Angular Velocity, RPM

Max energy stroed at 20,000 RPM

$E_{stored}(\omega_{max}) = 33.328\,kJ$

Energy Density up to 20,000 RPM for high speed implementation

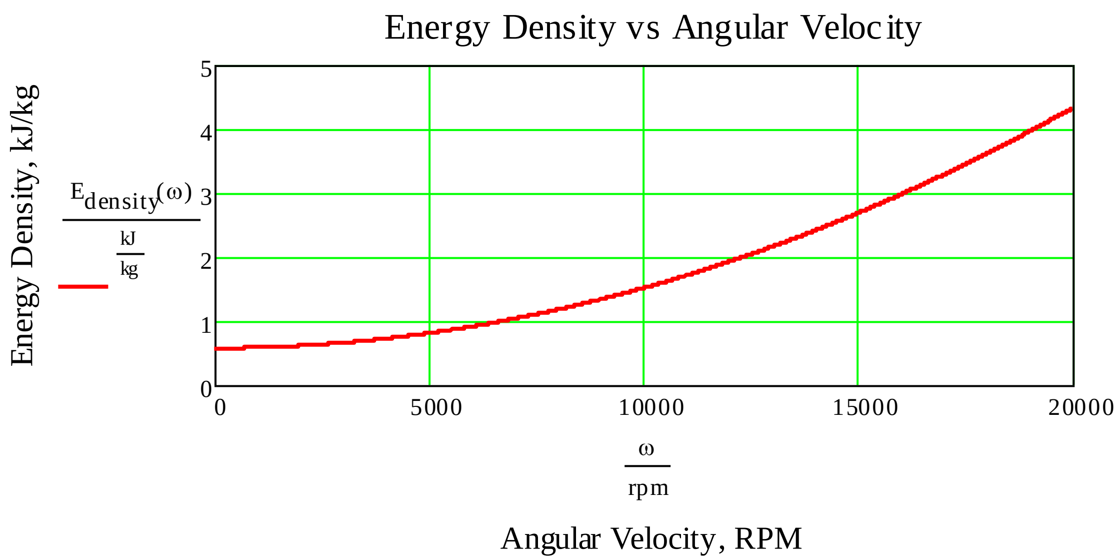

Energy Density up to 3,000 RPM for low energy prototype

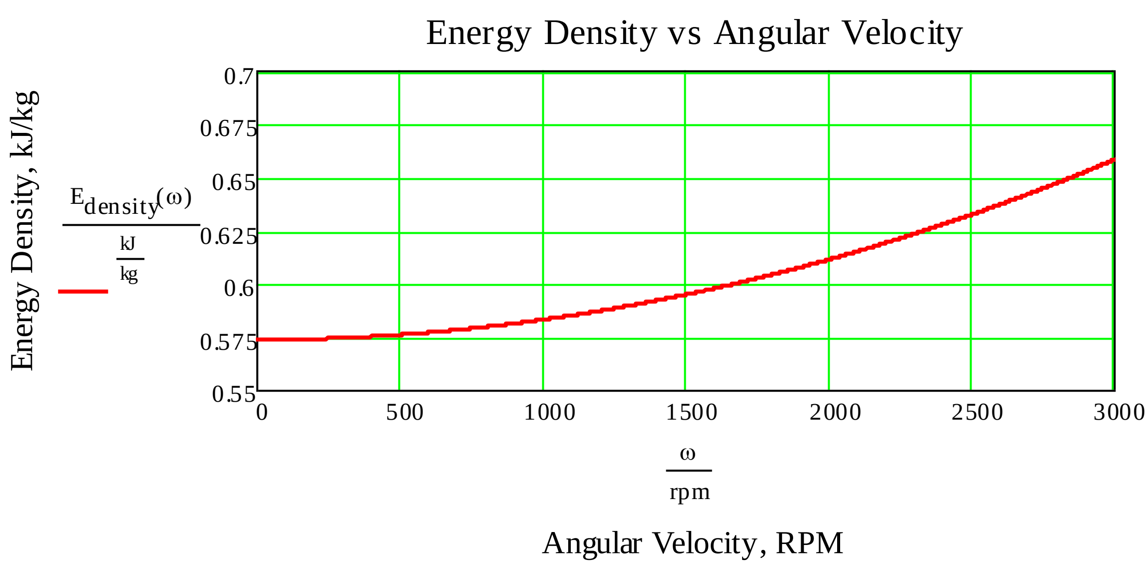

Maximum Energy Density at system spec of 3000 RPM

$$E_{density}(3000\,rpm) = 0.658\frac{kJ}{kg}$$

Appendix N: Xbee Schematic

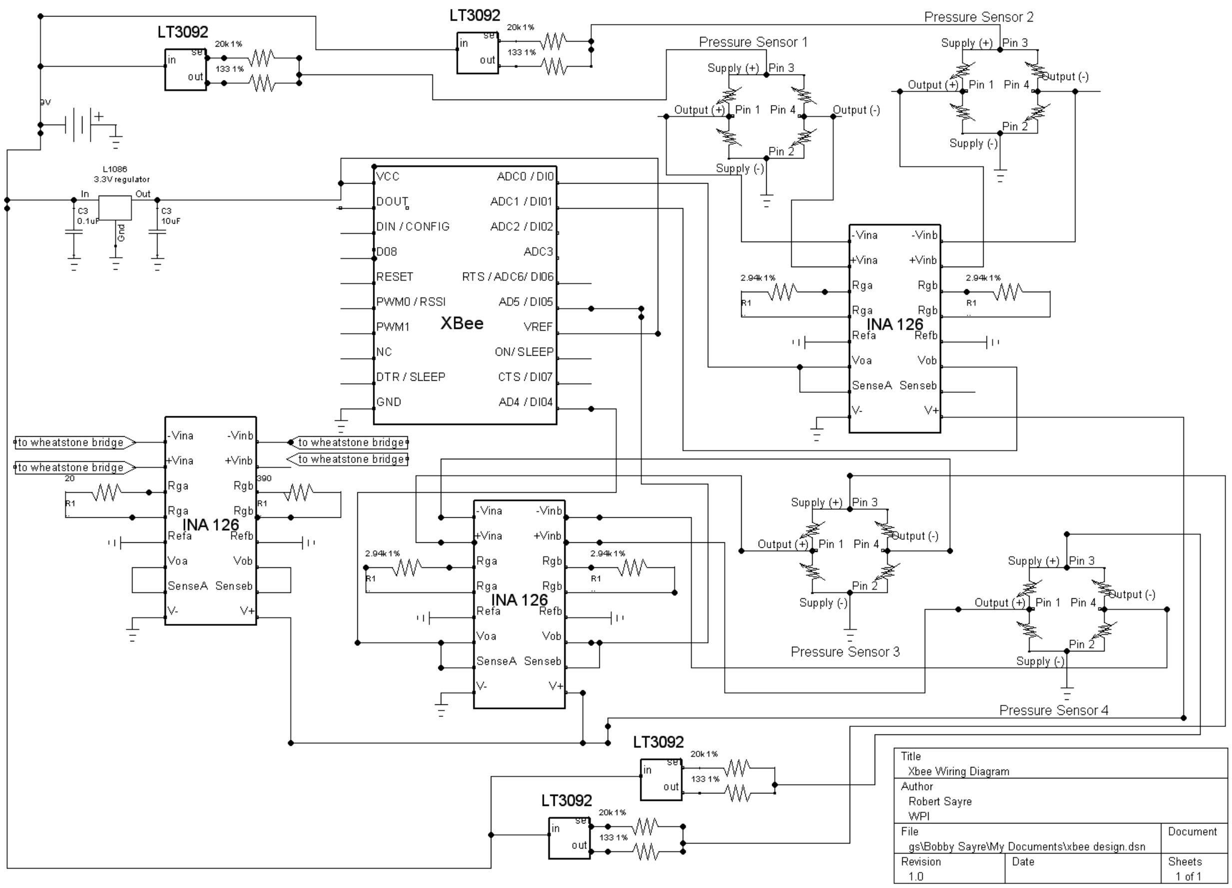

Appendix O: Vision System LabVIEW VI